



IONIC LIQUIDS FOR KERATIN FIBRE MODIFICATION

Margarida João de Morais Sarmento Póvoas Trindade, MSci

Thesis submitted to the University of Nottingham

for the degree of Doctor of Philosophy in Chemistry

February 2022

Acknowledgments

I would like to thank my Supervisor, Prof. Pete Licence for all the guidance and support throughout my PhD project. His constant encouragement was essential during my PhD. I would like to thank Doctor Paul Pudney and Doctor Ken Lee for the support during my visits to Unilever. I gratefully acknowledge the funding received towards my PhD from Unilever.

I would like to thank Doctor Elisabeth Steer for SEM training and help throughout my PhD. I extend my gratitude to Doctor Nichola Star for the assistance with ToF-SIMS studies.

I would like to thank members of the Licence Group for the laughter and for being a good source of support and knowledge: Ste, Aki, Ejike, Astrid, Laís, Patrick, Meike and Zé. A special thank you goes to Doctor Ana and Doctor Calum for the support, knowledge, sarcasm and tough-love. A special thank you to Luiz for all the scientific discussions and all the support during his time in Nottingham. I would like to extend my sincere thanks to Doctor Coby Clarke for performing the FTIR spectroscopy analysis.

To my best friend Tatiana for being by my side since day one of my PhD, you made me feel at home. My experience would definitely have not been the same without you by my side. I would like to thank Jorge for all the patience and support and for being by my side throughout my roller coaster of emotions throughout my PhD. Lastly, I would like to thank my parents and my brother for all the support, optimism, encouragement and for being there for me.

Abstract

The human hair has been wasted in many parts of the world and even considered useless, however human hair is a great source of keratin. Keratin represents an important renewable biomaterial which could be further explored. The number of applications is vast and due to its potential, the dissolution of human hair was further investigated in this Thesis.

It has been demonstrated that ionic liquids have the ability to dissolve cellulose and other keratin sources, such as feathers and wool. For this reason, the dissolution of human hair with ionic liquids was investigated in this study. Imidazolium and pyrrolidinium based ionic liquids were studied, and the impact of the cation on dissolution was found to be marginal. Conversely, the anion plays an important role disrupting the hydrogen and disulfide bonds, which leads to the dissolution of hair. This is due to nucleophilic anions such as acetate, dimethylphosphate or chloride. Increasing the aliphatic chain length of the cation was also shown to have an impact on the dissolution of hair due to the increase of the viscosity of the ionic liquid. The efficiency of the dissolution process was also considered, where dissolution assisted by microwave radiation proved to be faster than conventional heating.

It was found that keratin, extracted from waste biomass, has many applications, and as such, it was investigated whether it was possible to extract keratin material from the dissolution of hair. Recovery of keratin material was possible using $[C_2C_1Im][OAc]$ and $[C_2C_1Im][Me_2PO_4]$. The recovery of keratin material was further analysed in order to investigate its chemical characterisation. In terms of efficiency, greater amounts of keratin material was recoverable from the dissolution with $[C_2C_1Im][Me_2PO_4]$ than $[C_2C_1Im][OAc]$. This may be related to the higher affinity of the dissolved particles to the ionic liquid phase which makes the regeneration process challenging.

Since the dissolution of hair was possible with ionic liquids, the ability ionic liquids to modify the structure of hair in specific bonds was investigated. These modifications were then investigated by infrared spectroscopy. During this investigation a deeper analysis was conducted to understand the natural structure of hair and how to identify possible modifications in its structure by infrared spectroscopy.

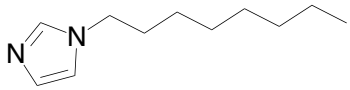
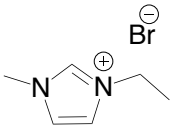
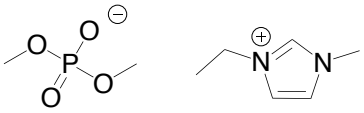
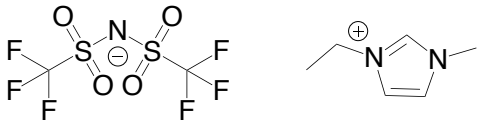
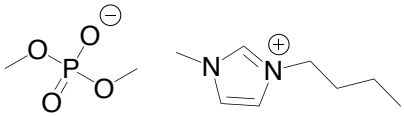
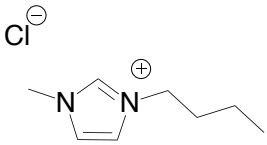
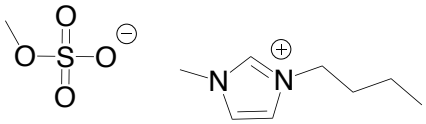
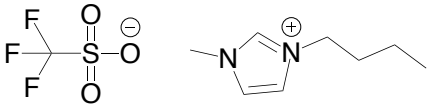
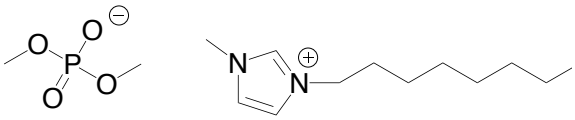
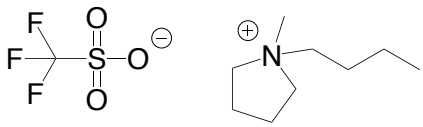
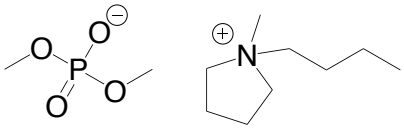
Abbreviations & Acronyms

[AmIm]Cl	1-allyl-3-methylimidazolium chloride
$[C_4C_1Im][OAc]$	1-butyl-3-methylimidazolium acetate
$[C_4C_1Im]Cl$	1-butyl-3-methylimidazolium chloride
$[C_2C_1Im]^+$	1-ethyl-3-mehtylimidazolium cation
$[C_2C_1Im][OAc]$	1-ethyl-3-methylimidazolium acetate
[TMGH][OAc]	1,1,3,3-tetramethylguanidinium acetate
18-MEA	18-methyleicosanoic acid
$[OAc]^-$	Acetate
ALP	Alkaline phosphatase
θ	Angle
a.u.	Arbitrary units
RGD	Arginine-glycine-aspartic acid
Ar^+	Argon
AAS	Atomic Absorption Spectroscopy
AES	Atomic Emission Spectroscopy
AFM	Atomic Force Microscopy
ATR-FTIR	Attenuated Total Reflectance Fourier-Transform Infrared Spectroscopy
NTf_2^-	Bis(trifluoromethane)sulfonimide anion
Bi_3^+	Bismuth cluster
CO_2	Carbon dioxide
CMC	Cell Membrane Complex
cm	Centimetres
δ	Chemical Shift
CHO	Chinese Hamster Ovary
J	Coupling constant
θ_c	Critical angle
d_p	Depth of penetration
$(CD_3)_2CO$	Deuterated acetone

DSC	Differential Scanning Calorimetry
$[Me_2PO_4]^-$	Dimethylphosphate anion
π^*	Dipolarity/polarizability
DSL	Dynamic Light Scattering
eV	Electron volt
ESI-MS	Electrospray Ionisation Mass Spectrometry
EDX	Energy Dispersive X-Ray Emission
ECM	Extracellular Matrix
FoV	Fields of view
FIDs	Free Induction Decay
GRAS	Generally recognised as safe
PF_6^-	Hexafluorophosphate anion
HCl	Hydrochloric acid
SH^-	Hydrogen sulfide
α	Hydrogen-bond acidity
β	Hydrogen-bond basicity
n	Index number
ICPMS	Inductively Coupled Plasma Mass Spectrometry
IR	Infrared Spectroscopy
ILs	Ionic Liquids
KRT	Keratin
KAPs	Keratin Associated Proteins
KIF	Keratin Intermediate Filament
kDa	Kilodalton
kV	Kilovolt
LC_{50}	Lethal concentration
LDU	Leucine-aspartic acid-valine
m/z	Mass-to-charge ratio
MALDI	Matrix Assisted Laser Desorption Ionization
EC_{50}	Measure of concentration
LD_{50}	Median lethal dose

µg	microgram
µm	micrometre
mbar	milibar
mg	milligram
mm	millimetre
MIC	Minimum Inhibitory Concentration
min	Minutes
M	Molarity
NAA	Neutron Activation Analysis
NMR	Nuclear Magnetic Resonance
PIXE	Particle Induced X-Ray Emission
ppm	Parts per million
Phe	Phenylalanine
rmp	Revolutions Per Minute
SEM	Scanning Electron Microscopy
TBAH	Tetrabutylammonium hydroxide
$BF4^-$	Tetrafluoroborate anion
TG	Thermograms
TGA	Thermogravimetric Analysis
ToF-SIMS	Time of Flight Secondary Ion Mass Spectrometry
$[N2221]^+$	Triethylmethylammonium cation
Trp	Tryptophan
Tyr	Tyrosine
VOC	Volatile Organic Solvents
W	Watt
w	Weight
XRD	X-Ray Diffraction
XRF	X-Ray Fluorescence
XPS	X-Ray Photoelectron Spectroscopy

Table of Structural Abbreviations

Structure	Name	Abbreviation
	1-octylimidazole	
	1-ethyl-3-methylimidazolium bromide	$[C_2C_1Im]Br$
	1-ethyl-3-methylimidazolium dimethylphosphate	$[C_2C_1Im][Me_2PO_4]$
	1-ethyl-3-methylimidazolium bis(trifluoromethanesulfonyl) imide	$[C_2C_1Im][NTf_2]$
	1-butyl-3-methylimidazolium dimethylphosphate	$[C_4C_1Im][Me_2PO_4]$
	1-butyl-3-methylimidazolium chloride	$[C_4C_1Im]Cl$
	1-butyl-3-methylimidazolium methylsulphate	$[C_4C_1Im][MeSO_4]$
	1-butyl-3-methylimidazolium trifluoromethanesulfonate	$[C_4C_1Im][CF_3SO_3]$
	1-octyl-3-methylimidazolium dimethylphosphate	$[C_8C_1Im][Me_2PO_4]$
	1-butyl-1-methylpyrrolidinium trifluoromethanesulfonate	$[C_4C_1Pyrr][CF_3SO_3]$
	1-butyl-1-methylpyrrolidinium dimethylphosphate	$[C_4C_1Pyrr][Me_2PO_4]$

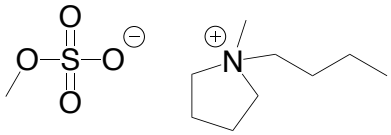
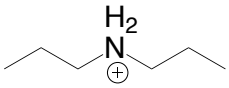
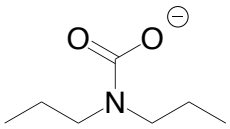
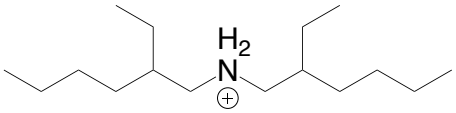
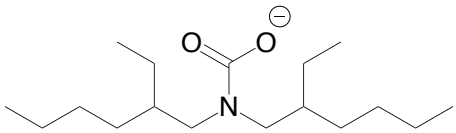
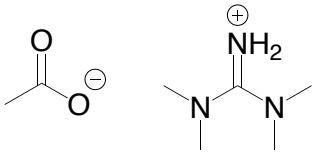
	1-butyl-1-methylpyrrolidinium methylsulfate	$[C_4C_1Pyrr][MeSO_4]$
 	*N,N*-dipropylammonium *N',N'*-dipropylcarbamate	DPCARB
 	Bis(2-ethylhexyl)ammonium bis(2-ethylhexyl)carbamate	DBCARB
	1,1,3,3-tetramethylguanidinium acetate	[TMGH][OAc]

TABLE OF CONTENTS

Acknowledgments ..... *I*

Abstract ..... *II*

Abbreviations & Acronyms ..... *III*

Table of Structural Abbreviations ..... *VI*

Chapter 1 Introduction *1*

1.1 Overview **1**

1.2 Human hair **1**

1.2.1 The structure of hair 1

1.2.2 Human hair from different ethnicities 4

1.3 Hair material application **6**

1.3.1 Amino acids from human hair 7

1.3.2 Keratins from human hair 8

1.3.3 KAPs from human hair 10

1.4 Extraction **11**

1.4.1 Extraction of keratin from natural sources 11

1.4.2 Dissolution of macromolecules with Ionic liquids 12

1.4.3 Diffusion into hair fibres 15

1.4.4 Ionic liquid selection based on Kamlet-Taft parameters 17

1.4.4.1 Toxicity of Ionic liquids 18

1.4.5 Recovery of keratin material from dissolution of wool and feathers 20

1.5 Modification of the structure of hair **21**

1.5.1 Reversible methods 21

1.5.2 Permanent methods 21

1.5.3 How ionic liquids could target specific bonds in hair structure 22

1.5.3.1 ATR infrared spectroscopy on human hair 22

1.5.3.2 Vibrational spectroscopy of human hair 23

1.6 Analysis of the structure of hair **26**

1.7 Aims **27**

Chapter 2 The study of the dissolution of hair with ILs *28*

2.1 Influence of the anion of the ILs on the dissolution of hair. **30**

2.2 Influence of the cation of the ILs on the dissolution of hair 32

2.3 Influence of alkyl side chain of cation of ILs on the dissolution of hair 33

2.4 The influence of the temperature on the dissolution of hair with ILs 35

2.4.1 Dissolution of hair 36

2.5 Dissolution of hair with [C_2C_1Im][OAc] and [C_2C_1Im][Me_2PO_4] assisted by microwave radiation 38

2.6 Dissolution of different hair types with [C_2C_1Im][OAc] 40

2.7 Conclusions 42

Chapter 3 Material recovery from the dissolution of hair with ILs and its chemical characterisation 44

3.1 Material recovery from the dissolution of hair with [C_2C_1Im][OAc] 44

3.2 Material recovery from the dissolution of hair with [C_2C_1Im][Me_2PO_4] 46

3.2.1 Material recovery from dissolution of hair assisted by microwave radiation 48

3.3 Characterisation of recovered materials from dissolution processes 49

3.3.1 Scanning Electron Analysis Energy-dispersive X-Ray spectroscopy (SEM-EDX) 49

3.3.2 Thermal stability analysis of hair 51

3.3.3 Thermal stability analysis of recovered material from dissolution assisted by microwave radiation 57

3.3.4 Material recovery from dissolution of hair from different ethnicities 59

3.3.5 FTIR spectroscopy of the recovered material 61

3.4 Chemical characterisation (MALDI) 63

3.5 Dissolution of hair with distillable ionic liquids 67

3.6 Conclusions 68

Chapter 4 Modification of hair fibres with ILs and subsequent characterisation ... 71

4.1 Modification of hair fibres with ILs 71

4.2 ATR analysis on the impact of ILs on the structure of hair 87

4.3 Natural variation of hair fibre 88

4.3.1 Natural variation along hair fibre hair 91

4.3.1.1 Natural variation among different hair fibres 94

4.4 Conclusions 98

Chapter 5 Experimental.....101

5.1 Preparation of solvents..... 101

5.1.1 Methods of analysis 101

5.1.1.1 Nuclear Magnetic Resonance (NMR)..... 101

5.1.1.2 Electrospray Ionisation Mass Spectrometry (ESI-MS) 101

5.1.2 Ionic liquid synthesis 101

5.1.2.1 Imidazolium based Ionic Liquids..... 103

5.1.2.1.1 1-octylimidazole. [304] 103

5.1.2.1.2 1-ethyl-3-methylimidazolium bromide, $[C_2C_1Im]Br$.[306] 104

5.1.2.1.3 1-ethyl-3-methylimidazolium dimethylphosphate, $[C_2C_1Im][Me_2PO_4]$.[137] 105

5.1.2.1.4 1-ethyl-3-methylimidazolium dimethylphosphate, $[C_2C_1Im][Me_2PO_4]$.[137] 106

5.1.2.1.5 1-ethyl-3-methylimidazolium bis(trifluoromethanesulfonyl)imide,$[C_2C_1Im][NTf_2]$.[309] 107

5.1.2.1.6 1-butyl-3-methylimidazolium dimethylphosphate, $[C_4C_1Im][Me_2PO_4]$.[312] 108

5.1.2.1.7 1-butyl-3-methylimidazolium chloride, $[C_4C_1Im]Cl$.[259] 109

5.1.2.1.8 1-butyl-3-methylimidazolium methylsulphate, $[C_4C_1Im][MeSO_4]$.[315] 110

5.1.2.1.9 1-butyl-3-methylimidazolium trifluoromethanesulfonate, $[C_4C_1Im][CF_3SO_3]$.[318] .. 111

5.1.2.1.10 1-octyl-3-methylimidazolium dimethylphosphate, $[C_8C_1Im][Me_2PO_4]$.[312] 112

5.1.2.2 Pyrrolidinium Ionic Liquids 113

5.1.2.2.1 1-butyl-1-methylpyrrolidinium trifluoromethanesulfonate, $[C_4C_1Pyrr][CF_3SO_3]$.[318] 113

5.1.2.2.2 1-butyl-1-methylpyrrolidinium dimethylphosphate, $[C_4C_1Pyrr][Me_2PO_4]$.[136] 114

5.1.2.2.3 1-butyl-1-methylpyrrolidinium methylsulfate, $[C_4C_1Pyrr][MeSO_4]$.[280] 115

5.1.2.3 Distillable ILs 116

5.1.2.3.1 *N,N*-dipropylammonium *N',N'*-dipropylcarbamate, DPCARB.[323] 116

5.1.2.3.2 Bis(2-ethylhexyl)ammonium bis(2-ethylhexyl)carbamate, DBCARB.[323] 117

5.1.2.3.3 1,1,3,3-tetramethylguanidinium acetate, [TMGH][OAc]. [294] 118

5.1.3 Water content of IL 118

5.2 Keratin process 119

5.2.1 Pre-treatment 119

5.2.2 Dissolution method 120

5.3 Regeneration process of recovered material 120

5.3.1 Dissolution assisted by microwave radiation 125

5.4 Instrumentation 126

5.4.1 Thermogravimetric analysis (TGA) 126

5.4.1.1 Analysis of the recovered hair material 126

5.4.1.2 Analysis of the precipitate from IL water-soluble fraction 126
5.4.2 FTIR spectroscopy: Attenuated Total Reflectance (ATR) 127
5.4.3 FTIR spectroscopy 127
5.4.4 Scanning Electron Microscopy (SEM) 127
5.4.4.1 Analysis of the recovered hair material 127
5.4.4.2 Analysis of the treated hair fibres 127
5.4.5 Time of Flight (ToF) Mass Spectrometer Coupled with Matrix Assisted Laser Desorption Ionization (MALDI) 128
5.4.5.1 Analysis of the recovered hair material 128
5.4.5.2 Analysis of the treated hair fibres 128
5.4.6 Mass spectrometry 129
5.4.6.1 Analysis of the ionic liquids 129
5.4.7 Polarised light microscopy 129

Chapter 6 Conclusions and Future work 130

References 133

Appendix: 151

TGA for Chapter 3 151

Distortion of hair fibres during ATR sampling for Chapter 4 154

Pressure variation among different hair fibres 161

Differential Scanning Calorimetry (DSC) 163

Chapter 1 Introduction

1.1 Overview

Every month, thousands of kilograms of human hair are thrown away by the hair salon industry. Every year, 6.5 million kilograms of human hair waste is generated by the UK, which most of it is thrown away in landfills or ended up decaying in the environment.[1] Of particular concern is the accumulation of human hair waste in landfill, which is magnified by the fact that human hair waste is discarded mostly in plastic bags. Generally, plastic bags can take up to 1000 years to decompose and consequently during that time hair inside the bags can cause several problems. To name a few, the lack of oxygen in bagged hair bags leads to the production of methane, a powerful greenhouse gas.[2,3] Furthermore, human hair waste often collects in streams and blocks drainage systems for large periods of time occupying great volumes of space due to the slow degradation of hair. This leads to eutrophication, this happens when the nitrogen content of water bodies increases, which can harm marine life due to a potential growth of the algae in waters. To overcome these problems, human hair waste is frequently burned, which produces hazardous by-products and toxic gases.[4] Finally, open dumps of waste of human hair can generate dust, which can cause respiratory problems and distress for people living nearby.[5]

1.2 Human hair

1.2.1 The structure of hair

Hair fibres have an average diameter between 60 to 80 μm, however these values may vary depending on the ethnic origin of hair fibre. For instance, Asian hair is thicker than European hair, where the average diameter of the fibre varies between 80 and 120 μm.[6] Human hair fibres are mainly composed by α-keratin proteins, more than 90% of dry weight, and lipids about 1-9% dry weight.[10] Human hair present different types of lipids in

its composition. Those lipids are composed by free fatty acids, cholesterol esters, cholesterol sulphate and ceramides. The cuticle of the hair fibres shows lipids covalently bonded, via thioester linkage, to the proteins presented on surface of the hair fibres 18-methyleicosanoic acid (18-MEA).[7] Hair lipids can be divided into two categories depending on their origin. Either from sebaceous glands or hair matrix cells, which are considered exogenous or endogenous lipids, respectively.[8] Also, the medulla contains the highest amount of lipids within the whole hair fibre.[9] In human hair, lipids have the essential role of maintaining the internal water content inside the fibre. They also promote a barrier and prevent external materials from penetrating the fibre.[10,11] Studies on human hair lipids have reported internal lipids consist of 2.5% of the whole fibre, while external lipids account less than that 1%.[12] Internal lipids include free fatty acids, sterols and polar compounds, such as cholesterol sulphate and can be found in the hair matrix cells. Contrarily, external lipids, such as squalene and sterol esters, are apolar lipids, and are best known for creating the sebaceous surface lipids.[12] A study reported the human sebum contains triglycerides (30-50%), as the major component, wax esters (26-30%), fatty acids (15-30%) and squalene (12-26%).[13]

Hair fibres are formed by a compact group of cells within the fibre follicle and are not continuous in their length.[14,15] However, despite all the complexity of the hair structure, one can highlight three major structures: the cuticle, the cortex and the medulla, as- well as other keratin fibres.[16]

The cuticle of the hair fibre is the outermost layer of the fibre, and it is the first to be damaged when hair is mistreated by shampoo, brushing, perms, or straightening treatments. The cuticle contributes to the physical properties of the hair fibres, since it manages the specific superficial properties of the hair fibre.[17] Studies have shown the importance of the cuticle on the mechanical properties of the hair fibre, particularly on the bending properties. The cuticle is presented in hair as flat square sheets around 0.5 μm thick and 60 μm long, where about seven to ten layers are overlaid inside the cuticle edges pointing towards the tip of the fibre, as shown in Figure 1.[15,18] The cuticle structure is complex and can be divided into smaller components, such as the epicuticle, the exocuticle and the endocuticle.

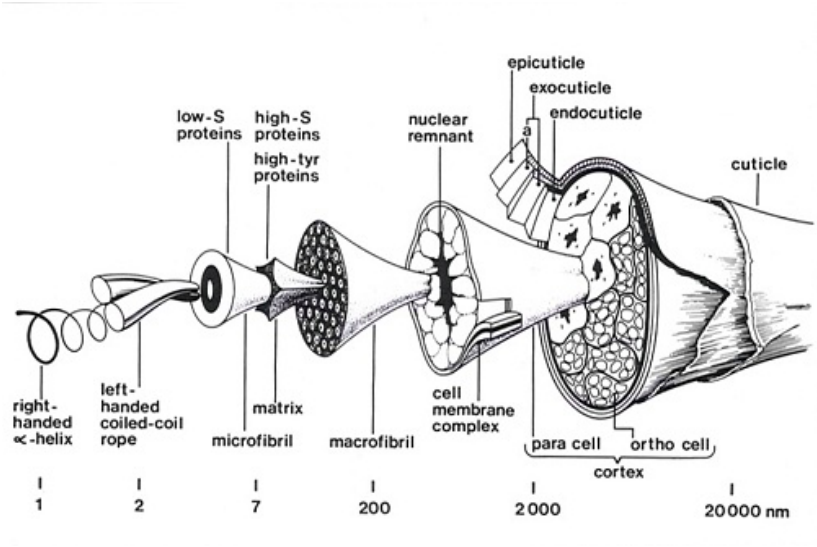


Figure 1. Schematic diagram showing the various components of human hair fibre. Reproduced from reference 19.

The epicuticle is a cross-linked thin lipid layer, that coats the outer surface of the cuticle, covering the exocuticle, a very cysteine-rich layer.[20] Finally, the endocuticle is located in the interface of the cortex, and is very low in sulfur content, which enables it to swell considerably more in water than the cysteine-rich exocuticle.[21] Another component of the cuticle is the cell membrane complex (CMC), this component is one of the pathways present on the hair structure for the water molecules go through the cuticle to the central cortex.[22] The composition of proteins within the CMC is not fully understood, since it is very difficult to is isolate these proteins from the components adjacent to the CMC. The CMC presents a complex structure of three layers with a central core (δ-layer) bonded on both sides by 2 lipid-endowed β-layers. The central core is assumed to be composed of proteins with a polysaccharidic nature.[15]

The cortex comprises 80% of the hair mass and it is made up of cortical cells surrounded by the CMC, which are embedded in a hydrophilic sulfur-rich matrix. The cortical cells, ~100 μm in length and 3 μm wide, contain the macrofibrils (0.4 μm diameter). In addition, macrofibrils are formed by keratin intermediate filaments (KIF) and they present a diameter around 10 nm and a low cysteine content. This intermacrofibrillar material is less cross-linked and similar to CMC, and could be a preferred diffusion pathway for water.[23] Cortical cells are embedded in the matrix that surrounds the KIF. The matrix presents a high mechanical strength, inertness and hardness to the keratin fibres.[14,20] These properties of

the matrix are due to keratin associated proteins (KAPs), through an extensive disulfide bond cross-linking with KIF. KAPs are hydrophobic proteins with sizes between 10 and 50 kDa and they can be found in the matrix around KIF.[24]

The last component of the hair structure discussed in this subchapter is the medulla, which is located in the centre of the fibre and presents an amorphous structure with high lipid content.[9] The medulla is not always present in human hair and even when it is present it may be fragmented or discontinuous along the hair fibre.[25] The study of the medulla however is not an simple and straightforward task due to the difficulty in its isolation and its poor solubility in most solvents.[22]

1.2.2 Human hair from different ethnicities

Human hair is classified into three major distinct groups according to their ethnic group: Caucasian, Asian and African. Some factors vary among different hair ethnic groups, such as diameter, shape and mechanical properties.[15] Each individual is unique regarding hair size, shape and production rate.[26,27] The geometry of hair varies depending on the ethnicity. Caucasian for instance, can present straight or curly hair, with about 45% being straight, 40% wavy and 15% curly.[28,29]

Early reports suggested that the shape of the hair fibre was determined by the shape of the follicle in the keratinization zone.[30] This is the designated region where the fibre is formed. Consequently, if the follicle was curved, the emerging hair fibre would be wavy or curly. Therefore, a straight follicle will emerge a straight hair fibre. A representation of this effect can be depicted in Figure 2.[31,32]

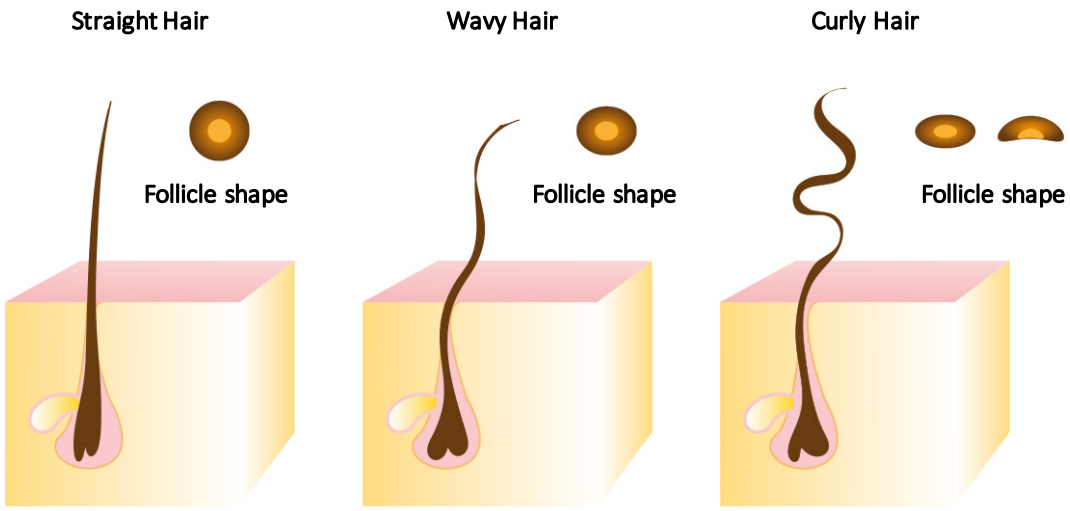


Figure 2. Scheme of hair shaft cross-section of hair follicle shapes. The shape of the follicle determines the shape of hair. Reproduced from reference 33.

However, this theory has been disproven and more recent studies suggest that curly hair may in fact result from variations in the content and distribution of cortical cells.[34,35]

Curly and straight hair present different ratios of the macrofibrils, such as orthocortical, mesocortical and paracortical.[22,36,37] Transmission electron analysis of hair fibres has shown the orthocortical region present a great number of intermediate filaments bundles with fewer matrix content. The hair matrix is composed of keratinocytes, which are cells in which keratin is synthesised inside the follicle. Furthermore, the mesocortical region shows a hexagonal arrangement of the intermediate filaments and almost no matrix. Finally, the paracortical regions presents loose intermediate filaments and the matrix content is very large.[24]

There is a correlation between the degree of curvature of hair and the distribution of cortical cells, where straight hair presents paracortical cells surrounded by mesocortical and orthocortical cells and consequently, as the degree of curvature of the hair fibre increases, the mesocortical cell concentration decreases.[36] The distribution of cortical cells on the hair structure is exemplified in Figure 3.

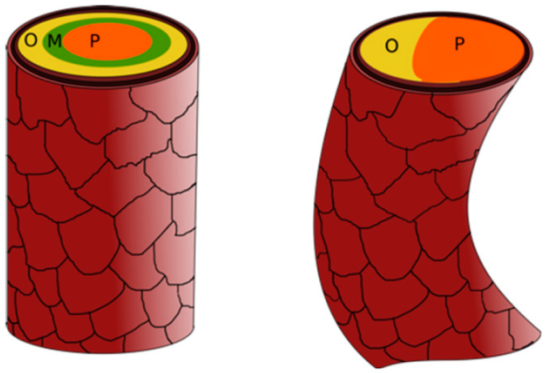


Figure 3. Scheme of orthocortical (O), mesocortical (M) and paracortical (P) cells in straight (a) and curly (b) hair fibres, as suggested by Thibaut.[36] Mesocortical cells may be absent on curly (b) fibres. Adapted from reference 38.

The chemical composition of the hair fibre can be described by the average of a mixture of proteins. Some studies on the extraction of proteins from hair reported the lowest protein recoveries were from hair samples with least pigment, such as blonde hair.[39] The same study has reported the differences between dark and light hair may be related to the number of reducible cross-links. It was suggested that the formation of these cross-links may be related to genetic control or in combination with pigment formation.[39]
Investigations on chemical composition has shown the amino acid profiles from different background hair types do not change.[40]

1.3 Hair material application

Firstly, the hair waste problem needs to be addressed, and for that it is important to develop systems that can use this waste as a resource. Additionally, reducing waste would improve the economy as well. Several applications of hair have been developed. Human hair waste has been used in wigs and hair extensions.[41] Human hair shows excellent properties such as a slow degradation rate, high tensile strength, thermal insulation, elastic recovery and exceptional interactions with water and oils. Due to these properties, the number of applications for human hair waste are unlimited. For example, swatches of human hair are frequently used to develop new hair care products as test materials.[5]

Interestingly, human hair can also be used to fabricate cosmetic brushes, where usually all types of straight hair can be used.[42]

One of the major properties of human hair is its great tensile strength, due to this reason human hair has been used for reinforcing clay-based constructions. The addition of hair with other binders reinforces the strength and reduces the cracking of construction materials, such as plastering house walls. Not only does hair reinforces the strength but it also has been shown to improve the thermal insulation capacity of the clay structures.[43,44]

Human hair has been used in other applications. For example, wavy hair has been included in composite materials to make moulded structures, such as furniture.[45] Oil spill remediation is another field where the application of human hair has been critical. Due to the highly affinity for oils, human hair has been used to clean up seaside oil spills. In this method, the oil can be recovered from the hair, which can then be recycled up to 100 times. This is a great advantage when compared to other oil spill remediation methods.[46]

The high strength of human hair has also been used as sutures in surgeries. The high compatibility with the human body is another advantage of human hair in medical fields.[47]

In several cultures, human hair has also been used to create ropes due to its high tensile strength properties. These ropes were used to lift heavy beams or domestic purposes and they are still appreciated for horse riding.[48,49]

1.3.1 Amino acids from human hair

In terms of its chemical composition, human hair has approximately 16% along with sulfur, carbon and other elements fundamental to plants.[50] Latest investigations have revealed that nutrients needed for plants can be delivered by direct application of human hair to soils.[51] However, this process can take up months due the biological decomposition of human hair. Alternatively, chemical hydrolysis can decompose hair in a few hours. The hydrolysis solution, which is essentially amino acids with fatty acids and nucleotides, can be used as a liquid fertilizer after neutralization.[52]

Human hair applications are very promising in areas such pharmaceutical and biological. For example, amino acids extracted by hydrolysis of hair are then used in cosmetics and pharmaceutical formulations.[22] Depending on the demographic area, the abundance of

amino acids in human hair may vary. For example, hair that has never been treated chemically is better, as some chemical procedures can alter the chemical structure of hair. For example, hair treated for permanent waving will make cysteine extraction difficult.[53]

1.3.2 Keratins from human hair

In the field of biomedical engineering, human hair keratins have been given attention due to their outstanding biocompatibility and biodegradability, and their capability to function as a synthetic extracellular matrix (ECM). The field of application of keratin-based biomaterials is vast, from hydrogels or films for wound healing or other forms for tissue renewal.[54]

The properties of films derived from human hair keratin were investigated for drug delivery, during which the controlled-release of alkaline phosphatase (ALP) was investigated and shown to retain its biological activity as a minimum of 14 days after being incorporated into keratin films.[55] Furthermore, keratin has been shown to improve the release in highly hydrophobic and non-degradable systems.[56]

In 2002 a method was developed to extract protein quickly and effectively from human hair. This method brought the possibility to develop several materials with novel properties, such as hair protein based thin films, or protein scaffolds and hydrogels for tissue engineering.[57,58]

The keratin spontaneous self-assembly has been widely investigated at both microscopic and macroscopic levels.[59–62] The ability to support cell attachment and cell growth is another interesting property of keratin biomaterials, which is related to the presence of cell adhesion sequences, such as arginine-glycine-aspartic acid (RGD) and leucine-aspartic acid-valine (LDV) on the keratin proteins derived from wool or hair.[58,63] The first device consisting of keratin biomaterial reported in the literature was a vascular implant coated with keratin implanted into a dog.[64] After that, keratin biomaterials have been used for wound healing, bone regeneration and more recently in peripheral nerve healing.[65–73]

Some keratin films have been produced by solvent casting, where the thickness distribution and other properties such as maximum optical purity or extremely low haze are some advantages of this technique that stand out.[74] Some studies on the analysis of films from

different keratin sources, such as feathers, wool or hair led to the preparation of films with different mechanical properties. The properties of solvent cast keratin films were investigated in more depth, during some studies on the physiochemical properties, as well as where the biodegradation properties of these materials were investigated.[74] Due to the fragility of pure keratin films, glycerol was added to improve the strength of wool keratin films, which resulted in a transparent, strong, flexible and biodegradable film.[74] Many years of research have been dedicated to optimise the physical strength and flexibility of keratin films, while their biological activity is preserved. To improve the properties of keratin-based materials, several approaches have been considered, such as the addition of natural and synthetic polymers to keratin-blended systems, and new techniques for pure keratin films.[57,75–83] Alternative methods to produce blended keratin systems have been considered, where natural or synthetic polymers with great mechanical properties have been investigated.[84]

The investigation of scaffolds for biomedical devices arises from the ability of the keratin extracted self-assembly into three dimensional porous structures. Lyophilization was the main technique used to produce sponges with homogeneous porous microstructures. The size of the pores can be controlled during the technique, by freezing rate and pH. For instance, faster freezing rates leads to smaller pores, as the diameter of the pores is an important factor, which determines the cellular infiltration and nutrient delivery. The sponges reported in the literature were derived from wool keratin.[63]

It has been observed an increase of the investigation of electrospinning of biocompatible polymeric materials.[84] Electrospinning is a method that uses a high voltage to create an electrically charged jet of polymer which is drawn to a grounded collector.[82] The resulting fibres have shown great potential in several applications, such as drug delivery, vascular tissue engineering or heavy metal ion adsorption. These applications are due to exact structural features and functional properties of the nanofibers.[85–89] The electrospinning process has been expanded to include recovered keratin extracted from human hair fibres.[84]

Wet-spinning, used in textile industry for the production of synthetic fabrics, has been used to create single fibre biomaterials. This method includes extrusion of a homogeneous solution through a spinneret into a coagulation bath and following drawing/stretching to promote polymer chain alignment and fibre formation. Once again, due to the physical

limitations of pure keratin fibres, researchers have overcome these challenges using mixtures of synthetic and natural polymers with improved material properties.[84]

Some studies on keratin materials have revealed outstanding biocompatibility. Also, to create new biomaterials with suitable features for their application, researchers have shown new approaches to modify the physical and mechanical properties of keratins.[84]

Keratin proteins with high molecular weight are hydrophilic and have the ability to form films, which make them very appealing for skin care purposes. They can provide a coating on the skin, which offers a smooth and soft sensation.[90] Moreover, keratin peptides used in cosmetics and hair products, improve the shine and softness of the hair fibres providing hydration and seal of the cuticles with the keratin peptides, which results in a healthy fibre.[91]

1.3.3 KAPs from human hair

KAPs are amorphous cysteine-rich proteins, they are a major component of human hair structure and are very important in forming strong hair shafts, due to the cross-linked network with KIF. Due to their high cysteine content, KAPs can be classified according to their amino acid composition, less than 30% mol of cysteine content they are classified as high sulfur, however if that value is higher than that they are considered as ultrahigh sulfur and the last classification as glycine/tyrosine KAPs. For comparison proposes, keratins can have between 17 and 32 cysteines, while KAPs present much higher values.[92] Occasionally, keratins have to be modified before their application to increase materials strength, however KAPs contain multiple disulfide bonds in their composition and they have the advantage to be very resistant to physicochemical and biological modifications. KAPs have been used as a natural source to isolate cysteine for cosmetics and chemical applications. Moreover, KAPs can be applied in 3D tissue harvesting or as carriers of biological active materials in areas such as medicine or cosmetics.[93]

1.4 Extraction

1.4.1 Extraction of keratin from natural sources

The extraction of keratin is not a simple task owing to the strong internal interactions that stabilise the protein structure, which makes the dissolution of keratin based materials in water or organic solvents very challenging.[94–96] The dissolution of keratin requires the disruption of disulfide linkages and hydrogen bonds and numerous methods have been reported for the dissolution of wool or feathers, such as reduction.[74,97–100] The reduction methods uses reducing agents such as 2-mercaptoethanol, this technique allows the breakage of cystine disulfide bonds (R-S-S-R)(two cysteine amino acids residues) and the formation of cysteine (R-S-H), Figure 4. The advantage of this technique is the preservation of the keratin structure, however 2-mercaptoethanol is expensive and can be toxic and harmful.[100,101] Besides the reduction method, there are also other processes such as oxidation and sulfitolysis of the disulfide bonds.[48,61-64] Nevertheless, all these methods currently used to extract the keratin have a lot of associated problems, namely the toxicity of the solvents involved in the process, as well as the difficulty of the recovery of the solvents afterwards and, finally the impact of the waste solution on the environment.[104] In order to minimise these problems, different approaches to extract keratin from natural sources have been studied, and are discussed followingly.

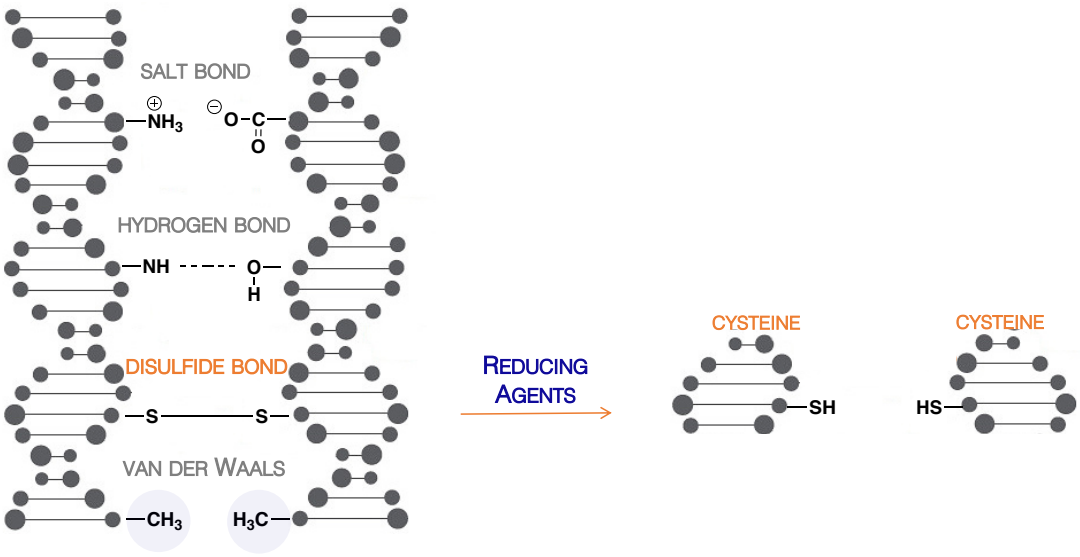


Figure 4. Schematics of the reducing agents in the structure of keratin. (Source: Personal collection)

1.4.2 Dissolution of macromolecules with Ionic liquids

Ionic liquids (ILs) are alternative solvents to volatile organic solvents (VOCs). VOCs are volatile, flammable and health hazards, which have a negative impact on the environment and human health. ILs have been proposed as alternatives to VOCs due to their reusable, non-volatile, and relatively nontoxic properties.[105]

Usually, ionic liquids have an organic cation and organic/inorganic anion. Cations can vary from tetra-alkyl ammonium or tetra-alkylphosphonium to imidazolium, pyrrolidinium or pyridinium. On the other hand, anions can vary from halides, acetate, nitrate to dimethylphosphate.[106,107]

Ionic liquids belong to a class of molten salts with melting points below 100° C, they have attracted the attention of researchers due to their unique properties, such as insignificant vapour pressure, non-flammability, high thermal stability, as well as a wide conductivity window. The physical properties of the ILs, polarity, solubility, viscosity, etc can be designed by combining and modifying their cations and anions.[108] For these reasons ILs have been used in dissolution of macromolecules. The dissolution of cellulose with ILs and the recovered cellulose was tested with no significant changes in the degree of polymerization and dispersibility, this study has attracted the attention of researchers to the study of ILs as solvents for the natural polymer materials.[108] The strong polar ILs would be able to destroy the strong intermolecular effect, such as hydrogen bonding in natural polymers and enhance their dissolution. The question whether ILs are strong polar molecules is ongoing, while other conductivity tests indicate the possibility of ion pairs, other studies definitely contest their existence.[109]

ILs are a new class solvents for natural polymer materials.[110–113] Recent studies have discovered ILs are able to dissolve cellulose up to a concentration of 30-40 wt%. Dissolution of cellulose by ILs has fabricated a great variety of cellulose-based materials, such as fibres, films, hydrogels, aerogels, composites and derivatives.[114] For dissolution of cellulose some ILs have been reported with the best dissolution capability, among the best ones 1-allyl-3-methylimidazolium chloride ([AmIm]Cl), 1-butyl-3-methylimidazolium chloride ($[C_4C_1Im]Cl$) and 1-ethyl-3-methylimidazolium acetate ($[C_2C_1Im][OAc]$) were highlighted as powerful solvents for cellulose.[108] The dissolution of cellulose by these ILs was related to their strong β Kamlet-Taft parameter and lower viscosity. These anions present the ability

to donate electron density to form a hydrogen bond with protons from the cellulose structure, disrupting the structure of cellulose which leads to its dissolution. Contrarily, ILs containing anions such as Tetrafluoroborate ($[BF_4]^-$), Hexafluorophosphate ($[PF_6]^-$) or bis(trifluoromethanesulfonyl)imide ($[NTf_2]^-$), which are weaker hydrogen bond acceptor anions.[108,115] As alkyl side chain of imidazolium cation increases, dissolution rate of cellulose decreases. This is related to increase of viscosity and/or decrease of the ability to form hydrogen bond with protons from the cellulose structure .[114] During dissolution of cellulose, disruption of hydrogen bonding network is crucial, and the literature suggests anions disrupts cellulose hydrogen-bond network.[116–123] The cellulose hydrogen-bond network is presented in Figure 5.

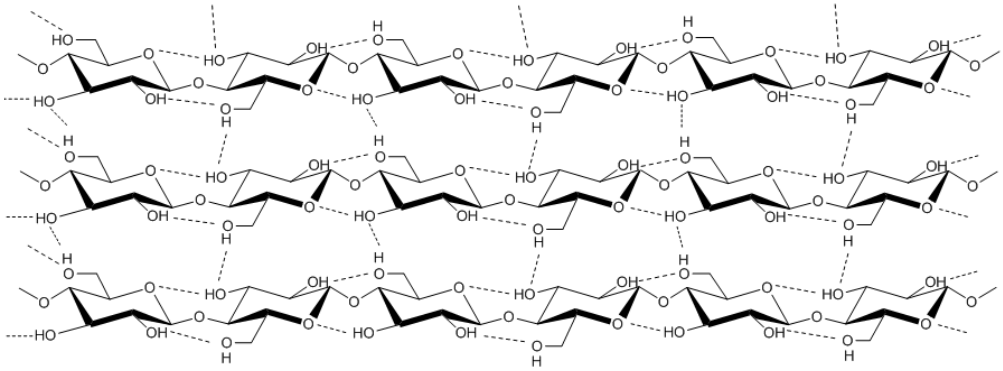


Figure 5. Diagram illustrating the generalised structure of cellulose. Adapted from reference 124.

These ILs have nucleophilic anions capable of disrupting the hydrogen bonding network within the cellulose structure, which results in the dissolution of the cellulose. Would these nucleophilic ILs be able to disrupt the hydrogen bonding and disulfide bonds within keratin fibres? It has been found in multiple studies that acetate, formate, phosphate and chloride are the most efficient anions to dissolve keratin fibres.[110,111,125–127] They have been selected due to their ability to dissolve cellulose based on hydrogen bond breaking abilities, since cellulosic fibres and protein fibres can be classified as natural fibres.[128] Researchers have reported recovered wool keratin from $[C_2C_1Im][OAc]$ and 1-butyl-3-methylimidazolium acetate ($[C_4C_1Im][OAc]$) had the lowest amount of disulfide bonds, more than 90% of the bonds were disrupted. That may be because these ILs have the ability of cleaving disulfide

bonds. However, while recovered wool keratin has the highest disulfide breaking percentage, they presented the lowest recovery percentage. Additionally, it was stated the capability of ILs to dissolve wool keratin is related to the ability of cleaving disulfide and hydrogen bonds. It was found that to achieve the total dissolution of wool keratin in ILs, at least 65% of disulfide bonds in keratin should be cleaved. This must be considered during the criteria for designing and screening suitable ILs to dissolve keratin-based biomass.[127]

Similarly, after some investigation on the dissolution capability and properties of the recovered keratin, dimethylphosphate ILs were selected as the optimal ILs.[125] In the case of the same anion, dimethylphosphate, on the investigation of the dissolution of wool keratin, the dissolution followed the order $[C_2C_1Im]^+ < [N_{2221}]^+$. This may suggest the anion plays a key role on the dissolution of wool keratin and once again, imidazolium-based ILs presented better dissolution ability.[125] Recovered material from the dissolution of wool with dimethylphosphate-based ILs showed a higher temperature stability than the ones from acetate-based ILs. The poor thermal stability of keratin recovered material from acetate-based ILs is consistent with the loss of crystallinity observed via X-ray Diffraction (XRD) reported in literature.[125] Moreover, dimethylphosphate-based ILs presented excellent potential for fibre spinning.[125]

Recently, keratin extracted from human hair has emerged as an alternative biomaterial for a variety of applications.[54,129] Generally, human hair is comprised of proteins, lipids, water and a small amount of trace elements. Due to its crosslinked polypeptide chain, human hair is a difficult protein to digest or solubilize.[130] The dissolution of human hair keratin follows the same traditional methods used on the dissolution/extraction of keratin from other natural keratin sources. But the toxicity and the harsh conditions of those methods frequently result in the formation of keratin with low molecular weight, which reduces the quality and therefore the applications of the protein.[131] More recently, as for the dissolution of other natural fibres, ILs are emerging as suitable and alternative solvent systems for the processing of various biopolymers including proteins in human hair systems. Although, few reports of dissolution of human hair with ILs are available in literature.[128,131,132]

According to a recent study in literature, it is possible to dissolve hair with tetrabutylammonium hydroxide, TBAH (40 % in water). The authors reported the dissolution of 0.0100 g to 0.3000 g of hair within 1.0000 g of TBAH (40 % in water) for 1 to

9 hours at room temperature.[131] Firstly, hair is washed and rinsed carefully with ethanol and distilled water, followed by a 24 hours de-lipidization, where fibres are soaked in chloroform and methanol (2:1 v/v), and afterwards the fibres are air-dried. After the dissolution of hair with TBAH, 1 M HCl is added to the solution until a precipitate is formed. In this case, the precipitate is found to be crude melanin. The remaining aqueous solution is evaporated to obtain a viscous liquid. This viscous solution contains the IL and keratin, which, after addition of acetone, a white precipitate is formed. The authors identified this as pure keratin that is then isolated by centrifugation and washed with acetone.[131]

The dissolution of biomaterials using ILs is an option for the use and conversion of biopolymers into useful materials with great potential in industrial applications.[133] In this work, the dissolution of hair will be studied taking into consideration the best ILs used either on dissolution of cellulose and keratin fibres. Furthermore, the ability of $[C_2C_1Im][OAc]$ and $[C_2C_1Im][Me_2PO_4]$ will also be assessed for the dissolution of hair.

1.4.3 Diffusion into hair fibres

Hair structure has been studied to improve and create new hair products. One of the approaches on these studies are the different pathways that cosmetic products can take to penetrate the hair fibre.[22] Therefore, considering those studies, some assumptions can made regarding the performance of the ILs on the dissolution of hair fibres. There are two main pathways to penetrate the hair fibre being the transcellular or intercellular diffusion.[22] The transcellular diffusion involves the most cross-linked regions, which are epicuticle, A-layer, exocuticle and endocuticle. On the other hand, intercellular diffusion involves the penetration between cuticle cells. Both routes may occur at the same time, nevertheless for large molecules, intracellular diffusion would be the preferred one due to low-sulfur content, which means these regions would more easily swell than high-cross-linked regions. Small molecules, on the other hand, will take the transcellular route due to the superior surface available for this type of diffusion.[22] Figure 6 below exemplifies the hair structure and pathways of human hair.

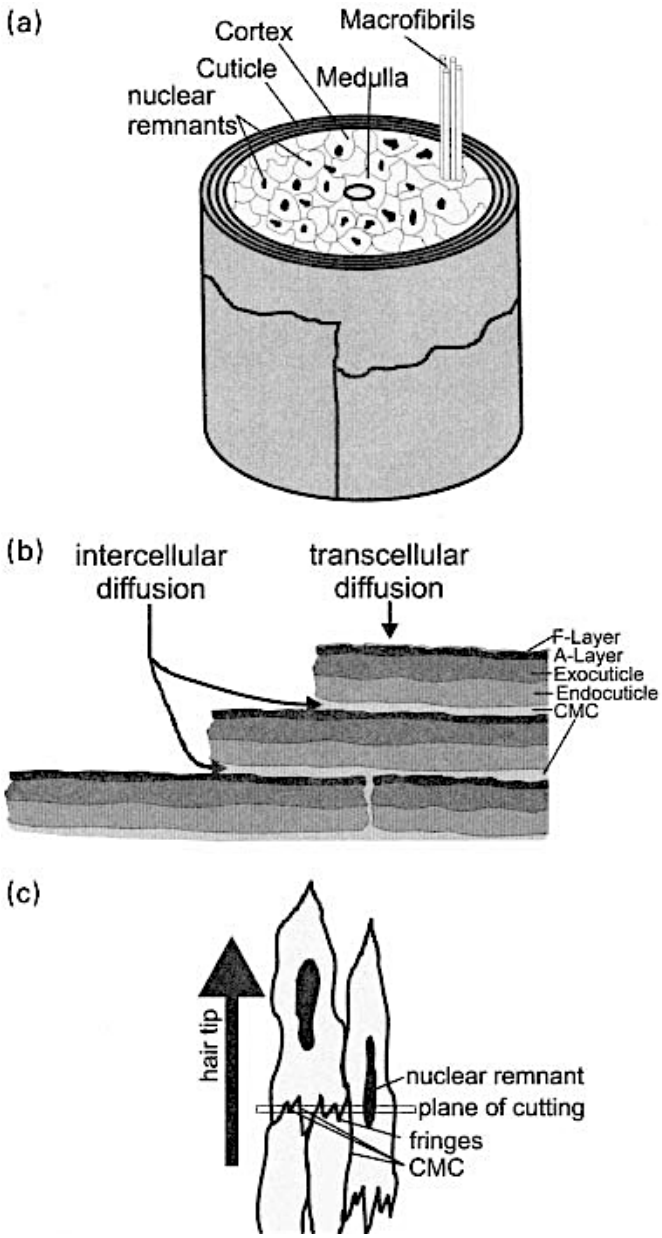


Figure 6. a) The main morphological structures of the inner region of human hair; b) Schematic of two major diffusion pathways of dye molecules into hair fibres; c) Model of longitudinal sections across cortical cells. Adapted from reference 134.

The dissolution of natural protein fibres in several IL using optical microscopy in real-time was reported.[128] In this publication hair was investigated and for the purpose of the study darkly pigmented hair was selected, during dissolution the coloured pigments within the cortex could be identified. During the study, the author reported the swelling of the fibre, which reached four times the original diameter of the fibre.[128]

1.4.4 Ionic liquid selection based on Kamlet-Taft parameters

Kamlet-Taft polarity parameters have been used to predict and explain the solubility of biomolecules and biopolymers in solvents.[135] Those parameters are determined by measuring the UV-vis spectra of a probe dye when dissolved in a solvent of interest. The Kamlet-Taft system presents different parameters, such as β which describes the hydrogen-bond basicity, α is hydrogen-bond acidity of the solvents and π^* of solvents interactions through dipolarity and polarizability. In the case of the ILs used in this work, because of the non-functionalised cations such as dialkylimidazolium, the hydrogen-bond basicity of β is primarily influenced by the anion.[136] As mentioned before, in the case the dissolution of natural fibres with ILs, we were looking for high values of the β parameter. Accordingly to several reported studies, $[C_2C_1Im][OAc]$ is a good candidate to dissolve keratin fibres. That may be related to the basicity nature of $[C_2C_1Im][OAc]$, in comparison to other imidazolium-based ILs. The strongest forces in $[C_2C_1Im][OAc]$ are exhibited by the basic anion, which can act as hydrogen bond acceptor and then is responsible for the dissolution of keratin.[137] The Kamlet-Taft parameters reported in Table 1.

Table 1. Kamlet-Taft parameters reported in literature for the ILs used on this study.

IL	α	β	π^*	Ref.
$[C_2C_1Im][OAc]$	0.40	0.95	1.09	138,139
$[C_2C_1Im][Me_2PO_4]$	0.51	1.00	1.06	140
$[C_4C_1Im][OAc]$	0.55	1.09	0.99	141
$[C_4C_1Im][Me_2PO_4]$	0.45	1.13	0.98	142
$[C_4C_1Im][MeSO_4]$	0.53	0.66	1.06	143
$[C_4C_1Im]Cl$	0.32	0.95	1.13	144
$[C_4C_1Im][CF_3SO_3]$	0.50	0.57	0.90	144
$[C_4C_1Pyrr][CF_3SO_3]$	0.40	0.46	1.02	145
$[C_4C_1Pyrr][Me_2PO_4]$	0.24	1.14	1.02	136

These parameters suggest both acetate $[OAc]^-$ and dimethylphosphate $[Me_2PO_4]^-$ anions are suitable to form strong hydrogen bonds with groups typically present in hair, such as for example, hydroxyl groups.[140,146] $[C_4C_1Pyrr][Me_2PO_4]$ also has a strong β parameter and for that reason its ability to dissolve hair will be tested.

From the analysis of Table 1 it is possible to conclude that the same anion for different cations do not show significant differences between β values, which can be justified by different sources of investigation. That once again suggests that the cation may have a marginal impact on dissolution of keratin fibres.

In this literature review it was not possible to find the Kamlet-Taft parameters for the distillable ILs listed in section 5.1.2.3. It was only possible to find the Kamlet-Taft parameters of 1,1,3,3-tetramethylguanidinium acetate ([TMGH][OAc]), as shown in Table 2. This ILs shows a β parameter of 1.095 which might indicate a good ability to dissolve hair.

Table 2. Kamlet-Taft parameters reported in literature for the ILs used on this study

IL	α	β	π^*	Ref.
[TMGH][OAc]	0.530	1.095	1.041	147

1.4.4.1 Toxicity of Ionic liquids

ILs have been applied in many processes such as separations, catalytic reactions, desulfurization, electrochemistry and hydrogenation.[148–157]

ILs used in the industrial field may end up in the aqueous or non-aqueous environment through the industrial waste watercourse, since several ILs are water soluble and exhibit high thermal and chemical stability.[158,159] However, there are a list of generally recognised as safe (GRAS) ILs list, some ILs that are more toxic may end up in the environment which may cause possible environment impact.[160–162] Another factor to take into account when use ILs in a large scale is their relatively high cost when compared with conventional solvents. This can be counterbalanced if the ILs can be recycled.[163] Among the methods of

recycling ILs are the distillation, extraction, adsorption, membrane separation, aqueous two phase extraction and crystallization etc.[164–170]

Imidazolium-based ILs are very often used as solvents in many industrial applications, such as catalysis, separations or dissolution.[171] An example is $[C_2C_1Im][OAc]$ that has been extensively used in the field of biomass dissolution.[172] The $[C_2C_1Im][OAc]$ has been showing ability to dissolve cellulose, wood, switchgrass, wheat straw, silkworm, chitin, other raw biomass and wool keratin.[172,173,182–189,174–181] The available information of $[C_2C_1Im][OAc]$ toxicity is very low and non-conclusive. However, a trend for imidazolium based ILs can be taken. The main toxicity effect can be associated to the cation, where the increase in of the alkyl side chain to a certain length leads to an increase of the toxicity. On the other hand, the contribution of anion to the toxicity of the ILs is very low. This is not the rule with fluorinated anions, that show higher toxicity.[190] Based on this, $[C_2C_1Im][OAc]$ is excepted to be less toxic than other imidazolium-based ILs, due to its small alkyl side chain and acetate anion.[191]

The toxicity of ILs can be made based on measured parameters, such as the EC_{50}. The EC_{50} represents the concentration resulting in 50% of reduction of the growth or reproductive activity, of the exposed organism comparative to the control. The different ranges of the EC_{50} indicate different levels of toxicity and they are presented on Table 3.[192]

Table 3. Levels of toxicity depending on the range of EC_{50}. Data from reference 192.

EC_{50} range (mg/L)	Level of toxicity
100-1000	No toxicity
10-100	Moderate toxicity
1-10	Mild toxicity
0.1-1	High toxicity
0.01-0.1	Extremely toxic
< 0.01	super toxic xenobiotics

There are, however, another indices frequently used to estimate the ILs toxicity, such as LC_{50} – Lethal concentration or dose, where half of the population tested is killed in a specific

time; IC_{50} – inhibitory concentration, 50% inhibition of the biological activity; LD_{50} – median lethal dose; MIC – minimum inhibitory concentration, the minimum concentration that inhibits the growth of a microorganism over a certain time of incubation.[193]

The effect of $[C_2C_1Im][OAc]$ was studied on zebrafish and Chinese hamster ovary (CHO) cells, it was shown that $[C_2C_1Im][OAc]$ can be classified as non-toxic, showing EC_{50} lower 100 mg/L on Zebrafish and 16717 ± 1379 mg/L (98.22 ± 8.10) on CHO.[194]

In summary, the imidazolium, pyrrolidinium and pyridinium-based ILs have been proven to be non-toxic to fish. Although, ammonium salts seemed to be more toxic.[195]

1.4.5 Recovery of keratin material from dissolution of wool and feathers

The dissolution of keratin natural sources with ILs is promising. Having into consideration Kamlet-Taft parameters and the studies on the dissolution of keratin it is possible to find good candidates for the dissolution of keratin fibres. However, another question that needs to be answered is whether after dissolution is it possible to recover high value material from the dissolution of keratin with ILs. In literature studies, it has been reported that it is possible to recover about 57 wt% after dissolution of wool keratin with $[C_4C_1Im]Cl$ at 120° C, a ratio of 1:6 (solid : liquid) was tested.[196] A similar percentage (about 60 wt%) was obtained after dissolution of feathers at 130° C, however in this case a lower ratio was selected 1:2 (solid : liquid).[133] The looser structure of feathers, when compared to wool may promote better dissolution, although the dissolution of feathers was driven with higher temperatures than wool keratin. Moreover, the amino acid composition of the recovered material was not reported, which makes it difficult to compare both studies.[198,133]

The temperature of the dissolution of wool with $[C_4C_1Im]Cl$ was investigated. In this study three temperatures were selected, 120° C, 150° C and 180° C, with a 1:6 ratio (solid : liquid) for 30 minutes.[196] A maximum of 57 wt% was obtained at 120° C, where the yield decreased at 150° C (35 wt%) and 180° C (18 wt%). About 90 % of wool weight is keratin. The decrease of the yield of the recovered keratin after the regeneration process might be related to the solubility of the keratin, which did not precipitate and remained in the water phase.[196] This was considered as one of the limitations of this method, which not only affects the rate of

regeneration of keratin but also affects the quality of the recovered material. The quality of this material is then compromised by the loss of cysteine, a valued water soluble amino acid.[197,198]

1.5 Modification of the structure of hair

1.5.1 Reversible methods

A few methods are design to temporarily modify the structure of hair. Thermal techniques such as hair combs, straightening irons or hair dryers have the ability to straighten curly hair by modifying the physicochemical properties of hair. The straightening effect is only temporary and as soon as hair is in contact with water or humidity will curl again. Thermal straighteners only modify the weaker hydrogen bonds in the cortex of the hair.[199,200]

1.5.2 Permanent methods

Chemical relaxers are hair straighteners which are responsible for the permanent straightening effect on the hair. These relaxers are alkaline straighteners and usually contain between 1 and 10% of sodium hydroxide, lithium hydroxide or calcium hydroxide. Similarly, different combinations, such as guanidine carbonate and calcium hydroxide are often used. The high pH, between 9 and 14, allows the swelling of the hair fibre consequently the alkaline agent (-OH) can penetrate up to the endocuticle. These chemicals will react with keratin, breaking and rearranging the disulfide bonds, which allows the stretch of the fibre.[22,201,202]

The reaction between alkaline reagents and cystine groups will produce lanthionyl residues. This process is called lanthionization, where the relaxer removes a sulfur atom from the disulfide bond and converts them to lanthionine bonds. While disulfide bonds contain two sulfur atoms, lanthionine bonds only contains one sulfur atom.[22,201]

Another reducing agent to straighten curly hair is Ammonium Thioglycolate, this relaxer weakens the hair's cystine bonds instead of disrupting the entire protein. After this first

process, thioglycolate must be neutralized with a solution of hydrogen peroxide. To achieve the permanent straight hair, a hot iron tool must be applied during this method. In this method the supercontraction of the fibre occurs and α-helix is transformed in amorphous proteins. After this process, 90% of the original cystine content is kept and 10% is converted as cysteic acid.[203]

1.5.3 How ionic liquids could target specific bonds in hair structure

The human hair, as reported before in section 1.2.1, presents disulfide and hydrogen bonds, covalent bonds, Columbic interactions and van der Walls interactions.[15] As ILs have been reported to dissolve biomass, due to their ability to disrupt the most important bonds in biomass, would it be possible to disrupt these bonds in the hair structure without the total dissolution of the fibre?
Investigation on hair chemically treated has been analysed by ATR infrared spectroscopy, in these studies only some bonds have been affected. Similarly, to these studies, ILs could be investigated to target these bonds and then the fibres analysed by ATR Infrared spectroscopy.

1.5.3.1 ATR infrared spectroscopy on human hair

Human hair appears to be relatively uniform when observed with the naked eye however, the structure and composition of human hair is very complex, as previously detailed.[126] Keratins in human hair have different secondary structures and their content may vary on different hair components. For instance, α-helical keratin structures are mainly found in the cortex material, while the cuticle has a higher content of the β-sheet structures.[204]
Due to the bonds in the protein structure, several vibrational bands can be detected in the IR spectrum of α-keratin.[205] On the mid-IR range (4000 to 400 cm^{-1} in this investigation), there are major absorptions characteristic of the peptide bond, such as Amide I (1690-1600 cm^{-1}), Amide II (1575-1480 cm^{-1}) and Amide III (1320-1210 cm^{-1}), which are bands for α-

keratin.[205] In the human hair IR spectrum there are other important vibration modes, however that will be discussed further in section 1.5.3.2.

The thickness of the cuticle of human hair has been reported to be between 2.5 to 5 μm, therefore the Attenuated total reflectance Fourier-transform infrared spectroscopy (ATR - FTIR) analysis is assumed to be sampling cuticle and part of the cortex of the hair. [206,207,208] Figure 7 shows the average dimensions of the different components of the hair structure.

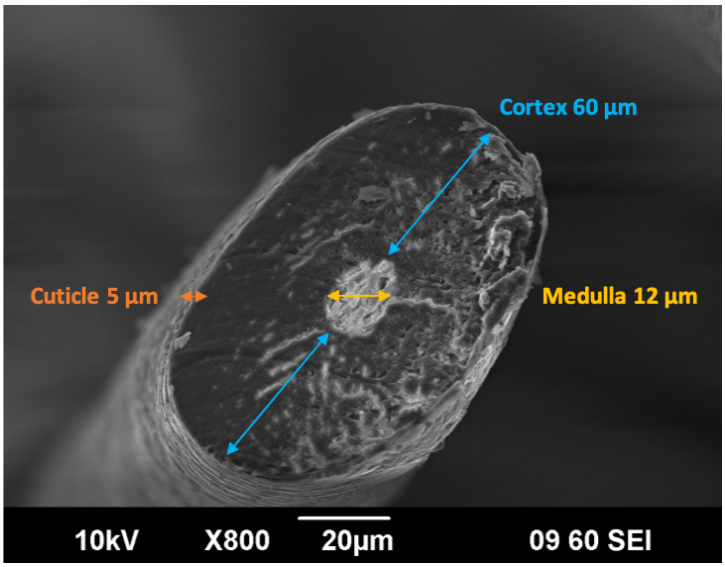


Figure 7. SEM profile picture of European curly hair with schematic dimensions of the hair components. (Source: Personal collection)

The exact dimension of hair components dependent upon the origin and type of hair, however in the context of this study, the size of the cuticle will be assumed to be between 2.5 and 5μm.[208] It is important, however, to consider that these dimensions are an average approximation and will vary from fibre to fibre.

1.5.3.2 Vibrational spectroscopy of human hair

Vibrational spectroscopy is very sensitive to molecular conformation and the structure of proteins, hence it has been used to study the properties of hair.[209] There are several studies using Infrared spectroscopy (IR) and Raman spectroscopy to identify modifications on the hair structure after cosmetic treatments.[210–216] Indeed, the cosmetic industry routinely use

IR and Raman spectroscopies to study the penetration of cosmetic products into hair fibres.[214,217]

ATR-FTIR is an established technique for qualitative and quantitative analysis of the surface of the keratin fibres. Researchers have used this technique for the identification of cysteic acid and intermediate oxidation products of cystine. This technique allows the comparison between untreated and bleached fibres.[218–221] These chemical changes may be due to oxidative damage on the fibre, from cosmetic treatments such as bleaching or permanent waving.[205] The changes on the hair spectrum result from the oxidation of the cystine disulfide to cysteic acid detected at 1040 cm^{-1} and the oxidative intermediates such as cystine monoxide (1071 cm^{-1}) or cystine dioxide (1114 cm^{-1}).[222–224] The fibres in this study are untreated hair fibres, however those bands may also be expected to be observed, since hair suffers from natural weathering (wind, grooming, exposure to sunlight, etc) and other external factors such as combing or drying processes.[225] Additionally, Raman spectroscopy has been used to measure the protein denaturation of the α-helix to random conformations due to oxidation and reduction.[226,227] Other FTIR analyses have been used to analyse other keratin fibres, such as horse hair, human skin, nails and lipids.[228,229]

ATR-FTIR was the selected technique on this study since it can provide molecular level information about the composition and the nature of the fibres.[230]

Chemically untreated hair spectrum showed spectral fingerprints according to their functional groups, where the Amide bands were identified. Figure 8 presents the spectrum of European curly hair. This spectrum itself is very complex, especially on the region between 1750-800 cm^{-1}, as known as the fingerprint region. This complexity is due to the chemistry of the protein-polypeptide structure of the hair keratin.[205]

Amide I band is the result of the stretching vibration of the peptide carbonyl group (C=O), likewise Amide II band corresponds to the C=O stretching coupled with C-N stretching and bending deformation of N-H in the protein backbones. Amide III is assigned to stretching modes of nucleic acids.[205,231] Besides the complexity of the fingerprint region, it is possible to highlight the band at 1180 cm^{-1} (C-OH groups of amino acid and C-O groups of carbohydrate).[232] and a band associated to glycogen at 1118 cm^{-1}.[233]

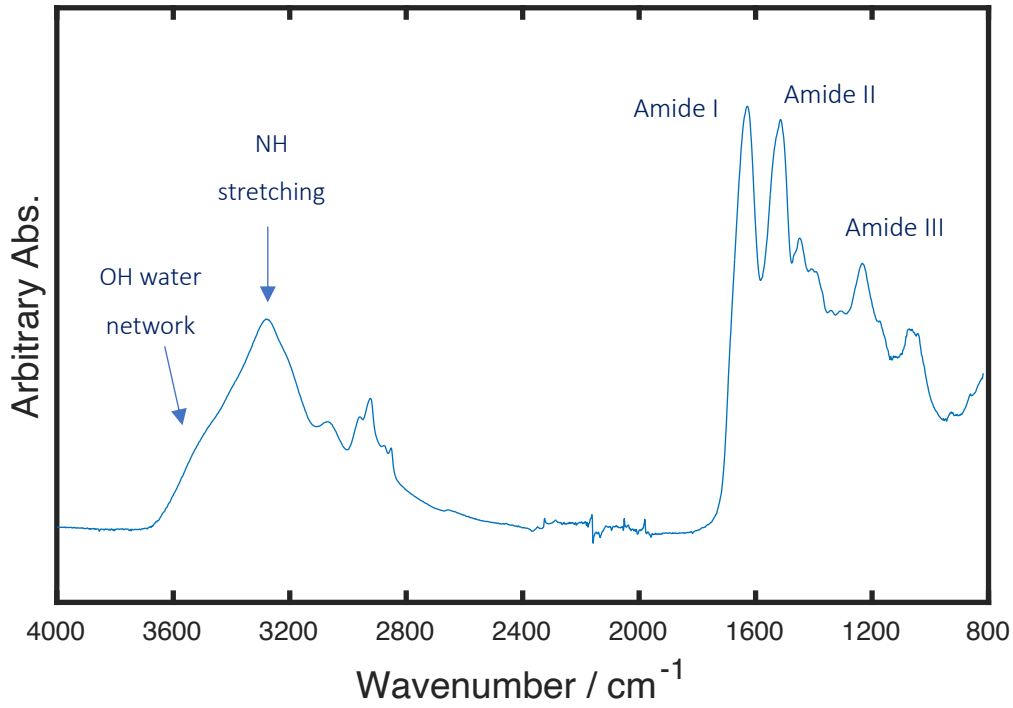


Figure 8. ATR-FTIR spectrum of a single chemically untreated hair fibre. (Source: Personal collection). OH water network: 3500 cm^{-1}, N-H stretch: 3280 cm^{-1}; Amide I: 1690-1600 cm^{-1}; Amide II: 1575-1480 cm^{-1} and Amide II 1320-1210 cm^{-1}.

At higher wavenumbers, the band at 3500 cm^{-1} corresponds to OH bonded water networks, as suggested in the literature.[234] The band at 3280 cm^{-1}, could be the consequence of free N-H stretch or hydrogen bond N-H stretch. But while the former band is primarily from the cuticle material, the second one is from the cortex.[235] The following band, 3200 to 3000 cm^{-1} is assigned to the aromatic C-H stretching of the Tyrosine (Tyr), Phenylalanine (Phe) and Tryptophan (Trp) groups in the composition of the keratin in the hair structure.[236] Moving towards lower wavenumbers, the set of bands 3000 to 2800 cm^{-1} result from the stretching of C-H bands. The band at 2924 cm^{-1} corresponds to long chain of CH_2 antisymmetric stretching vibration of a lipid component[236]. The band at 2960 cm^{-1} is mainly due to keratin CH_3 stretching bands. [231,236] At the fingerprint region, Amide I (1690-1600 cm^{-1}), Amide II (1575-1480 cm^{-1}) and Amide II (1320-1210 cm^{-1}) are the main structures to be identify.[205]

Finally, the region from 1130 to 1000 cm^{-1} normally provides information about chemical changes on hair. The changes on the hair spectrum is detected by the oxidation of the

cystine disulfide to cysteic acid at 1040 cm^{-1} and the oxidative intermediates such as cystine monoxide (1071 cm^{-1}) or cystine dioxide (1114 cm^{-1}).[222–224]

Now that the chemically untreated hair spectrum has been investigated, it is important to understand whether it is possible to identify any variation on the composition of hair throughout the fibre. It is known that the fibre may suffer from natural weathering and other destructive external factors which may result in variations on the spectrum of the fibre.[225]

1.6 Analysis of the structure of hair

Optical microscopy has been previously used to analyse human hair and fibres.[237] In the past, scanning probe microscopy techniques, such as scanning electron microscopy (SEM), have been utilised to characterise the hair morphology and its mechanical surface properties. These techniques allow the study of microstructure, ethnicity, treatment and damaged of the fibres.[238,239] However, optical microscopy can only provide structural information, it is not possible to obtain information about physical properties of hair and its chemical composition.[240] Instead, the elemental analysis of hair fibres is measured using bulk techniques, which makes the identification of the location of these elements in the hair structure very difficult to find. Among these techniques are inductively coupled plasma mass spectrometry (ICPMS), energy dispersive X-ray emission (EDX), atomic absorption spectroscopy (AAS), atomic emission spectroscopy (AES), X-ray fluorescence (XRF), particle induced X-ray emission (PIXE) and neutron activation analysis (NAA).[241–247]

The elemental distribution in hair structure is not achievable by conventional techniques, therefore time-of-flight ion mass spectroscopy (ToF-SIMS) has been used to localise the distribution of elemental species in hair structure. Time-of-flight ion mass spectroscopy can provide chemical information due to its ability to provide a two-dimensional view of the elemental and molecular composition of solid samples. ToF-SIMS allows the detection of elemental species that may not be detected by other techniques, such as EDX or X-ray

photoelectron spectroscopy (XPS).[248] Nonetheless, the analysis of hair fibres is particularly challenging due to the highly complexity of the hair structure.[248–252]

ToF-SIMS has been used to investigate the presence of silicones, anionic surfactants and cationic conditioners on the surface of the hair fibre.[253] Also, it has the ability to examine longitudinal sections without the influence of underlying volume, this allows the investigation of elemental distribution.[254] More studies have shown ToF-SIMS and Atomic force microscopy (AFM) allows the observation of the main regions of hair, cuticle, cortex and medulla.[240] This technique could be used to analyse forensically to determine the location of drugs.

Matrix Assisted Laser Desorption Ionization (MALDI) has been used for the detection and imaging of drugs and pharmaceutical in tissues. It has been widely used for the detection of drugs incorporated into hair, as required few hair samples, easier and faster preparation of the sample and provides more accurate information in hours or days.[249]

A study reported the characterisation of microstructures of keratin extracted from wool according to peptide sequences by MALDI-ToF/ToF. The results from this study were then compared to untreated wool powder. The aim of this study was to provide knowledge about extracted keratins and their potential to be used in biomaterials.[255]

1.7 Aims

The dissolution of hair is of great interest for the obtention of keratin, since this material has a vast number of applications from cosmetics to medical devices.[82,256,257] The main aim of this work is the study of the dissolution of hair with ILs, and this is further investigated in Chapter 2. The second study of this Thesis, Chapter 3, focuses on the chemical characterisation of the recovery material from dissolution of hair with ILs. Finally, the impact of the ILs in the hair structure was investigated by infrared spectroscopy. Since the dissolution of hair with ILs was achieved, it is important to understand which specific bonds in the hair structure were affected by dissolution, and this is further investigated in Chapter 4.

Chapter 2 The study of the dissolution of hair with ILs

Previous studies have demonstrated that cellulose and hard keratins can be dissolved successfully by ILs. However, the question whether ILs can dissolve human hair remains open. For that reason, the current study aims to answer this question by investigating the use of ILs in the dissolution of human hair.

As previously reported in section 1.4.2, ILs such as [AmIm]Cl, [C_4C_1Im]Cl and [C_2C_1Im][OAc] have been reported as good candidates to disrupt the hydrogen bonds of the cellulose structure.[108] Furthermore, [C_4C_1Im]Cl and [C_2C_1Im][OAc] has shown good results on the dissolution of wool keratin and was able to disrupt disulfide bonds within the keratin structure.[127] Imidazolium based ILs presented a better dissolution ability when compared with ammonium based ILs, and for that reason imidazolium based ILs were selected for this study.[125] Other factors such as the ability of the ILs to disrupt either hydrogen and disulfide bonds were taken into consideration in order to achieve successful dissolution of hair fibres. According to the literature, [C_2C_1Im][OAc] was shown to be a good candidate to dissolve cellulose and keratin fibres. The nucleophilic acetate can act as hydrogen bond acceptor, which allows the disruption of intra-molecular hydrogen and disulfide bonds, important in the dissolution of natural fibres.[137] Hence, [C_2C_1Im][OAc] was selected to investigate the dissolution of hair with ILs. Several studies have reported possible ratios (mass of hair : mass of IL) for the dissolution of wool with imidazolium based ILs, where it is possible to dissolve up to 0.4 g of wool in 5g of ILs at 120-130° C.[125,126] Assuming a broadly similar molecular weight distribution in hair, our first experiments were a like-for-like study where it was attempted to dissolve 0.04 g of hair in 0.5 g of [C_2C_1Im][OAc] at 120° C (temperature as reported in literature [125,126]), a second experiment was also run concurrent to investigate and increase in the concentration of hair subjected to the dissolution process, the outcome of these experiments is summarised in Table 4. In this investigation the processing of European curly hair was used as a demonstration case and is used as benchmark, unless stated otherwise.

Table 4. Investigation of the dissolution of hair with $[C_2C_1Im][OAc]$.

Ionic Liquid	IL(g)	Hair(g)	Time (h)	Temperature (° C)
$[C_2C_1Im][OAc]$	0.5	0.04	3	120
	0.5	0.5	24	

Table 4 provides insight into the duration of dissolution experiment as a crude measure of how long it took to dissolve the hair samples in 0.5 g of $[C_2C_1Im][OAc]$. The hair was considered completely dissolved by optical evaluation, *i.e.* the observation that no fibres of hair or lumps of solid material remained. Optical methods including dynamic light scattering (DLS) were not utilised due to the very dark nature of the resultant solution. In all cases the resulting sample was recovered as a dark-brown viscous liquid, as shown in Figure 9 (Dissolution image).

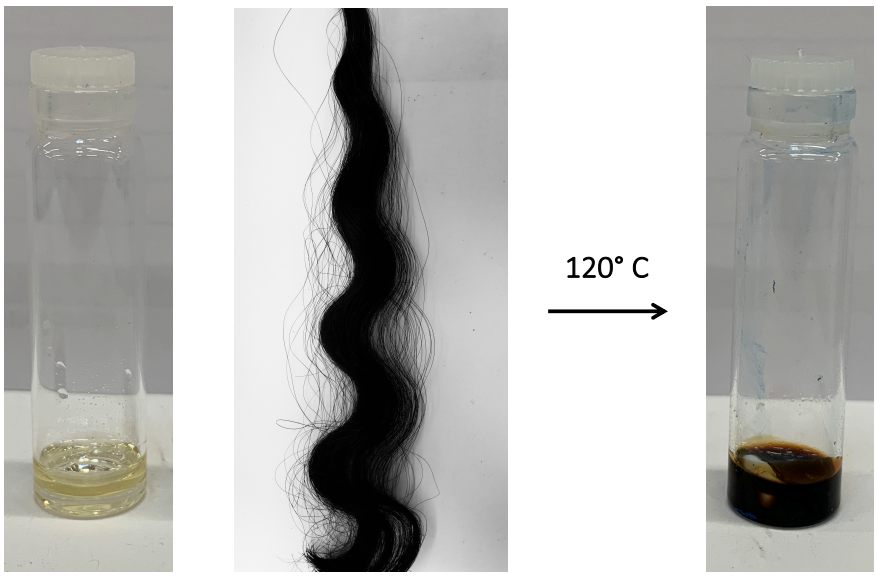


Figure 9. Scheme of the dissolution of hair with ILs. Note: Dissolution image (right image on the Figure) on the diagram represents the dissolution of hair, detected by visual observation. The picture of hair does not represent the amount of hair added to dissolution, the picture aims to show the morphology of hair before dissolution.

From the data in Table 4 it is possible to conclude on the dissolution of hair with ILs. The time of dissolution appears to be directly related to the amount of hair initially added, thus

it was expected that 0.5 g of hair would take longer to dissolve than 0.04 g in the same amount of IL (0.5 g).

It was possible to dissolve up to 0.5 g of hair in $[C_2C_1Im][OAc]$, nonetheless another question arises as whether it is the dissolution limited by the choice of the IL. The next sections aim to investigate the impact of the anion and the cation of the IL on the ability of the IL to dissolve hair.

2.1 Influence of the anion of the ILs on the dissolution of hair.

In this study several anions were investigated: acetate [OAc], dimethylphosphate $[Me_2PO_4]$, chloride (Cl), methylsulphate $[MeSO_4]$, triflate $[CF_3SO_3]$ and bis(trifluoromethanesulfonyl) amide $[NTf_2]$.

The study on the impact of the anion on the dissolution of hair was initiated with [OAc] and $[NTf_2]$ anions. Table 5 presents the experimental data of the dissolution of hair with [OAc] and $[NTf_2]$ anions with 1-ethyl-3-methylimidazolium based cation.

Table 5. The study of the influence of the anion on the dissolution of hair with 1-ethyl-3-3methylimidazolium cation. ND = no dissolution after 24 hours

Ionic Liquid	IL(g)	Hair(g)	Time (hours)	Temperature (° C)
$[C_2C_1Im][OAc]$	0.5	0.04	3	120
$[C_2C_1Im][NTf_2]$	0.5	0.04	ND	120

As it can be observed from the table above, the dissolution of hair was only achieved with $[C_2C_1Im][OAc]$ (the dissolution was considered completed by visual observation). The performance of dissolution with $[C_2C_1Im][OAc]$ can be explained by hydrogen-bond basicity (ß) of 0.95, as discussed previously in section 1.4.4.[138,139] This parameter is primarily influenced by the anion and according to our study the [OAc] anion showed the strongest force to act as an hydrogen bond acceptor. The dissolution of hair only occurs when hydrogen and disulfide bonds are disrupted, and, in the present study, $[C_2C_1Im][NTf_2]$ was not able to fulfil this requirement since it did not dissolve hair. It is important to mention

that $[C_2C_1Im][NTf_2]$ has an hydrogen-bond basicity of 0.28, which is lower than $[C_2C_1Im][OAc]$, and this might explanain why the dissolution did not occur.[147] Other anions were investigated, as shown in Table 6, where 1-butyl-3-methylimdazolium was kept constant.

Table 6. The study of the influence of the anion on the dissolution of hair with 1-butyl-3-methylimidazolium cation. ND = no dissolution in 24 hours.

Ionic Liquid	IL(g)	Hair(g)	Time (hours)	Temperature (° C)
$[C_4C_1Im][OAc]$	0.5	0.04	3	120
$[C_4C_1Im][Me_2PO_4]$	0.5	0.04	4	120
$[C_4C_1Im]Cl$	0.5	0.04	6	120
$[C_4C_1Im][MeSO_4]$	0.5	0.04	ND	120
$[C_4C_1Im][CF_3SO_3]$	0.5	0.04	ND	120

What stands out from the results obtained from the dissolution of hair with different anions is the dissolution of hair when the anion present is [OAc], $[Me_2PO_4]$ and Cl. These ILs present a ß value of 1.09, 1.13 and 0.95, respectively, and the anion acted as a hydrogen bond acceptor being able to dissolve hair. The dissolution with $[C_4C_1Im][MeSO_4]$ and $[C_4C_1Im][CF_3SO_3]$ was not observed after 24 hours. These two ILs exhibit the lowest ß value of 0.66 and 0.57, respectively. An additional factor that might have had an impact on these results is the viscosity of the ILs. Table 7 shows the viscosity of each IL in this study and according to its information, $[C_4C_1Im][OAc]$ and $[C_4C_1Im][Me_2PO_4]$ show the highest viscosity. Curiously they were both able to dissolve hair.

Table 7. Published viscosity data of several ILs at 25° C.

Ionic Liquid	Viscosity (mPa.s)	Reference
$[C_4C_1Im][OAc]$	293	258
$[C_4C_1Im][Me_2PO_4]$	642	258
$[C_4C_1Im]Cl$	64	259
$[C_4C_1Im][MeSO_4]$	213	260
$[C_4C_1Im][CF_3SO_3]$	99	258

These results indicate that the choice of the anion showed to have a bigger impact on the performance of the IL on the dissolution of hair, when looking at the influence of the anion in the IL the following anions [OAc], $[Me_2PO_4]$ and Cl with 1-butyl-3-methylimidazolium as cation.

2.2 Influence of the cation of the ILs on the dissolution of hair

The dissolution of hair was achieved with different anions, yet it is not known if the selection of the cation has an impact on the dissolution of hair.

For this investigation both imidazolium and pyrrolidinium based ILs were studied to evaluate their ability to dissolve hair fibres, with the alkyl side chain kept constant on both cations, the study was carried out with butyl alkyl side chain for both cations in study.

On this investigation, 0.04 g of hair was added to 0.5 g of IL at 120° C. Table 8 presents the result of this investigation.

Table 8. Parameters of dissolution of hair with 0.5 g of IL and 0.04 g of hair at 120° C for the study of the influence of the cation, Imidazolium and Pyrrolidinium based cations. ND = no dissolution after 24 hours

Ionic Liquid	IL(g)	Hair(g)	Time (hours)	Temperature (° C)
$[C_4C_1Im][OAc]$	0.5	0.04	3	120
$[C_4C_1Im][Me_2PO_4]$	0.5	0.04	4	120
$[C_4C_1Pyrr][Me_2PO_4]$	0.5	0.04	4	120
$[C_4C_1Im][MeSO_4]$	0.5	0.04	ND	120
$[C_4C_1Pyrr][MeSO_4]$	0.5	0.04	ND	120
$[C_4C_1Im][CF_3SO_3]$	0.5	0.04	ND	120
$[C_4C_1Pyrr][CF_3SO_3]$	0.5	0.04	ND	120

Three sets of experiments were taken in which the cation was varied. The dissolution was achieved after 4 hours with $[C_4C_1Im][Me_2PO_4]$ and $[C_4C_1Pyrr][Me_2PO_4]$, however, the other two sets of ILs were not able to dissolve hair in 24 hours. The time of dissolution was equivalent for both ILs, and, once again, the dissolution was considered completed by visual observation. $[C_4C_1Im][OAc]$ was reported as a comparison. According to the dissolution with $[C_4C_1Im][Me_2PO_4]$ and $[C_4C_1Pyrr][Me_2PO_4]$, the nature of the cation does not seem to be a decisive factor on the dissolution of hair. This assumption seems to agree with a previous study where $[C_4C_1Pyrr]Cl$, $[C_4py]Cl$ and $[C_4C_1Im]Cl$ showed similar dissolution trends on the dissolution of keratin, the three cations had a moderate effect on the dissolution of keratin.[261] Nonetheless, it can be concluded that it is possible to dissolve hair with imidazolium and pyrrolidinium based ILs.

2.3 Influence of alkyl side chain of cation of ILs on the dissolution of hair

As reported before, longer alkyl side chains of the cation would only penetrate keratin structure with difficulty.[133] Therefore, the influence of the aliphatic side chain of the imidazolium cation in the dissolution of hair was investigated. In this study 1-ethyl-3-methylimidazolium ($[C_2C_1Im]$) and 1-butyl-3-methylimidazolium ($[C_4C_1Im]$) were

investigated coupled with [Me_2PO_4] anion. These results were then compared to [C_2C_1Im][OAc] and [C_4C_1Im][OAc]. The impact of the anion can be ignored since the only variable changing in the study is the alkyl side chain length. Figure 10 presents the results obtained from the analysis of the dissolution of hair with alkyl side chain length variation of the imidazolium cation, and the data can be accessed in Table 25, Table 26, Table 27 and Table 28 in section 5.2.2.

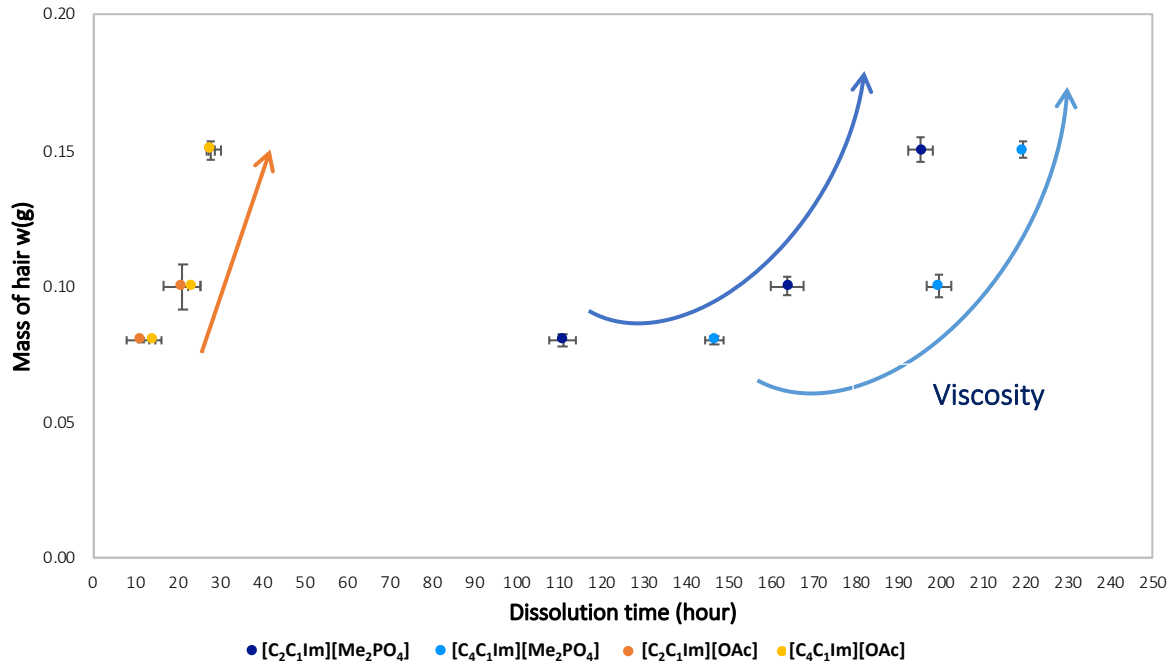


Figure 10. Scheme of the study of the impact of the aliphatic side chain on dissolution of hair. IL in this study [C_2C_1Im][Me_2PO_4], [C_4C_1Im][Me_2PO_4], [C_2C_1Im][OAc] and [C_4C_1Im][OAc], 0.7700 ± 0.0043 g of IL at 100° C.

The experiments were prepared separately, which means each data point is taken from each individual experiment. Only three masses of hair (0.0800 ± 0.0017 g, 0.1000 ± 0.0047 g, and 0.1500 ± 0.0037 g) were considered in this study.

The imidazolium-based acetate ILs exhibited consistently the same dissolution time for all ratios tested, as shown in Figure 10 (Table 25 and Table 26 in section 5.2.2). These reports suggest that the increase of the aliphatic side chain of the imidazolium-based IL coupled with acetate anion has no impact on the dissolution of hair. The analysis of imidazolium-based ILs coupled with dimethylphosphate showed slight differences, where the IL with shorter aliphatic side chain showed a faster dissolution time when compared with

butylimidazolium-based IL. However, it might be because of viscosity. Table 9 compares the viscosity of the ILs in this study at 25° C.

Table 9. Published viscosity data of several ILs at 25° C.

Ionic Liquid	Viscosity (mPa.s)	Reference
$[C_2C_1Im][OAc]$	144	262
$[C_4C_1Im][OAc]$	293	258
$[C_2C_1Im][Me_2PO_4]$	317	263
$[C_4C_1Im][Me_2PO_4]$	642	258

*Temperature = 30° C

As shown in Table 9 the dimethylphosphate based ILs reported significantly higher viscosity than acetate based ILs. It is important to mention that the viscosity data was reported at 25° C, and the dissolution studies were performed at 100° C. Nevertheless, these results may indicate that the viscosity of the ILs impacts the rate of dissolution of hair.

2.4 The influence of the temperature on the dissolution of hair with ILs

An important factor to have into consideration during dissolution is temperature. A previous study has reported that higher temperature can compromise the properties of the recovered material.[196] Researchers have suggested the temperature of dissolution have a big impact on both keratin solubility in ILs and physicochemical characteristics of the recovered keratin.[196] Furthermore, with increasing dissolution temperatures, the loss of cystine and sulfur was found to increase.[196] High dissolution temperatures can lead to an acceleration of the degradation rate of keratin, which is related to the rupture of the α-helix structure and disulfide bond fracture. The level of degradation of the recovered material increased with time at 120° C. In addition, the recovered percentage of the recovered keratin material decreases with increasing temperature. This is in agreement with the modification of disulfide bond content in the recovered keratin.[127] With this in mind the dissolution temperature was decreased to 100° C, in contrast to earlier reported

studies (120 - 130° C) in order to avoid compromising the properties of the proteins. Moreover, by doing so, it will not compromise the yield of the recovered keratin, as the increase of the temperature of the dissolution can lead to a decrease in the yield of keratin recovered material.[127] Therefore, the following investigations on the dissolution of hair were carried out at 100° C.

2.4.1 Dissolution of hair

The study of the dissolution of hair was continued with $[C_2C_1Im][Me_2PO_4]$ and $[C_2C_1Im][OAc]$ at 100° C, at different ratios of hair to investigate the limit on the dissolution. From Figure 11 we can see that for the maximum amount of hair added (0.30 g) both ILs were able to dissolve hair. As previously shown in section 2.1, [OAc] presented a better ability to dissolve hair.

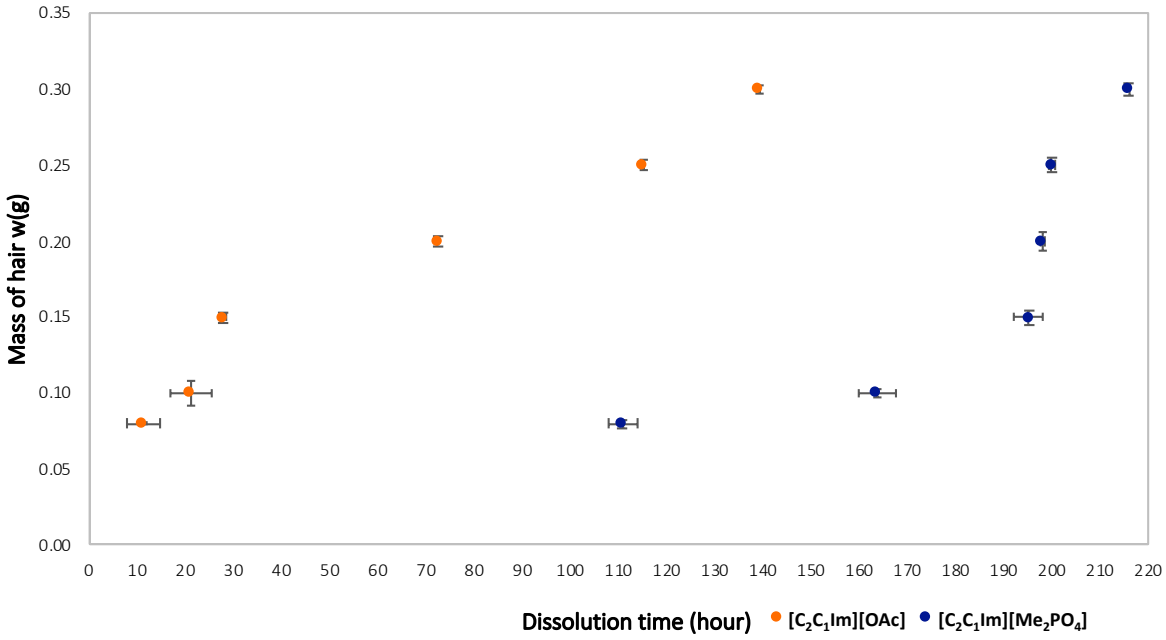


Figure 11. Scheme of comparison of time of dissolution of curly hair with $[C_2C_1Im][OAc]$ and $[C_2C_1Im][Me_2PO_4]$. IL was constant for all data points 0.7700 ± 0.0043 g. Dissolution was performed at 100° C and each data point corresponds to the mean of 3 independent dissolution tests.

A few discrepancies on the time of dissolution by these two ILs could be observed, however this may be associated to experimental error and the effect of the anion. The time necessary to dissolve 0.0800 ± 0.0008 g of hair was 112 ± 3 hours, when dissolution was performed by $[C_2C_1Im][Me_2PO_4]$, while $[C_2C_1Im][OAc]$ this time was 11 ± 3 hours. The dissolution of hair with $[C_2C_1Im][Me_2PO_4]$ showed that it takes longer for the dissolution process to start, but as the mass of hair increases, the time of dissolution did not increase similarly. The dissolution of hair keratin results in the disruption of hydrogen and disulfide bonds, and the latter are mainly present in the cuticle layer of the hair fibre due to the high cysteine content.[127] According to Figure 11, acetate-based ILs might have a higher ability to disrupt these bonds than dimethylphosphate ILs. These results corroborate the ones presented for dissolution of wool, where acetate imidazolium-based ILs exhibited the fast dissolution rate when compared to dimethylphosphate imidazolium-based ILs.[127]

As mentioned in section 1.4.3, there are two main paths on the structure of hair by which dissolution can happen, being the transcellular and intercellular. On one hand, the transcellular path involves the most cross-linked regions, which indicates higher content of disulfide bonds. On the other hand, intercellular diffusion takes place between the cuticle cells, and is the preferred route of larger molecules. However, the process can occur via both routes at the same time.[22] According to this, and the results in Figure 11, a mechanism of dissolution can be proposed. In section 4.1, the dissolution of hair with ILs was initiated by the swollen of the cuticle, followed by the dissolution of the cortex. Having into consideration that larger molecules preferred the intercellular path between the cuticles, this might be the case in the current investigation. Nevertheless, the dissolution might take place by both routes. The IL might penetrate through the cuticle cells, breaking the disulfide bonds and hydrogen bonds along the way to the cortex where the dissolution initially takes place. However, at this stage it is not possible to identify the mechanism of dissolution, with this being only an assumption.

2.5 Dissolution of hair with $[C_2C_1Im][OAc]$ and $[C_2C_1Im][Me_2PO_4]$ assisted by microwave radiation

The dissolution of keratin with ILs assisted by microwave radiation has recently been investigated in the literature under different set of conditions.[84,264–266] The conventional heating dissolution method on section 2.4.1 took up to 50 hours to completely dissolve hair. Now we are trying to improve the dissolution time of hair with microwave radiation. From the literature, it is possible to find reports on the dissolution of keratin fibres assisted by microwave radiation.[264] For instance, it was reported that feathers had faster dissolution times with super-heated water when compared to conventional heating.[197,265] The decrease in the dissolution time assisted by microwave radiation may be related to the homogenous heat distribution and internal heat generation, which reduces the processing time and decreases the energy required to dissolve keratin. Yet, the exact role of electromagnetic radiation is not yet fully understood and its interactions with wool matrix are also mostly undetermined. One hypothesis for the reduction in the dissolution time of keratin previously suggested is the hydrolysis of the ester groups due to microwave irradiation, which in turn reduces the activation energy.[267]

In this study, the dissolution of hair was also investigated by microwave radiation. The ratio masses of hair:IL were selected based on conventional heating dissolution method. In this investigation triangular stir bars were used to improve the mixing during the reaction. The dissolution of hair was tested with 0.1500 ± 0.0010 g of hair and 0.7700 ± 0.0055 g of IL. The parameters of the mass of hair:IL ratio and temperature were the same as conventional heating dissolution method to conclude about the efficiency of dissolution assisted by microwave. Table 10 presents the conditions and time of dissolution assisted by microwave radiation.

Table 10. Conditions of the dissolution of hair with $[C_2C_1Im][OAc]$ assisted by Microwave radiation.

IL	IL content w(g)	IL (mol)	Hair w(g)	Temperature (° C)	Power (W)	Time (min)
$[C_2C_1Im][OAc]$	0.7733	0.0045	0.1507	100	100	5
$[C_2C_1Im][Me_2PO_4]$	0.7719	0.0033	0.1503	100	100	5

During this process, the total dissolution was determined by visual observation, exactly as performed for conventional heating dissolution method. At this stage the samples were not pre-filtered and this will be discussed in detailed in Chapter 3.

Using the microwave method, the time of dissolution was reduced drastically. Figure 12 represents the visual dissolution of hair before and after dissolution assisted by microwave.

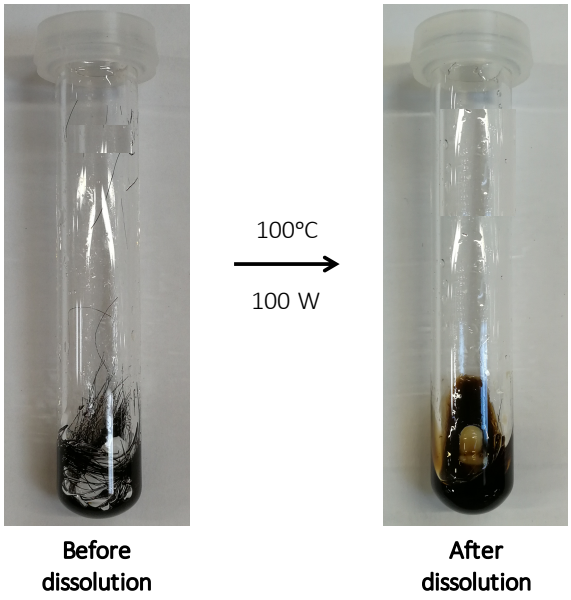


Figure 12. Dissolution of hair assisted by Microwave irradiation. Scheme before (IL + hair) and after dissolution of hair. Dissolution conditions: 100° C at 100 W, 0.7733 g of IL and 0.1507 g of hair.

The dissolution assisted by microwave radiation showed a faster dissolution rate when compared to conventional heating method, as shown in Table 11.

Table 11. Comparison between dissolution of European curly hair with $[C_2C_1Im][OAc]$ and $[C_2C_1Im][Me_2PO_4]$ assisted by Microwave radiation and conventional heating method.

IL	Hair w(g)	Temperature (° C)	Dissolution assisted by Microwave Time (min)	Conventional heating dissolution method Time (hours)
$[C_2C_1Im][OAc]$	0.1507	100	5	28
$[C_2C_1Im][Me_2PO_4]$	0.1503	100	5	194

In the microwave-assisted dissolution the molecules in the microwave tube can absorb the microwave radiation, and therefore the temperature of the ILs and hair fibres increases very quickly. Furthermore, the reaction time is then highly reduced with a consistent saving of energy.[264]

Both dissolutions presented similar dissolution time, and these times are comparatively much faster than the conventional heating method. Additionally, according to these results no significant differences were found among these anions.

2.6 Dissolution of different hair types with $[C_2C_1Im][OAc]$

The study on the dissolution of hair with ILs proved to be possible. However, until now only European curly hair was studied. This section will investigate whether it is possible to dissolve different hair types and if IL has the capability to dissolve different hair types.

As mentioned in section 1.2.2, the structure of the human hair does not differ from different ethnicities. However, a positive correlation between hair pigmentation and the degree of crosslinking in the hair structure has been observed elsewhere.[22] This means that lighter hair presents a less crosslinked structure than darker hair, and consequently it would be expected that lighter hair would dissolve faster when compared to darker hair.[22]

For the study of the dissolution with $[C_2C_1Im][OAc]$, different hair types were selected: dark European curly, straight and blond European straight hairs and dark straight Asian hair. The Table 12 below shows the hair's characteristics according to their ethnicity.

Table 12. Hair characteristics by ethnicities.[268] Note: the pictures on top of the table show the fibres used at dissolution of hair with ILs and the length of the fibres.






Ethnicity	European blonde hair	European hair	European hair	Asian hair
	Straight	Straight	Curly	Straight
Colour	Light		Dark	
Diameter (µm)	40-80	40-80	50-90	80-100
Cross-section shape of the fibre	Elliptical	Elliptical	Elliptical	Circular
Fibres length (cm)	15	15	20	15

According to Table 12, Asian hair presents the biggest diameter from the 4 types of hair tested which may suggest this hair type would require more time to be dissolved.

To investigate the dissolution of different hairs with ILs, the experimental procedure was based upon earlier keratin dissolution studies, most commonly wool fibres.[128]

Different masses of hair were systematically increased from 0.0800 g to 0.3000 g, with mass of IL set constant at 0.7700 g. Three repetitions of each mass:IL ratio were prepared, and each repeated result corresponds to a unique experiment.

During the dissolution, flasks were placed inside a sand bath to improve the temperature homogeneity around flasks at 100° C. After complete dissolution, *i.e.,* the observation that no fibres of hair or lumps of solid material remained, the flasks were removed from the sand bath to cool down.

All samples, for all mass of hair:IL ratio, after complete dissolution presented a consistency like a gel and very dark in colour, as presented before in Figure 9 (Dissolution).

The time that it took to dissolve hair with acetate-based IL was very similar among different hair types. The dissolution of 0.0800 and 0.1000 g of hair took up to 25 hours to completely dissolve, this observation was common among different types of hair. When the amount of hair increased to 0.1500 g, complete dissolution was reached at up to 50 hours. Finally, higher amounts of hair (0.2000 and 0.2500 g) took more than 50 hours to completely dissolve, as it would be expected, since there was less IL available to dissolve hair. However, no hair type is significantly distinct during this analysis. From the dissolution point of view, it is possible to dissolve hair with ILs as it is also possible to dissolve different hair types with ILs. From the literature review of dissolution of cellulose and other keratin fibres it is possible to speculate what may be happening during dissolution. Since the cation has been shown to have a minor effect on dissolution, the acetate anion may have the ultimate importance during dissolution of hair, as discussed in section 2.1. The study can be consulted in Table 25.

At this stage, the results obtained show that the dissolution of hair with ILs can be achieved. Additionally, it was possible to dissolve different hair types, and this may indicate that ILs are able to dissolve hair independently of its ethnicity. [C_2C_1Im][OAc] showed dissolution at higher masses of hair, but higher dissolution times were recorded. Complete dissolution was assumed using the visual observation method as no hair yet to be dissolved could be observed.

2.7 Conclusions

The aim of Chapter 2 was to show that ILs are able to dissolve hair. The influence of the anion was investigated, and the results suggests that [OAc], [Me_2PO_4] and Cl can achieve the dissolution of hair when coupled with 1-butyl-3-methylimidazolium cation. From section 2.1 was possible to conclude that these nucleophilic anions, have the ability to disrupt the hydrogen and disulfide bonds of the hair structure, which ultimately leads to a successful dissolution of hair. The impact of the cation on the dissolution of hair was also investigated with imidazolium and pyrrolidinium cations. Both cations were able to dissolve hair, however it was possible to conclude that the cation has a marginal impact on

dissolution. The increase of the aliphatic chain of the cation, showed to have an greater impact on the dissolution of hair due to the increase of the viscosity of the IL.

Another factor that impacts the dissolution of hair is temperature. This parameter was decreased to 100° C during dissolution of hair to avoid compromising the properties of the keratin. The hair fibres were then heated at 100° C with two different ILs, $[C_2C_1Im][OAc]$ and $[C_2C_1Im][Me_2PO_4]$. The limit of the dissolution of hair with $[C_2C_1Im][Me_2PO_4]$ and $[C_2C_1Im][OAc]$ was also investigated, and the results showed that the $[C_2C_1Im][OAc]$ has the fastest dissolution rate (see Figure 11). This might suggest that acetate anion can easily penetrate the structure of hair, from the cuticle cells to the cortex.

The time required to dissolve hair with ILs showed to be rather high. Consequently, to improve the dissolution time with ILs, the use of microwave radiation was investigated. This section was also essential to comprehend if the time of the dissolution process could be decreased in comparation to the conventional heating method. The time of dissolution of 0.15g of hair was able to be reduced to approximately 5 min for both ILs, $[C_2C_1Im][Me_2PO_4]$ and $[C_2C_1Im][OAc]$ (Table 10). The dissolution of 0.15g of hair with conventional heating method lasted 28 hours with $[C_2C_1Im][OAc]$ and 198 hours with $[C_2C_1Im][Me_2PO_4]$ (Table 11). From this investigation, it was possible to improve the time of dissolution and dissolution can be more efficient when assisted by microwave radiation.

A mechanism of dissolution was proposed: in the current investigation, the larger molecules might prefer the intercellular path between the cuticles. Still, the dissolution might take place by both routes (transcellular and intercellular). The cuticle cells might be the preferred route by the IL to penetrate through and breaking the disulfide bonds and hydrogen bonds along the way to the cortex where the dissolution initially takes place.

Lastly, the investigation of the dissolution of hair from different ethnicities was studied where it was possible to conclude that the nature of the hair has no impact on its dissolution with ILs.

From now on, it is possible to investigate the extraction of value-added material, such as keratins, and KAPs from the dissolution of hair with ILs, and this is presented in the following Chapter 3.

Chapter 3 Material recovery from the dissolution of hair with ILs and its chemical characterisation

The previous Chapter helped determine the ability of ILs to dissolve hair. The study showed that the dissolution of hair can be successfully achieved, however it is now important to understand whether it is possible to recover material (keratin) from the dissolution process.

The central aims of the current Chapter are to determine the recovering of hair material from the dissolution and, consequently analyse and characterise the chemical composition of such materials.

3.1 Material recovery from the dissolution of hair with $[C_2C_1Im][OAc]$

Firstly, it is important to understand whether hair material can be recovered from the dissolution of hair with ILs. Unless stated otherwise, European curly hair will be the object of study in the current Chapter.

The dissolution of 0.3000 g of hair with $[C_2C_1Im][OAc]$ was investigated, as this was the first condition selected due to the highest amount of hair dissolved. The regeneration process was followed and is described elsewhere in this Thesis (section 5.3). After this procedure it was possible to recover 0.0467 g of material from the 0.3000 g of hair initial added. At this point, it was possible to recover material from the dissolution of hair process, therefore there is a need to investigate how much can we recover from the previous dissolutions.

Following the same procedure, other ratios of hair and $[C_2C_1Im][OAc]$ were investigated. It was firstly expected that the higher amount of hair initially added in dissolution would provide the highest amount of material recovered. The results of the recovered material from dissolution of hair with $[C_2C_1Im][OAc]$ are presented in Table 13, the results obtainable are the average of three masses.

Table 13. Recovered material (recovered keratin) masses from dissolution of European curly hair with $[C_2C_1Im][OAc]$.

Mass of hair initially added w(g)	Recovered material w(g)	Recovered material (%)
0.0800 ± 0.0009	0.0450 ± 0.0311	56.3%
0.1000 ± 0.0083	0.0295 ± 0.0083	29.5%
0.1500 ± 0.0033	0.0502 ± 0.0398	33.5%
0.2000 ± 0.0036	0.0161 ± 0.0003	8.1%
0.2500 ± 0.0035	0.0751 ± 0.0729	30.0%
0.3000 ± 0.0024	0.0233 ± 0.0474	7.8%

Comparison of the weight of recovered material with initial mass of hair dissolved, the mass of hair dissolved initially increases down the columns.

According to the results in Table 13, solutions with higher amount of hair dissolved, showed a lower weight of the recovered material, which contradicted the initial expectations, and this may be associated to experimental errors during recovered material process. Nonetheless, the maximum amount of recovered material obtained from the dissolution of hair with $[C_2C_1Im][OAc]$ was 56.3%, this value was higher than the amount of material recovered from the dissolution of wool with $[C_2C_1Im][OAc]$ (15.8%). The conditions of this dissolution were different, the dissolution was performed at 120° C for 30 min.[127] Moreover, the lower percentage of recovered material might be due to the higher affinity of hair to the ionic liquid phase, which result in less material recovered. This will be further discussed in section 3.2.

The regeneration method showed some limitations, which may be the result of the methodology chosen. The procedure has several steps where the loss of sample may

happen, such as when solvent is separated from the recovered keratin material after centrifugation step. Thus, the inconsistence on results may be related to experimental errors during recovered process. Nonetheless, at this stage the main object of study is recovery of material from the dissolution of hair and subsequent characterisation. Accordingly, it is possible to recover material from the dissolution of hair with $[C_2C_1Im][OAc]$ which fulfils the initial goal of the current Chapter.

3.2 Material recovery from the dissolution of hair with $[C_2C_1Im][Me_2PO_4]$

It is now possible to affirm that material from dissolution of hair with acetate-based IL can be recovered, and, following the same procedure, we can now investigate the material recovered from dissolution of hair with $[C_2C_1Im][Me_2PO_4]$. These results are presented in Table 14.

Table 14. Recovered material masses from dissolution of European curly hair with $[C_2C_1Im][Me_2PO_4]$.

Mass of hair initially added w(g)	Recovered material w(g)	Recovered material (%)
0.0800 ± 0.0026	0.0354 ± 0.0059	44.3%
0.1000 ± 0.0031	0.0558 ± 0.0086	55.8%
0.1500 ± 0.0046	0.0998 ± 0.0116	66.5%
0.2000 ± 0.0060	0.1028 ± 0.0124	51.4%
0.2500 ± 0.0054	0.1162 ± 0.0075	46.5%
0.3000 ± 0.0043	0.0855 ± 0.0674	28.5%

Comparison of the weight of recovered material with initial mass of hair dissolved, the mass of hair dissolved initially increases down the columns.

Recovered material from dissolution of hair with $[C_2C_1Im][Me_2PO_4]$ showed higher weights when compared with $[C_2C_1Im][OAc]$. Also, $[C_2C_1Im][Me_2PO_4]$ results showed a proportional increasing trend as the increase of initial hair added presented higher recovered material

weights. These results are in agreement with the dissolution of wool with $[C_2C_1Im][Me_2PO_4]$ reported in the literature. In that investigation it was possible to recover 76.6% of material after dissolution at 120° C for 30 min. It was possible to recover higher material content from the dissolution of wool with $[C_2C_1Im][Me_2PO_4]$ than from the dissolution with $[C_2C_1Im][OAc]$ (15.8%).[127]

The weight variation of the recovered material results from dissolution with different ILs may be the consequence of the ILs high ability to cleave hydrogen and disulfide bonds, which may be related to the distribution of the ILs components around keratin.[127] Furthermore, the size of anion and the ability to cleave H-bonds and disulfide bonds will primarily determine the capability to dissolve hair.[106] That may explain why $[C_2C_1Im][OAc]$ presented fastest dissolution time but lower weight mass of recovered material. Due to its efficiency to cleave such bonds, the dissolution particles may have a better affinity to IL phase and, in turn make it difficult for their precipitation during the recovery method. This may be justified by the observation during these procedures, as the IL solution presented a brownish colour after the regeneration process, which may indicate that the presence of some material left in the IL solution. Moreover, after 24 hours of resting it was possible to detect a precipitate layer in the IL solution (water-soluble fraction), as presented in Figure 13. This was observed by both ILs in this study, $[C_2C_1Im][OAc]$ and $[C_2C_1Im][Me_2PO_4]$

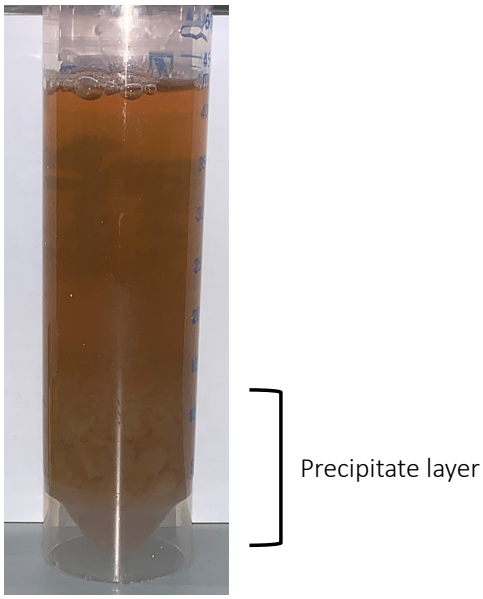


Figure 13. Ionic liquid solution after regeneration method. Formation of a precipitate layer.

Both regenerated material and IL solution were submitted to several techniques to firstly, understand what may have been left in solution and secondly to comprehend the composition of the recovered material. Section 3.3 will discuss the characterisation of the recovered material and ILs after the recovery process.

3.2.1 Material recovery from dissolution of hair assisted by microwave radiation

In this section, the recovered material from the conventional heating dissolution method will be compared with dissolution assisted by microwave radiation. In Chapter 2, it was shown that microwave assisted dissolution is faster than the conventional heating dissolution method. However, there is now a need to understand if any material can also be recovered from the dissolution assisted by microwave radiation. Table 15 shows the results of this study, where only one dissolution solution was tested, using 0.1500 g of hair. This combination was selected due to higher mass of recovered material from dissolution with $[C_2C_1Im][OAc]$ and $[C_2C_1Im][Me_2PO_4]$.

Table 15. Comparison of recovered material from conventional heating dissolution and dissolution assisted by microwave radiation with $[C_2C_1Im][OAc]$ and $[C_2C_1Im][Me_2PO_4]$.

IL	Hair initially added to dissolution w(g)	Recovered material from conventional heating dissolution w(g)	Recovered material from dissolution assisted by microwave w(g)
$[C_2C_1Im][OAc]$	0.1507	0.0566	0.0112
$[C_2C_1Im][Me_2PO_4]$	0.1503	0.1041	0.0208

The mechanism of dissolution of hair assisted by microwave radiation is not fully understood due to the complexity of the hair structure. However, one can conclude that the material retained in the IL solution is much higher than conventional heating dissolution method, reason why the weight of recovered material is lower than the one from the conventional heating dissolution method. A possible explanation for this could be

that during the dissolution process the clusters of hair dissolved are being broken down into continuously smaller and smaller monomers, when compared to the conventional heating dissolution method. Consequently, it may lead to an increase of the interaction between these monomers and the IL constituents, with these having a higher affinity to the IL phase. That way, the hair material content retained into the IL solution is much higher when using microwave irradiation thus explaining the lower percentage of recovered material.

The after analysis the IL solution (water-soluble fraction) was evaporated in order to remove the water, however the precipitated layer was not possible to be removed from the IL. Several attempts were performed, such as filtration, liquid-liquid extraction and IL washed with different solvents (such as chloroform, dichloromethane, ethyl acetate, methanol, petroleum ether, acetone and acetonitrile). However, recovering and/or recycling of the IL was not possible to achieve and the contaminated ILs were disposed of with the appropriate chemical waste treatment. Unfortunately, this process will have a negative impact on the environment, since new ILs will have to be synthesised for each new dissolution.

Section 3.3 will focus on the characterisation of the recovered material and possible characterisation of the IL after recovered material procedure.

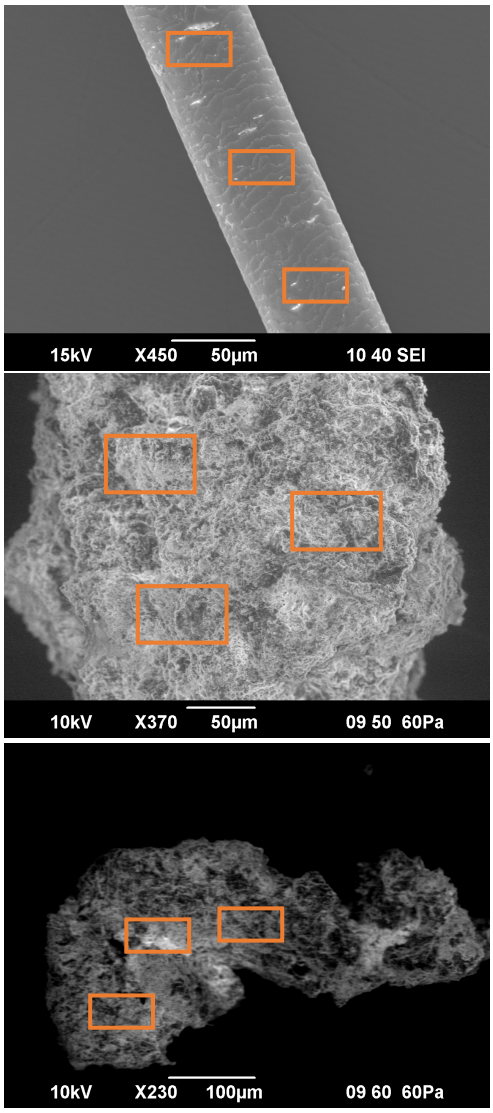
3.3 Characterisation of recovered materials from dissolution processes

3.3.1 Scanning Electron Analysis Energy-dispersive X-Ray spectroscopy (SEM-EDX)

The insolubility of the recovered material in most solvents made it impossible to utilise techniques that involve the dissolution of the material for its analysis, such as HPLC or gas chromatography-mass spectrometry headspace. The solubility of the recovered hair material was studied on several solvents with a wide range of polarity. However, these materials showed poor solubility in the majority of the solvents tested (chloroform, dichloromethane, Ethyl acetate, methanol, petroleum ether, acetone, acetonitrile). Because of this, scanning electron analysis couple to energy-dispersive X-ray spectroscopy (SEM-EDX) was the technique selected to investigate the morphology of these materials

after dissolution, and due to its versatility of elemental microanalysis method capable of identifying and quantifying elements.

The recovered hair material from $[C_2C_1Im][OAc]$ dissolution is noticeably different from chemically untreated hair, as shown in Figure 14. From the EDX analysis it was possible to identify a reduction on the sulfur content in these samples and by comparison with chemically untreated hair, as presented.



Element	Weight %
Sulfur	4.84

Element	Weight %
Sulfur	0.48

Element	Weight %
Sulfur	0.47

Figure 14. Scheme of the EDX results on cuticle of chemically untreated hair fibre (top image on this scheme) and recovered material from dissolution with $[C_2C_1Im][OAc]$. The results are the average of three spots on the sample represented by the orange boxes in the pictures.

The reduction of the sulfur content may be related to the exposure of the cuticle of the hair. The cuticle structure contains more sulfur content than the cortex, which could explain the reduction on sulfur content.[269] However, by using this technique only elemental sulfur was possible to identify and no insight could be attained regarding specific proteins.

3.3.2 Thermal stability analysis of hair

The thermogravimetric (TG) analysis of chemically untreated hair and recovered hair material from the dissolution with $[C_2C_1Im][OAc]$ and $[C_2C_1Im][Me_2PO_4]$ was investigated. In this section, the water-soluble fraction refers to the IL solution after the regeneration process, which contains IL and hair material that did not precipitate after the regeneration process. The water-soluble fraction showed the formation of a precipitate layer (suspension) after 24 hours standing, as shown in Figure 15. Both precipitate and water-soluble fraction were analysed by TGA.

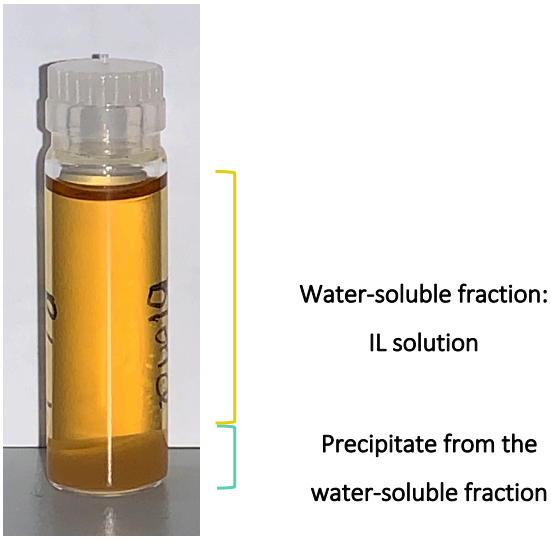


Figure 15. Scheme of the water-soluble fraction and precipitation of hair material after 24 hours standing.

Several attempts were made to separate/remove the precipitate from the water-soluble fraction, but this process showed to be a challenging and unsuccessful. Nonetheless, some aliquots from the precipitate were analysed by TGA.

The range of temperatures selected in this study was determined by the chemically untreated hair TG profile, where full degradation of keratin was reached at 600° C, as reported in the literature.[270] At the time of this study, it was not possible to perform TG profiles at temperatures higher than 600° C.

Figure 16 shows the TG curves or mass losses of chemically untreated European curly hair. Until stated otherwise, European curly hair is used as an analysis example in this study. Minute variations on the temperature of mass losses observed within all hair types analysed were observed, which are ascribed to the error associated with this technique.

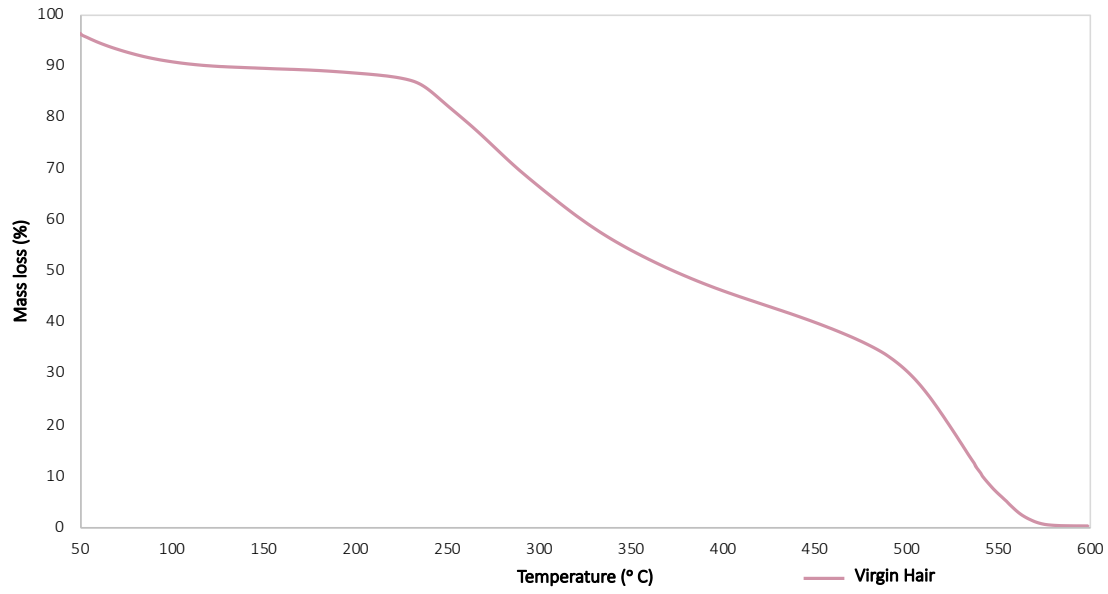


Figure 16. Thermogravimetric curves of European curly hair.

The TG curve for the hair exhibits three mass losses in the range of temperatures 50 to 600° C, similar to the behaviour reported in literature for Brown Caucasian hair.[270] The first mass loss around 100° C is related to water evaporation and the following two losses are associated with the denaturation of the keratin polypeptide chains.[270]

The TG profile of the recovered hair material from dissolution with $[C_2C_1Im][Me_2PO_4]$ is shown in Figure 17. The TG profile of recovered hair material showed a decrease on the mass losses when compared to chemically untreated hair.

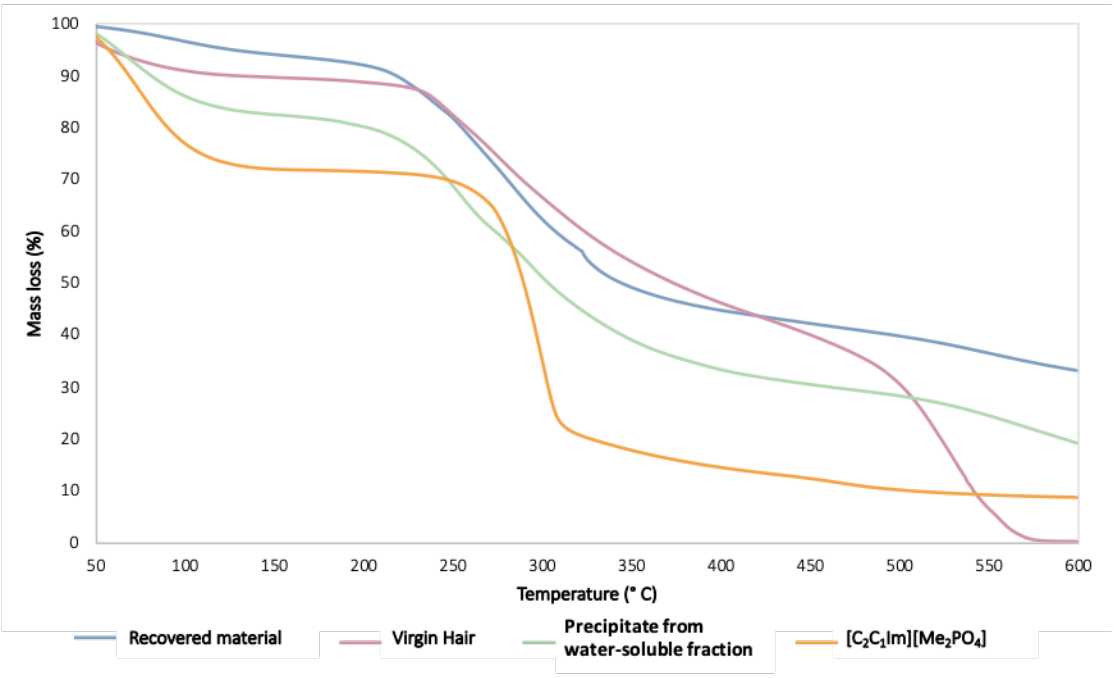


Figure 17. Thermogravimetric curves of European curly hair recovered hair material from $[C_2C_1Im][Me_2PO_4]$ dissolution, chemically untreated hair, precipitate from the water-soluble fraction and $[C_2C_1Im][Me_2PO_4]$.

According to literature, $[C_2C_1Im][Me_2PO_4]$ presents the first mass loss at 105° C, related to the evaporation of water content of the IL, followed by a decomposition at 264° C and another two mass losses at 363 and 800° C.[271,272] $[C_2C_1Im][Me_2PO_4]$ TG profile in Figure 17 does not show the last mass loss, 800° C, as full degradation of keratin was reached at 600° C, and it was not possible to perform TG profiles at temperatures higher than 600° C, at the time of this investigation.[270] The dissolution with $[C_2C_1Im][Me_2PO_4]$ showed a decrease on the mass losses of the thermogravimetric scheme of recovered hair material when compared to chemically untreated hair. This behaviour was observed within this range of temperatures, and since the thermogram at 600° C does not reach zero it may suggest that at higher temperatures another mass loss could be detected. This change in the TG profile

may be related to the modification caused by the ILs on the keratin structure of the hair. The hair keratin structure becomes more disorganised after the dissolution and regeneration process of the hair material and that disorganisation is characterised by a smaller number of mass loss stages on the TG graphic.[270] The same performance is observed for hair treated with cosmetic products, such as bleach or chlorinated solutions. The most affected bonds on these types of treatments are the disulfide bonds which maintain the keratin structure conformation. The modification on these bonds is represented on the TG profile by mass losses.[270] Although the decrease of mass losses on the TGA profile decreases from chemically untreated hair to recovered hair material, it is not possible to conclude which hair type showed the major modification on the keratin structure, since the temperatures on the profile are very similar. The TG profile of recovered material and precipitate from the water-soluble fraction showed similar profiles, where it was only possible to detect two mass loss on the analysed range of temperatures. They showed a mass loss around 100° C related to water evaporation and another one between 200 and 300° C very close to the first mass loss of chemically untreated hair. The IL, $[C_2C_1Im][Me_2PO_4]$, have the first mass loss around 100° C (water evaporation) and the second one between 250 and 300° C.[271,272] This mass loss is shifted to higher temperatures, which may suggest the mass loss around 200 and 300° C of recovered material and precipitate from the water-soluble fraction is not related to IL but keratin material. However, above 350° C, TG profile of recovered material and precipitate from the water-soluble fraction is very similar to the IL TG profile, which may suggest recovered material and precipitate still may have IL remaining. This fact could be corroborated by the aspect of recovered material after TGA analysis, Figure 18.



Figure 18. Recovered material from dissolution of $[C_2C_1Im][Me_2PO_4]$ after TG analysis.

The recovered material from the dissolution of hair with $[C_2C_1Im][OAc]$ was investigated by TG analysis. The TG profile of the recovered material from the dissolution with $[C_2C_1Im][OAc]$ and $[C_2C_1Im][Me_2PO_4]$ presented different behaviours. Figure 19 shows the TG profile of recovered material from the dissolution of hair with $[C_2C_1Im][OAc]$, the precipitate from the water soluble fraction and the IL TG profile.

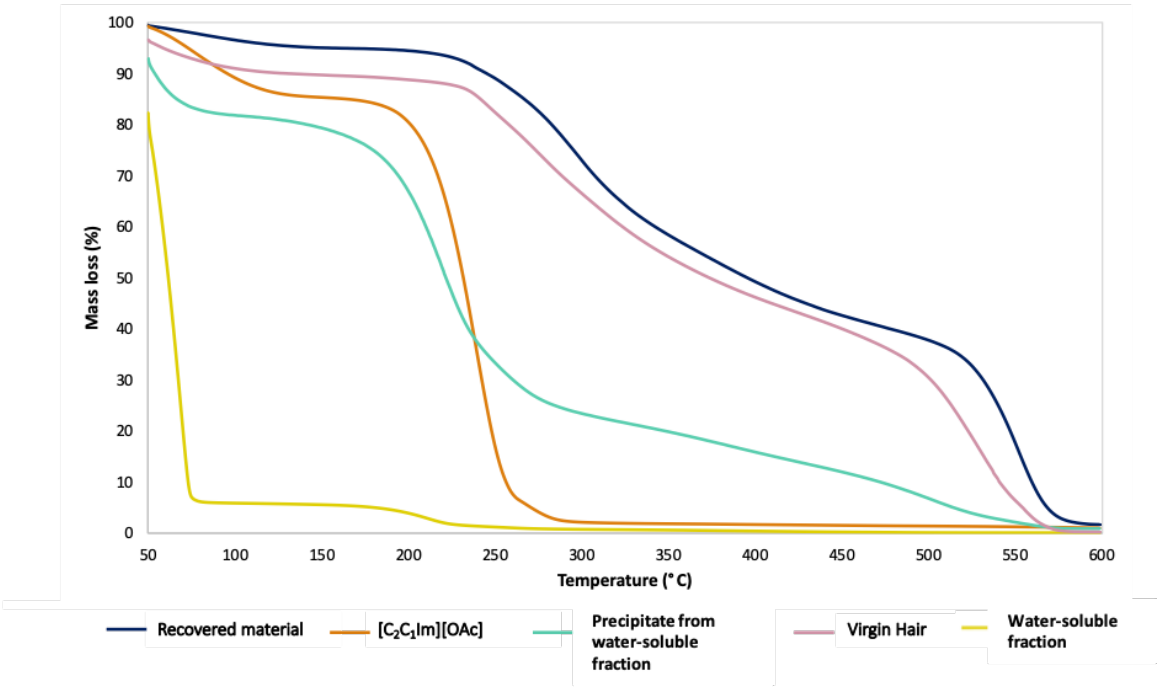


Figure 19. Thermogravimetric analysis of European curly hair recovered hair material from $[C_2C_1Im][OAc]$ dissolution.

Differences were found in the TG profile of the recovered material from the dissolution with $[C_2C_1Im][OAc]$ compared with $[C_2C_1Im][Me_2PO_4]$. The TG profile presents three mass losses similar to those observed in the chemically untreated hair TG profile, which may suggest that $[C_2C_1Im][OAc]$ does not have the same impact on the keratin structure as $[C_2C_1Im][Me_2PO_4]$. However, the morphology of the recovered hair material is not the same as chemically untreated hair, Figure 14 thus the TG analysis cannot provide information about the changes on the recovered hair material structure. The precipitate from the water-soluble fraction shows water evaporation around 100° C and another mass loss between 150 and 250° C, which is very similar to the IL one around the same range. This may indicate that the precipitate from the water-soluble fraction may still contain IL, however, the second mass loss is related to hair material, since the IL does not exhibit any mass loss between 300 and 600° C. Additionally, the water-soluble fraction showed a significant loss of water at around 75° C and another mass loss that might be related to IL (> 200° C), since they are very close.

The TG profiles of the recovered materials from both dissolutions are shown in Figure 20 for comparison purposes. The recovered hair material from $[C_2C_1Im][Me_2PO_4]$ dissolution showed fewer mass losses than chemically untreated hair TG profile, which may suggest that the keratin structure is more disordered after dissolution and regeneration processes. On the other hand, recovered hair material from $[C_2C_1Im][OAc]$ dissolution presented the same mass losses than chemically untreated hair, which could imply that $[C_2C_1Im][OAc]$ has a different impact on keratin structure than $[C_2C_1Im][Me_2PO_4]$. Another factor is the acetate-based IL is easier removed from recovered material than $[C_2C_1Im][Me_2PO_4]$ since the recovered material from dissolution with acetate-based IL did not show any mass loss related to IL. In principle both ILs are miscible with water. However, the dimethylphosphate anion might be a stronger hydrogen bond acceptor than acetate anion, which increases the complexity of the interaction between IL and hair. Recovered material from the dissolution of hair with $[C_2C_1Im][Me_2PO_4]$ shows a mass loss after 600° C, which is similar to the $[C_2C_1Im][Me_2PO_4]$ neat TG profile. [271,272] This might indicate that phosphate residues might be integrated in hair structure after dissolution, as shown in Figure 18. Nonetheless, more analysis needs to be made in order to understand the composition of the recovered hair materials and help infer about the mechanism of dissolution with different ILs. The

following section will discuss the results of the chemical analysis on recovered hair materials from $[C_2C_1Im][Me_2PO_4]$ and $[C_2C_1Im][OAc]$ dissolutions with all hair types in this study.

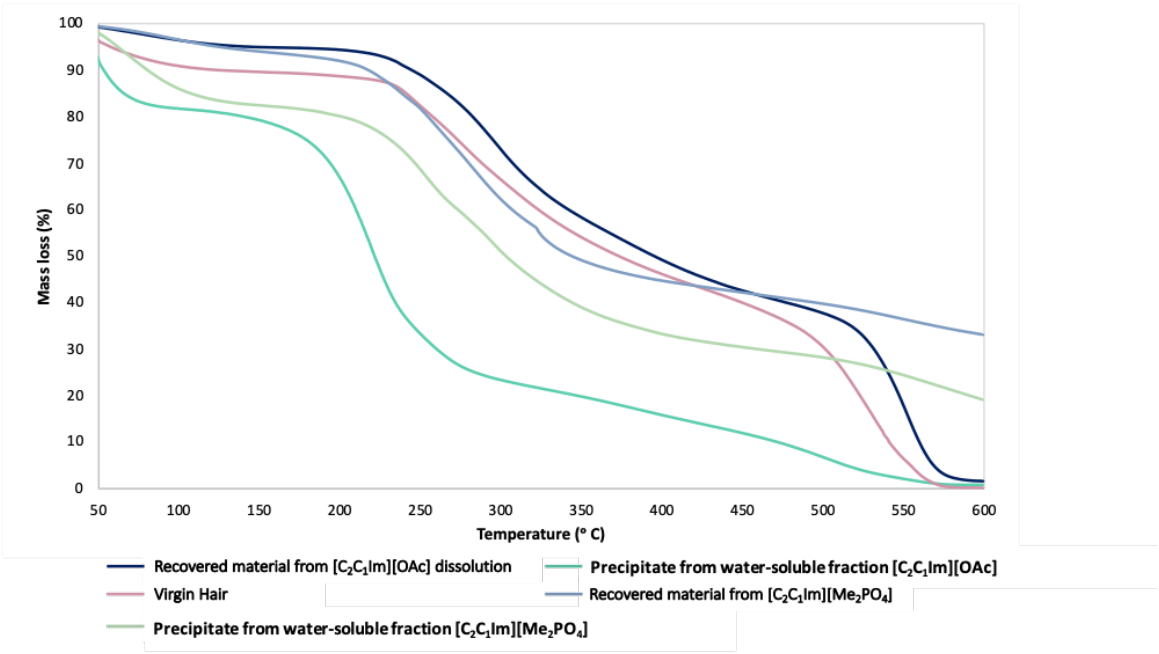


Figure 20. Comparison among recovered material and precipitate from water-soluble fraction from $[C_2C_1Im][OAc]$ and $[C_2C_1Im][Me_2PO_4]$ dissolution.

3.3.3 Thermal stability analysis of recovered material from dissolution assisted by microwave radiation

The dissolution of hair with ILs assisted by microwave irradiation was discussed previously in Chapter 2 which help conclude that a significant decrease of the time of dissolution is achieved when compared with conventional heating dissolution methods. The recovered material from dissolution assisted by microwave radiation was analysed by TGA to investigate the impact of ILs on hair's structure. Figure 21 presents the thermogram of recovered material from dissolution with $[C_2C_1Im][Me_2PO_4]$ and the comparison with neat IL and water-soluble fraction.

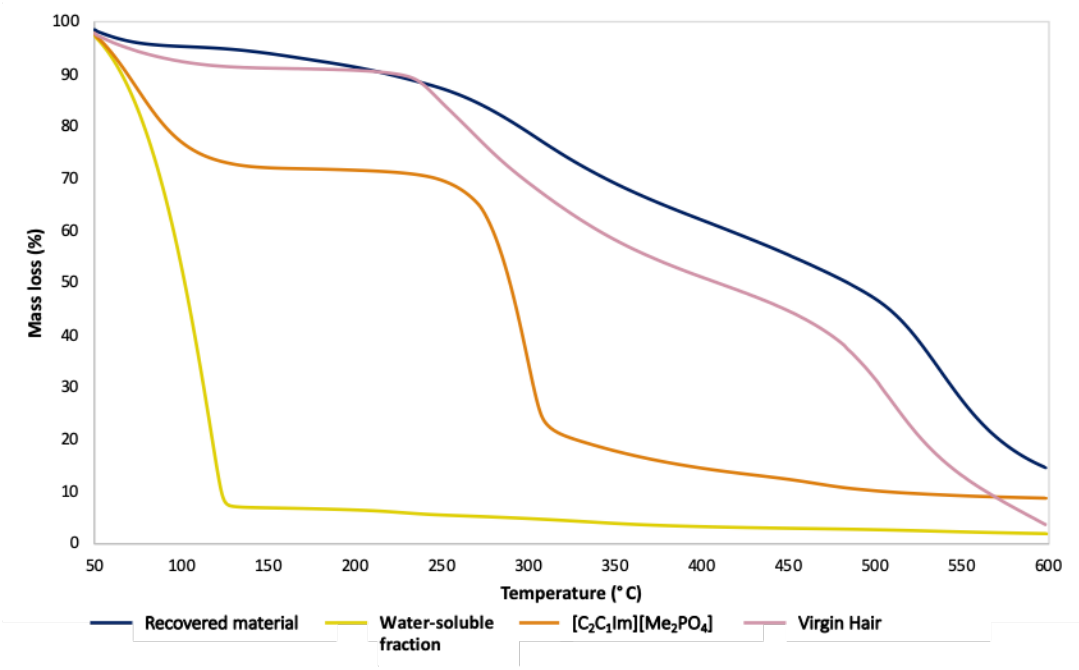


Figure 21. Thermogravimetric analysis of dissolution of European curly hair with $[C_2C_1Im][Me_2PO_4]$ assisted by microwave irradiation.

The analysis of Figure 21 showed some differences on the thermogram of curly hair from conventional heating dissolution with same IL. The thermogram of recovered material *via* microwave radiation (Figure 21) showed identical losses of mass to those observed for chemically untreated hair, which may indicate that both dissolution techniques have different impact on hair's structure. The number of mass losses are the same between the recovered material and the chemically untreated hair thermogram (three), which may indicate that dissolution with $[C_2C_1Im][Me_2PO_4]$ assisted by microwave radiation does not disturb the structure of hair the same way as conventional heating method. The mass percentage of the recovered material at 600° C is higher than zero and this may suggest that more mass may be lost at higher temperatures. The water-soluble fraction shows a small mass loss after 100° C in its TG profile, which may indicate that some hair material is still in the IL solution phase. However, the water-soluble fraction may still contain IL, and hence the mass loss may be associated to the IL degradation.

The recovered material from dissolution with $[C_2C_1Im][OAc]$ assisted by microwave shows similar thermogram behaviour has the conventional heating dissolution with $[C_2C_1Im][OAc]$. Figure 22 compares the recovered material from the dissolution with $[C_2C_1Im][OAc]$ assisted by microwave radiation with chemically untreated hair.

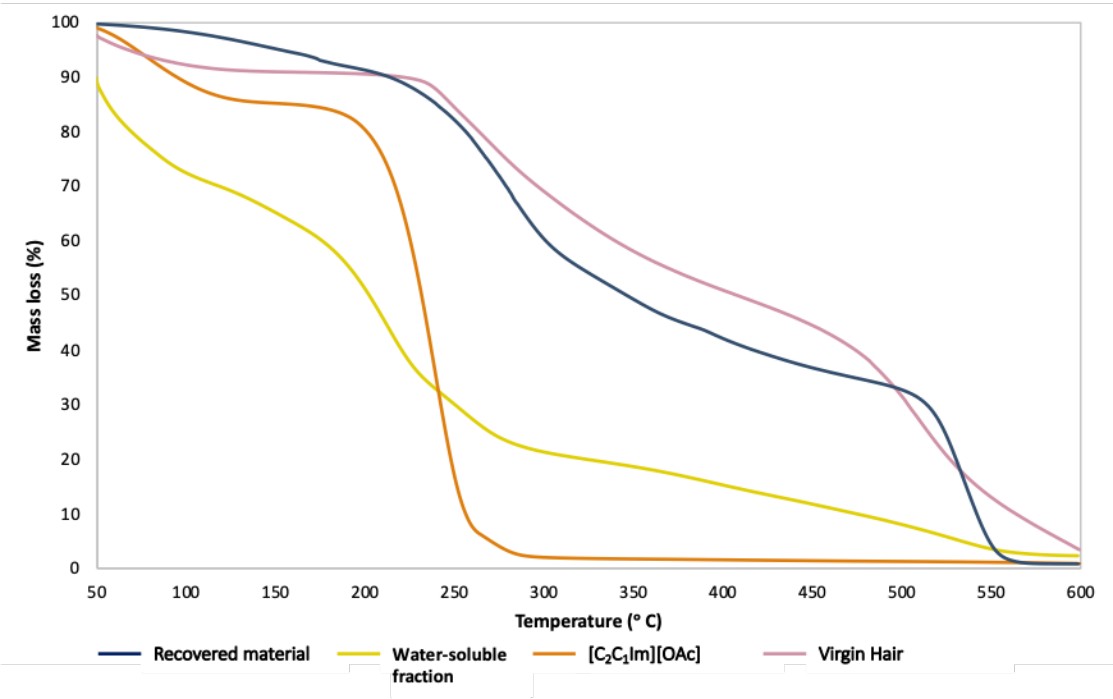


Figure 22. Thermogravimetric analysis of dissolution of European curly hair with $[C_2C_1Im][OAc]$ assisted by microwave irradiation.

The thermogram of the recovered material showed similar mass losses to that of chemically untreated hair. The last mass loss around 525° C is slightly shifted towards higher temperatures when compared to the chemically untreated hair (500° C). The water-soluble fraction exhibited the first mass loss at 200° C, which is related to IL, followed by another at 250° C related to hair material decomposition and finally the one last that may be associated to chemically untreated hair as it matches its thermogram. What is more, this indicates that the water-soluble fraction may still contains hair material in the form of the aforementioned precipitate which was not possible to be separated. As before, it is not possible to conclude on the nature of this hair material.

3.3.4 Material recovery from dissolution of hair from different ethnicities

The conditions of the dissolution of hair from different backgrounds performed with $[C_2C_1Im][OAc]$ did not show any significant dissimilarities among hair types. Nonetheless, the study of the recovered material must be carried out in order to understand a) whether

or not it is possible to recover material from the dissolution and b) what is the composition of this material.

The results of recovered material from different hair types are presented in Table 16. The detailed data can be accessed in Table 25.

Table 16. Scheme of the mass of recovered material from dissolution of different hair types with $[C_2C_1Im][OAc]$. *Value from one measurement as the remaining two were corrupted.

Mass of hair initially added w(g)	European Curly	European Straight	European Blonde	Asian
0.0800 ± 0.0034	56.3% ± 38.9%	86.1% ± 14.5%	53.5% ± 8.0%	24.1% ± 11.0%
0.1000 ± 0.0048	39.9% ± 18.9%	76.3% ± 8.1%	*	30.7% ± 6.4%
0.1500 ± 0.0047	33.5% ± 26.5%	33.3% ± 26.0%	79.1% ± 9.7%	30.5% ± 17.7%
0.2000 ± 0.0207	8.1% ± 0.2%	63.8% ± 19.9%	19.5% ± 25.0%	14.2% ± 18.2%
0.2500 ± 0.0102	30.0% ± 29.2%	24.6% ± 13.4%	25.9% ± 12.7%	29.2% ± 11.4%

Comparison of the weight of recovered material with initial mass of hair dissolved, the mass of hair dissolved initially increases down the columns.

The results from the recovered material from different hair types did not show significant differences among hair types. As mentioned before, some variations may be related to experimental errors during the recovery process, as some material is lost during decantation of the recovered material from the water-soluble fraction. Also, the optimum ratio of IL to hair was studied considering time and the highest amount of hair recovered after dissolution. The summary of this investigation is shown in Table 17 below.

Table 17. Summary of the optimum ratio of $[C_2C_1Im][OAc]$ to hair for each hair type.

Hair type	Hair w(g)	IL w(g)	Average Time (hours)	STDEV Time (hours)	Average Recovered material (g)	STDEV Recovered material (g)	Recovered material (%)
European Curly	0.08	0.77	11	0	0.0751	0.0729	56.3% ± 38.9%
European Straight	0.08		17	5	0.1276	0.0397	86.1% ± 14.5%
European Blonde	0.15		43	0	0.1187	0.0146	79.1% ± 9.7%
Asian	0.10		12	6	0.0730	0.0284	30.7% ± 6.4%

What stands out in Table 17 is the dissolution of straight and blonde hair allows the highest amount of recovered material. However, blonde hair takes the longest to be dissolved yet this could be due to the highest weight of initial hair. When we compared the same amount of hair dissolved, 0.08g of hair, blonde hair presents the longest time to be dissolved. As stated in section 1.2.2, hair from different ethnicities don't show differences on their structure. Nonetheless, it would be expected that lighter hair would dissolve faster when compared to darker hair, due to a less crosslinked structure of lighter hair than darker hair.[22] Moreover, dark hair has tightly packed melanin content.[273] This might indicate why is difficult to dissolve and recovered material from dark hair. However, this might explain the lowest recovered material percentage for European curly and Asian hair, but not why European straight hair shows higher recovered material percentage.

3.3.5 FTIR spectroscopy of the recovered material

To further understand the composition of the recovered material, FTIR spectroscopy was the technique selected. In this study, the recovered material from the dissolution of hair with $[C_2C_1Im][OAc]$ was supported on KBr pellets and analysed by transmission FTIR spectroscopy, through the investigation of the characteristic vibrational modes.

The IR spectrum is shown in Figure 23 and shows similar characteristics bands of those found for human hair, such as 3500 cm^{-1} (OH water network), 3280 cm^{-1} (NH stretching)

and the Amide I (1690-1600 cm^{-1}), Amide II (1575-1480 cm^{-1}) and Amide III (1320-1210 cm^{-1}) bands were identified with this technique.[205] Moreover, the band at approximately 1040 cm^{-1} is assign to the cysteic acid vibrational band ($-SO_3^-$) and as mentioned in section 1.5.3.2, this region can provide information about chemical changes on hair, more precisely the oxidation of the cystine disulfide.[222,223]

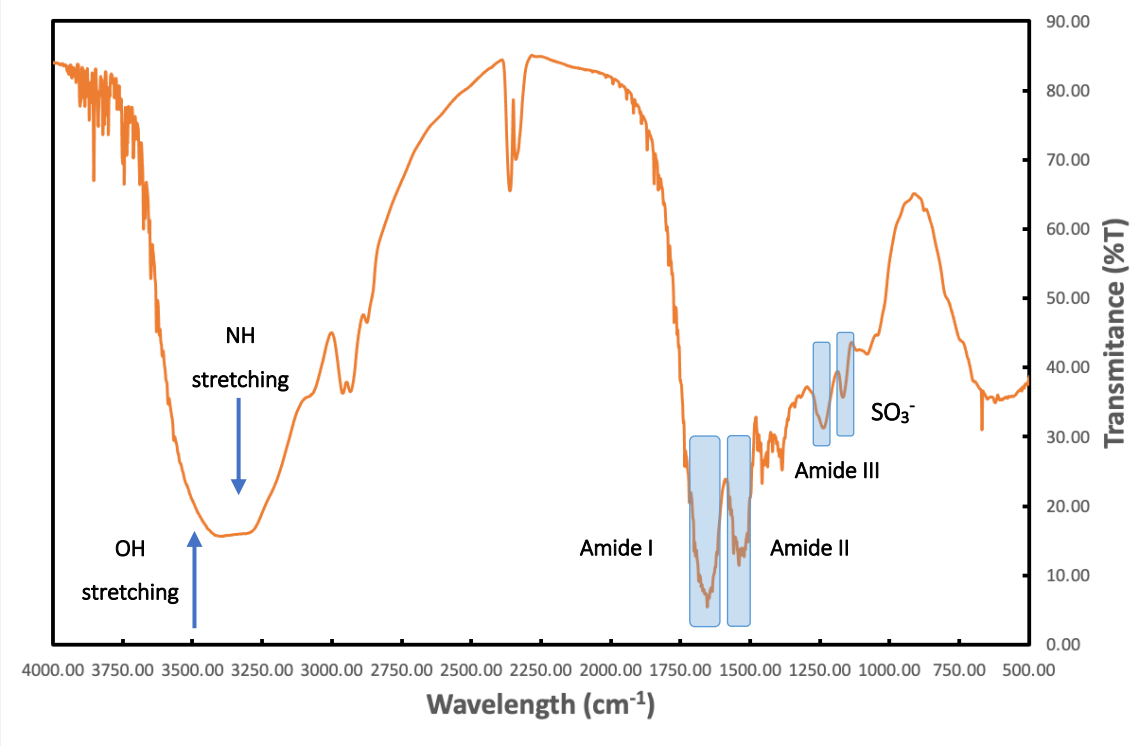


Figure 23. FT-IR spectra of recovery material from the dissolution of European curly hair with $[C_2C_1Im][OAc]$.

The results of this investigation are in agreement with the ones reported by Singh and Prasad.[131] Overall, the vibrational profile of the recovered material shows similarities to the spectrum of the human hair, Figure 8. Although the cysteic acid band was observed this was not enough to confirm modifications in the structure of keratin. The comparison between these spectra, *i.e.* Figure 8 and Figure 23, should be made carefully as the spectra were obtained by different FTIR techniques. However, the analysis in this section helped to further identify the chemical composition of the recovered material and showed identical conclusions from the ATR-FTIR analysis.

3.4 Chemical characterisation (MALDI)

MALDI-TOF was the technique selected to characterise recovered material from dissolution with $[C_2C_1Im][OAc]$ and $[C_2C_1Im][Me_2PO_4]$, due simple sample preparation. Samples were placed on top of the support and the matrix was placed on top of the samples. The samples were left to dry for a couple minutes and then analysed. Each sample was analysed three times, as MALDI-ToF is not an invasive technique.

The first step on this study was to determine the natural proteins present in human hair on literature.[24] After that, the molecular weight (m/z) of these proteins was identified. Only proteins in human hair structure between 20 kDa and 200 kDa were considered, value selected having into consideration KAP molecular weight.[24] Literature reported some proteins below this range such as KAP2-1 to KAP2-4, KAP3-2, KAP 3-3 and KAP11-1, however in this particular test we supressed the analysis below 20 kDa.[24]

Hair proteins can be in four different parts of the hair, as shown in Figure 24.

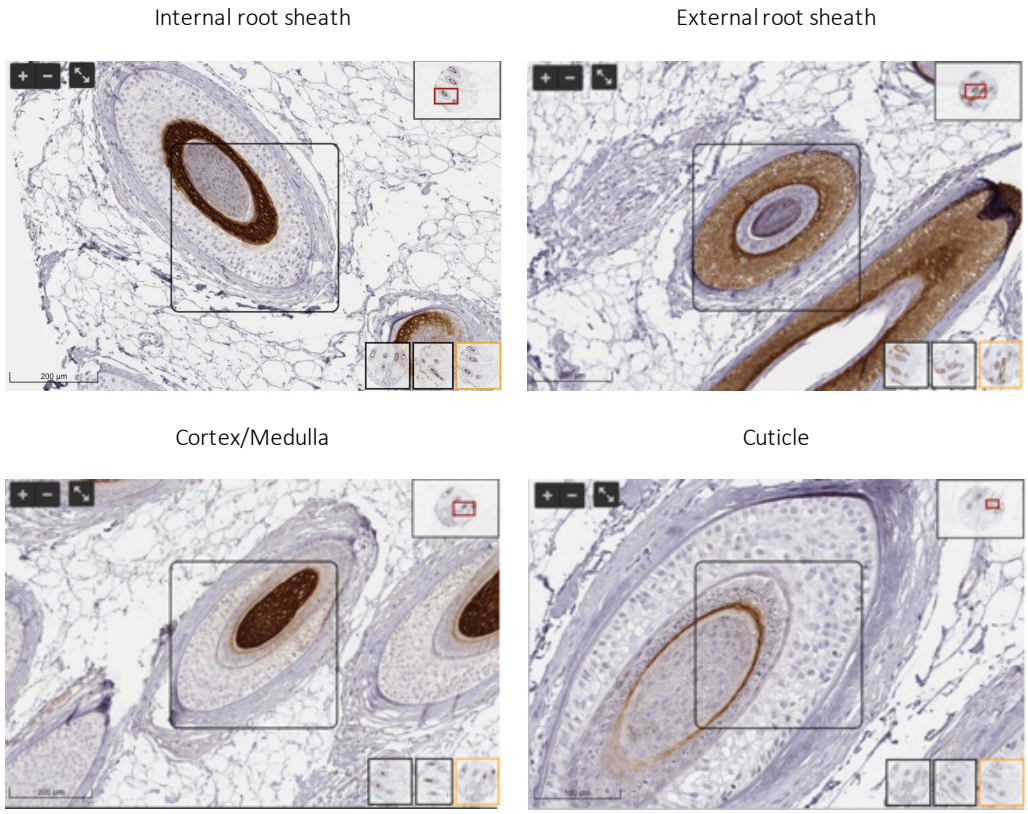


Figure 24. Location of proteins in human hair structure. The brown colour represents the location of the protein in the hair structure. The higher intensity of the colour, the higher quantity level of proteins. Adapted from reference 274.

The locations internal and external root will not be considered as these locations do not belong to the hair fibre, so in this current study only proteins located in the cortex/medulla and cuticle will be considered. Images presented in Figure 24 were obtained from literature.[274]

The proteins to be considered are represented in Table 18. Keratin can be divided into super families, which comprise one of the major groups of structural proteins. The proteins identified from MALDI analysis will be compared with Keratin known in literature.[24]

Table 18. Keratin proteins for MALDI analysis. Data from reference 24 and 274.

m/z of Protein (kDa)	Keratin	Location of the protein in the hair structure
35.3	HOXC13	Cortex/Medulla
53.9	KAP16-1	Cuticle
27.7	KAP24-1	Cuticle
47.2	KRT31	Cortex/Medulla
45.9	KRT33A	Cortex/Medulla
46.2	KRT33B	Cortex/Medulla
49.4	KRT34	Cortex/Medulla
55.9	KRT72	Cuticle
54.9	KRT81	Cortex/Medulla
56.7	KRT82	Cuticle
54.2	KRT83	Cortex/Medulla
55.8	KRT85	Cortex/Medulla
53.5	KRT86	Cortex/Medulla

There are two types of keratin compounds in hair structure, type I (acidic) and type II (basic). The type I is divided into 10 groups, KRT31-40. The molecular range varies between 45.9 and 49.4 kDa. On the other hand, the type II keratins are distinguished into six groups, which are KRT81-86, the molecular range of these keratins is 53.5 to 54.9 kDa. From type I group, only KRT31, KRT33A-B and KRT34 will be considered due to their location in hair structure. Type I proteins are characterised by their higher amount of cysteine and proline residues.[275] Keratin KRT31 is a major component of the cortex/medulla of the hair structure, this proteins contributes to the strength of the hair shaft.[276] Chemical

treatments on hair, such as bleaching, promotes damage in hair by penetrating deep within the hair fibre and cleaving the KRT31, which decreases the strength of hair.[277]

The ionization of recovered material during MALDI technique is not fully understood, therefore to investigate the proteins in hair structure, the average of the three results obtained with this analysis was used in this study. Table 19 presents the results of MALDI analysis of recovered materials from dissolution with $[C_2C_1Im][OAc]$.

Table 19. MALDI analysis of recovered material from $[C_2C_1Im][OAc]$ dissolution. NF=Not Found

m/z of Proteins (kDa)					
Curly	Straight	Asian	Blonde	Keratin	Protein location
45.4	NF	45.0	45.3	KRT33A	Cortex/Medulla
46.7	46.3	46.0	46.4	KRT33B	Cortex/Medulla
NF	47.5	NF	47.4	KRT31	Cortex/Medulla
49.9	49.4	49.8	49.4	KRT34	Cortex/Medulla
53.5	53.6	NF	53.5	KAP16-1	Cuticle
54.2	54.1	54.0	54.6	KRT83	Cortex/Medulla
55.5	55.6	55.1	55.1	KRT85	Cortex/Medulla
56.4	56.3	56.4	56.6	KRT82	Cuticle

All recovered materials showed proteins located at cortex/medulla and cuticle of initial hair structure. However, not all keratin proteins listed in Table 18 were found on recovered material from the dissolution of different hair types. Similarly, Table 20 shows the results of proteins presented in recovered material from dissolution with $[C_2C_1Im][Me_2PO_4]$.

Table 20. MALDI analysis of recovered material from $[C_2C_1Im][Me_2PO_4]$ dissolution. NF=Not Found

m/z of Proteins (kDa)					
Curly	Straight	Asian	Blonde	Keratin	Protein location
45.6	45.0	45.6	NF	KRT33A	Cortex/Medulla
NF	46.3	46.4	NF	KRT33B	Cortex/Medulla
47.5	47.7	47.3	47.1	KRT31	Cortex/Medulla
49.1	49.6	49.5	49.7	KRT34	Cortex/Medulla
53.4	53.6	53.4	NF	KAP16-1	Cuticle
54.4	54.2	54.7	NF	KRT83	Cortex/Medulla
55.6	55.5	55.5	NF	KRT85	Cortex/Medulla
56.7	56.4	56.5	56.2	KRT82	Cuticle

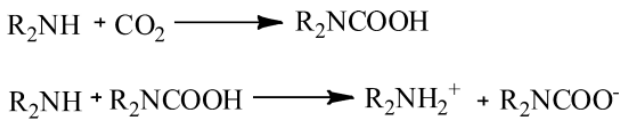
Results from Table 20 are very similar to proteins found in recovered material from acetate based ILs. However, analysis of recovered material from blonde hair dissolution with $[C_2C_1Im][Me_2PO_4]$ was difficult to achieve which is reflected in the lack of results. However, this is not fully understood, and it might be related to the way ILs dissolve hair. From the thermal stability of the recovered material it was possible to conclude that dissolution with two anions, acetate and dimehtylphophate, is different. This aligns with MALDI results, and at least with blonde hair it is possible to conclude that dissolution is different.

MALDI analysis on the recovered material helped to understand its composition. Nevertheless, during this investigation some challenges were faced. The lack of a database was one of them, also the preparation and the finding for the best matrix was very difficult to achieve. However, this technique seems promising for the analysis of recovered material.

3.5 Dissolution of hair with distillable ionic liquids

The recovery process proved to be a complex task, mainly because of the highly affinity of the recovery material with IL. Furthermore, dark colour of the recovered material and the water-phase fraction may be an indication of the presence of melanin. The extraction of melanin and further precipitation of keratin was not possible to achieve, contrary to of was reported in literature.[131] To improve this method investigations were done. Initially, a different class of IL was investigated, this new class of ILs belongs to protic class and, frequently they are distillable, which results on its ability to reverse back-transfer of the labile proton.[175,278–283] These classes of ILs are formed when CO_2 and a secondary dialkylamine are combine in a specific ratio (1:2).[284–292] A scheme of this reaction is shown in Scheme 1, where the carbamic acid adduct is generated during a Lewis acid/base reaction, followed by the loss of a proton to a second mole of amine to form the dialkyl ammonium cation and dialkylcarbamate anion.

Scheme 1. Scheme of distillable ILs reaction, where CO_2 and a secondary dialkylamine in an approximate 1:2 ratio form a distillable IL. Scheme adapted from reference 293.



The product of this reaction, in the majority of the cases, is liquid at suitable temperatures. This family of ILs allows the ability to dissolve an extensive range of organic compounds with the great facility to recover the ILs after dissolution. The ILs is easily distilled under moderate temperatures, and this process is facilitated due to the release of CO_2. After additional cooling inside the condenser, the IL is recombined and ready to be reused.[294] Hair dissolving and distillable ILs would allow to recover the totality of dissolved hair and circumvent the hair material to be retained in the IL phase during the regeneration process. In this study, three ILs were selected, *N,N*-dipropylammonium *N',N'*-dipropylcarbamate (DPCARB), bis(2-ethylhexyl)ammonium bis(2-ethylhexyl)carbamate (DBCARB) and 1,1,3,3-

tetramethylguanidinium acetate, [TMGH][OAc] (see section 5.1.2.3). These ILs were selected due to their potential ability to dissolve hair.[293] A study showed, [TMGH][OAc] has the ability to dissolve 5 wt% of microcrystalline cellulose at 100° C within 18 hours.[294] The temperature of dissolution was carefully selected to each IL to avoid distilling it during the experiment. DPCARB presents the lowest boiling point, 52° C, while DBCARB is distillable at a temperature range between 59 and 113° C.[293] [TMGH][OAc] has the highest boiling point at 165° C.[294] The dissolution of hair with distillable ILs is summarised in Table 21.

Table 21. Dissolution of hair with distillable ILs. ND = no dissolution in 48 hours

IL	Hair wt (g)	IL wt (g)	Dissolution time (hours)	Temperature (° C)
DPCARB	0.0802	0.7732	*ND*	40
DBCARB	0.0811	0.7746	ND	40
[TMGH][OAc]	0.0808	0.7755	ND	100

The dissolution of hair with distillable ILs was performed for 48 hours, with temperature kept under control to ensure ILs were not distilled during dissolution. However, after 48 hours it was not possible to observe any evidence of dissolution of hair. ILs remained colourless and hair fibres did not show any change with the naked eye. Nevertheless, SEM analysis of the fibres should be performed to determine whether any modification occurred at cuticle level. However, this was not possible to be performed at the time of this investigation.

3.6 Conclusions

The aim of this Chapter was to understand whether it was possible to recover material from dissolution of hair. Recovery of material was possible by the addition of water, which promotes the precipitation of some material. This material was analysed to investigate their chemical composition and then speculate the possible dissolution process of hair with ILs.

The recovered material from dissolution with $[C_2C_1Im][OAc]$ showed the lower results for recovered material weights when compared with dimethylphosphate-based IL. It was shown that as the initial mass of dissolved hair increased, the recovery material weight decreased. This could be a consequence of experimental errors, yet it may also be related to the way different ILs dissolve hair. One hypothesis can be the way that acetate anion cleaves hydrogen and disulfide bonds and the affinity of these particles to IL phase, which results in less recovered material as the majority has been retained within the IL. The recovered materials were later analysed to better understand their chemical composition. FTIR spectroscopy of the recovered material from the dissolution of hair with $[C_2C_1Im][OAc]$ did not show structural changes in the human hair proteins. Furthermore, this investigation showed similar results to the ones reported in literature for the dissolution of hair with TBAH.[131]

SEM was the technique selected to investigate the morphology of the recovered material, moreover EDX analysis helped with elementary characterisation. The morphology of the recovered material was demonstrated to be different from chemically untreated hair and it was possible to conclude that cuticle presents more sulfur content than the cortex by EDX analysis.

The thermal analysis of recovered material showed different behaviour depending on IL used on dissolution, however all hair types showed similar results. Also, it was observed the formation of a precipitate layer in the water-soluble fraction. The thermal properties of the precipitate were also analysed, and it showed the same behaviour as chemically untreated hair. This was observed for all hair types and recovered materials from dissolution of hair with $[C_2C_1Im][OAc]$. On the other hand, recovered material and precipitate from dissolution with $[C_2C_1Im][Me_2PO_4]$ presented similar behaviour, however they had a different thermal profile from chemically untreated hair. The thermal profile of recovered material and precipitate presented a step that belongs to phosphonate materials. That may indicate the presence of IL still in recovered material structure or that dissolution with dimethylphosphate-based IL form different compounds. The thermal profile of recovered material from dissolution of hair with $[C_2C_1Im][Me_2PO_4]$ assisted by microwave seems to present different impact in recovered material structure than conventional heating dissolution method. That may indicate recovered material from

conventional heating dissolution of hair with $[C_2C_1Im][Me_2PO_4]$ may still contain some IL left in their structure.

The last technique in the recovered material characterisation study was MALDI, that technique is very promising, however more investigation on the sample preparation needs to be further investigated. In this analysis only the keratin present in hair's cortex/medulla and cuticle were considered and it was possible to detect some keratins in recovered material structure. However, it was not possible to conclude about some differences among recovered materials from dissolution of hair with different ILs.

In the last section of this Chapter the possibility of dissolution of hair with distillable ILs to improve the recovery method was investigated. After dissolution of hair, these ILs would be distilled and then avoid the affinity of the hair particle with IL phase. However, the distillable ILs investigated in this Chapter were not able to dissolve hair. This might be due to the lower temperature of dissolution, as the maximum temperature of dissolution with DPCARB and DBCARB was 40° C. However, [TMGH][OAc] was studied at 100° C and dissolution of hair was not observed. The next step should be the investigation on the morphology and structure of hair, as the dissolution did not occur it might be impacted the morphology/structure of hair. Though, visually it was not possible to observe any modification.

Chapter 4 Modification of hair fibres with ILs and subsequent characterisation

The purpose of the previous Chapters was to investigate the dissolution of hair with ILs and also the characterisation of the recovered material obtained from the dissolution of hair. Nonetheless, another question results from these investigations about whether it would be possible to target specific bonds in hair with ILs to modify the structure of hair, and this is the key aim of the following Chapter.

4.1 Modification of hair fibres with ILs

Hair fibres were covered with IL at 100° C, in order understand if ILs can have an impact on the structure of hair. Visually degradation of the fibres was observed, and for that reason and to better understand what was occurring to the fibres, polarised light microscopy was utilised. In this study, European curly hair was investigated, this is the hair used until otherwise stated. Figure 25 shows the support used to follow this study of a single fibre by microscopy, the single hair fibre was placed on a glass slide fixed with tape and covered with IL, in this particular case $[C_2C_1Im][OAc]$ or $[C_2C_1Im][Me_2PO_4]$. A glass coverslip was placed on top of the hair fibre and the IL, the glass slip was then placed inside an oven set at 100° C. The hair fibre was observed at the beginning of the test and then every 45 minutes, to visually identify structural differences on the hair fibre.

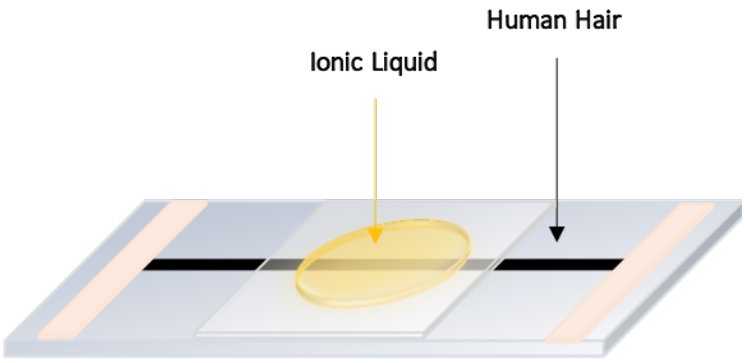


Figure 25. Illustration of the dissolution of a single hair fibre with ILs to be analysed by polarised optical microscopy. Adapted from reference 128.

During this study a modification of the morphology of hair was achieved by both ILs. Furthermore, it was detected that the modification of the morphology of hair with $[C_2C_1Im][Me_2PO_4]$ took longer to occur when compared to $[C_2C_1Im][OAc]$. The modification of the structure of the fibre was detected after 18 hours, while fibres treated with $[C_2C_1Im][OAc]$ took 90 minutes to achieve the same state of alteration. The follow-up of the modification of a single curly hair fibre by $[C_2C_1Im][OAc]$ and $[C_2C_1Im][Me_2PO_4]$ is summarised in Figure 26. The image of the single fibre treated with $[C_2C_1Im][OAc]$ for 90 minutes, in Figure 26, and the image of a single fibre treated with $[C_2C_1Im][Me_2PO_4]$ for 18 hours are the last stage followed by this study, where the fibre is almost dissolved. The dark spots dispersed on the ILs are colour pigments, it might be melanin, from the fibre.

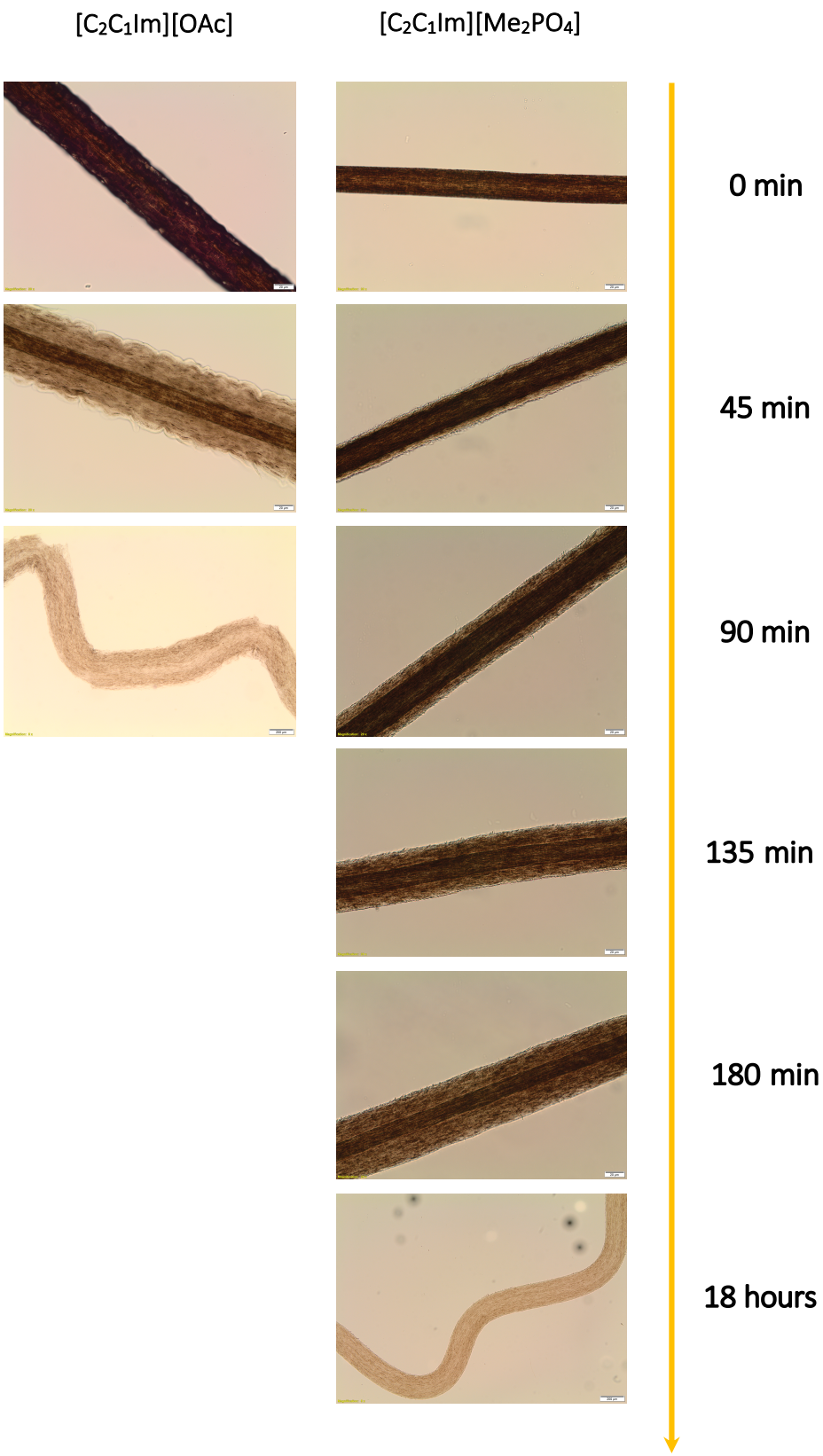


Figure 26. The follow-up of the dissolution of a single curly hair fibre with ILs by polarised light microscopy, Magnification used 20x.

An important observation can be highlighted after the analysis of the pictures in Figure 26, where both ILs showed the swelling of the fibre, at the beginning of this process, and then the dissolution of the cortex. Hair fibre presents a diameter of around 60 and 80 μm but after contact with IL at these conditions, the cuticle swells and the diameter of the fibre increases in comparison with the hair fibre picture.[208] Similarly, it was possible to visualise that the crystallinity of the cortex was decreasing while ILs were penetrating the inner part of the hair fibre. This may suggest that the cortex is the first thing to be affected by the IL, and the cuticle the last.[128] That evidence would be easily supported by the fact that the cuticle presents a higher content of disulfide bonds, while the cortex presents more hydrogen bonds and less cross-linked network.[21,295]

This is a visual study on the dissolution process of hair with ILs, however to better understand the process of dissolution another approach should be taken. During the SEM analysis of a single hair fibre, EDX analysis was also carried out on specific areas of the fibre. Each stage of modification of the structure of hair with ILs was prepared individually, so in total 5 samples were prepared. Two samples from the dissolution with $[C_2C_1Im][OAc]$, one at 45 minutes after the beginning of dissolution and another one closer to 90 minutes. The fibre could not be exposed to $[C_2C_1Im][OAc]$ for more than 90 minutes, as otherwise the damage on the fibre would make the SEM-EDX analysis pointless.

After 45 minutes the fibres on the glass slide were removed from the oven, placed inside the SEM chamber, the same procedure was followed for the other samples analysed in this study. The SEM-EDX analysis was challenging due to the presence of IL on the surface of the fibre, for this reason the fibre could not be detected underneath it. Nonetheless, EDX analysis of the IL on top of the hair fibre was performed to evaluate the presence of components of the hair fibre. Once again, this analysis was not successful as none or very low content of sulfur was detected on the IL on the surface of the hair fibre. To enable the analysis of the fibre, the IL had to be removed, thus the fibre was rinsed with methanol and dried after this step. To confirm that methanol has not had an impact on the surface of hair, control experiment was performed where a single chemically untreated hair fibre was washed with methanol and let it dry, after that the fibre was analysed by SEM. The results of SEM-EDX are presented in Figure 27.

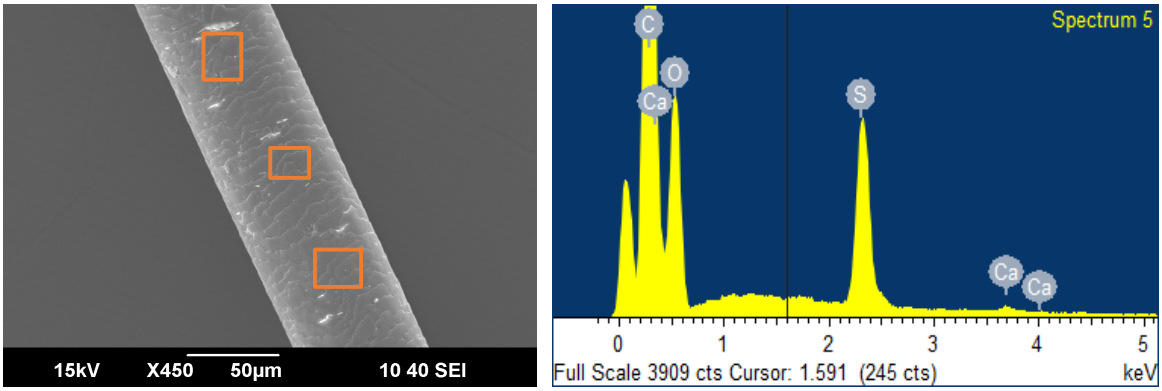


Figure 27. Illustration of SEM images of the hair fibres washed with methanol and analysed after drying. The fibre was analysed by EDX in three different spots represented by the orange boxes in the pictures. Each EDX spectra is an elemental analysis spectrum of one spot in the fibre that represents the elemental analysis in each spot.

After this procedure, the modification of the morphology of the hair fibre with $[C_2C_1Im][Me_2PO_4]$ and $[C_2C_1Im][OAc]$ could then be examined by SEM. The fibres with both ILs were investigated after 45 minutes of the beginning of dissolution. It was expected that the fibre with $[C_2C_1Im][OAc]$ would be half-way through dissolution, while the fibre with $[C_2C_1Im][Me_2PO_4]$ would be at the beginning stage of dissolution. Additionally, the fibre with $[C_2C_1Im][Me_2PO_4]$ was investigated after 90 min from the beginning of the study and then close to total dissolution, this procedure was followed with both ILs. Due to the complexity to remove ILs without losing the fibre components after total dissolution, the total dissolution of the fibre was not investigated by SEM. Figure 28 shows the SEM images and EDX spectra of single fibres during different stages of dissolution with $[C_2C_1Im][OAc]$ and $[C_2C_1Im][Me_2PO_4]$. During SEM analysis, EDX was performed to evaluate the sulfur content presented in the fibre during different stages of dissolution. In each fibre three spots with different dimensions were analysed. The spectra in the Figure 28 a1) and b1) correspond to one spot on the fibre, however the spectra did not show significant variations on the elemental analysis among the spots analysed, therefore only one spectrum is presented.

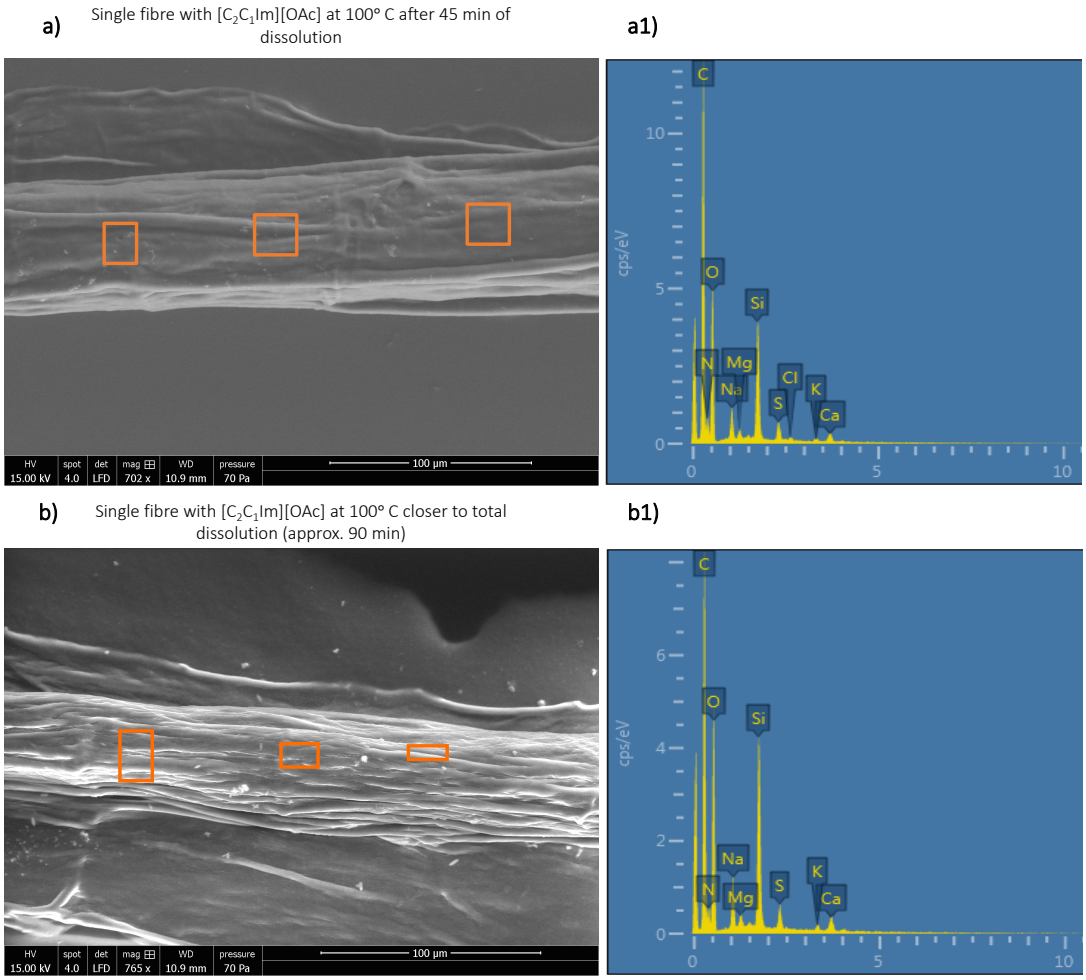


Figure 28. Illustration of SEM images of the dissolution of hair with $[C_2C_1Im][OAc]$. Each fibre was analysed by EDX in three different spots represented by the orange boxes in the pictures. Each EDX spectra is an elemental analysis spectrum of one spot in the fibre that represents the elemental analysis in each spot.

After 45 minutes of the beginning of the study, a single fibre with $[C_2C_1Im][OAc]$ showed a partial dissolution state, as shown in Figure 28b) where the fibre is very damaged. Although EDX analysis is only a quantitative analysis, it did not show any variation on the sulfur content of the hair fibre during dissolution. Nevertheless, previous analysis of SEM-EDX on chemically untreated hair fibres showed sulfur weight (%) around 5%, which is much higher than the sulfur content detected during dissolution. The results of the elemental analysis by SEM-EDX on chemically untreated hair fibres are shown in Table 22.

Table 22. Elemental analysis by SEM-EDX on chemically untreated hair fibres.

Element	Weight%
Carbon	52.33
Oxygen	28.05
Sulfur	**4.84**

The same procedure was followed with $[C_2C_1Im][Me_2PO_4]$, as shown in Figure 29. Each fibre was analysed by EDX in three different spots represented by the orange boxes in the pictures. The spectra in the Figure 29 a1), b1), c1) correspond to a single spot on the fibre, but as no significant variations were detected on the elemental analysis among the spots analysed, only one spectrum is presented.

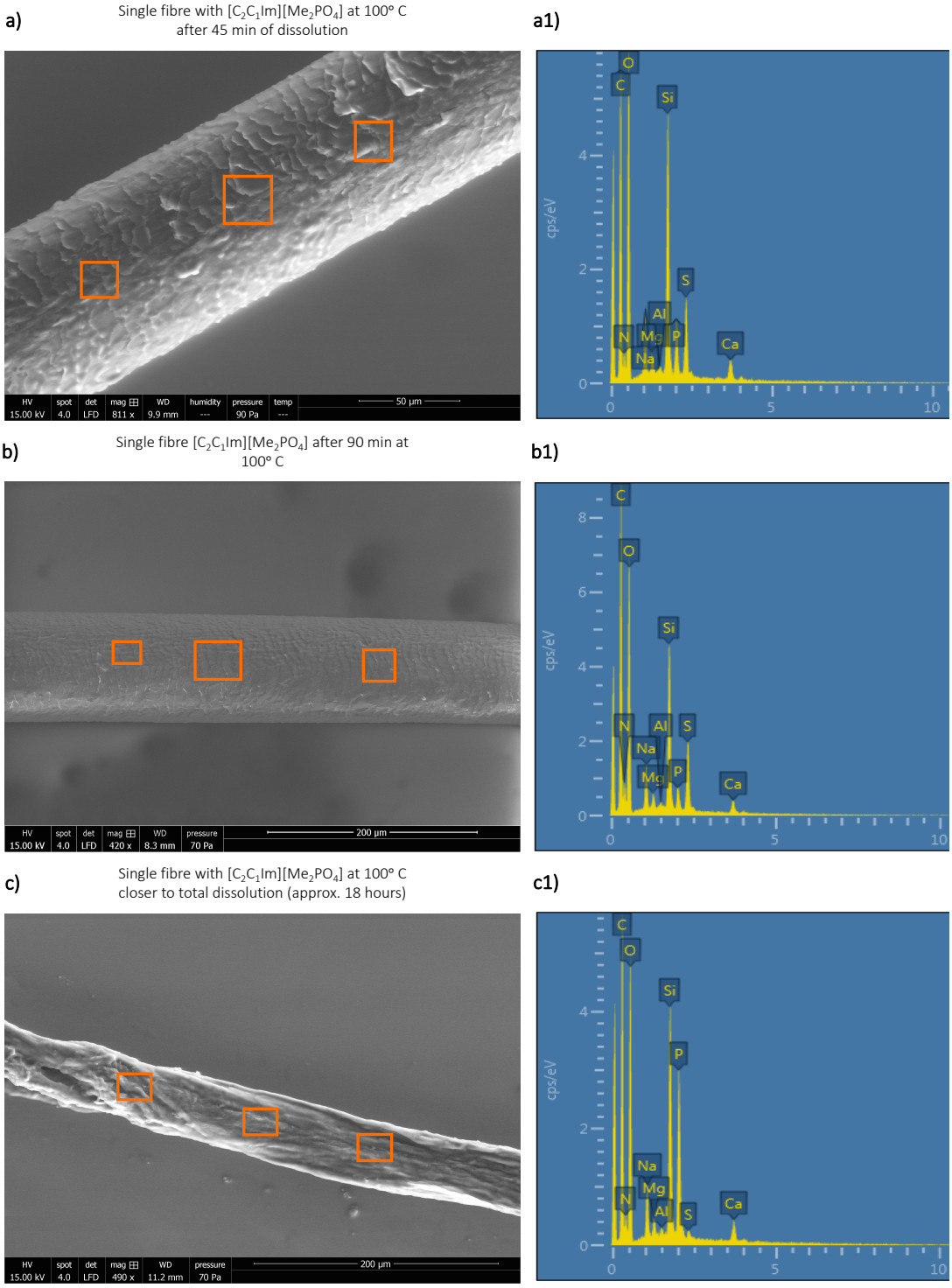


Figure 29. Illustration of SEM images of the dissolution of hair with $[C_2C_1Im][Me_2PO_4]$. Each fibre was analysed by EDX in three different spots represented by the orange boxes in the pictures. Each EDX spectra is an elemental analysis spectrum of one spot in the fibre that represents the elemental analysis in each spot.

Figure 29 a) and b), shows the fibre after 45 and 90 minutes at the beginning of the dissolution, and did not present any visual variation on the morphology of the fibre and by EDX analysis the sulfur content did not change considerably. The partial dissolution was reached after 18 hours. EDX analysis performed closer to that period showed that the sulfur content was reduced drastically.

The partial dissolution of hair by both ILs presented a reduction on the sulfur content. This may indicate that the cuticle has been modified or degraded since the higher sulfur content is presented in the cuticle of hair fibres. Table 23 compares the sulfur content among chemically untreated hair and the fibres from the partial dissolution of hair by both ILs. Table 23 shows that sulfur content is higher for fibres from the partial dissolution of hair with $[C_2C_1Im][OAc]$. Nevertheless SEM-EDX can only offer both semi-qualitative and semi-quantitative information, therefore what it is possible to conclude from this technique is that fibres from partial dissolution present lower sulfur content than chemically untreated hair.[296]

Table 23. Comparison of the elemental analysis by SEM-EDX on chemically untreated hair fibres with fibres dissolved with $[C_2C_1Im][OAc]$ and $[C_2C_1Im][Me_2PO_4]$.

Element	% Weight Chemically untreated hair	% Weight $[C_2C_1Im][OAc]$ (b) Figure 28)	% Weight $[C_2C_1Im][Me_2PO_4]$ (c) Figure 29)
Sulfur	4.84	2.81	1.42

To have a deeper understanding of the impact of the IL on the structure of hair, the fibres from the partial dissolution were analysed by Time-of-Flight Secondary Ion Mass Spectrometry (ToF-SIMS). Depth profile was the method selected to understand if any modification occurred and, when so, if those modifications were only at cuticle level or deeper in the cortex of hair. This technique can provide detail of the chemical composition and distribution of the hair sample surface, but also depth profile allows the analysis in a cross section of the fibre. The properties of the hair and the complexity of the hair structure make this analysis challenging.[250,251,297] ToF-SIMS uses an incident ion

source to impact on the solid samples, in our study hair samples, and generates secondary ions that then can be analysed by a time of flight mass spectrometer.[298] This way it is possible to determine the chemical composition of the hair surface.

For comparison proposes, European chemically untreated curly hair was analysed following the same parameters. Negative charges were performed with all samples. The analysis of hair by ToF-SIMS was challenging due to the nature and complexity of the sample. The analysis was carefully performed to guarantee the analysis of a single fibre. Due to the proximity of fibres, the beam can target more than one fibre, which could compromise the accuracy of the results.

Figure 30 presents the depth profile of chemically untreated hair under negative polarity. The analysis was performed with SH^- residue as a target. This way, it could be easier to identify modifications on the hair fibre treated with IL, since ILs are free of sulfur. Sputter time was considered higher than 1200 seconds (s) for this analysis, to guarantee the total penetration of the fibre. Similarly, other amino acids were analysed throughout this study, but due to similarities with ILs and complexity of the spectrum those are not presented in this section.

The purpose of this analysis is to investigate the SH^- residue profile from cuticle to the deeper hair structure, such as the cortex. Having that information, it would be possible to compare hair fibres modified by ILs.

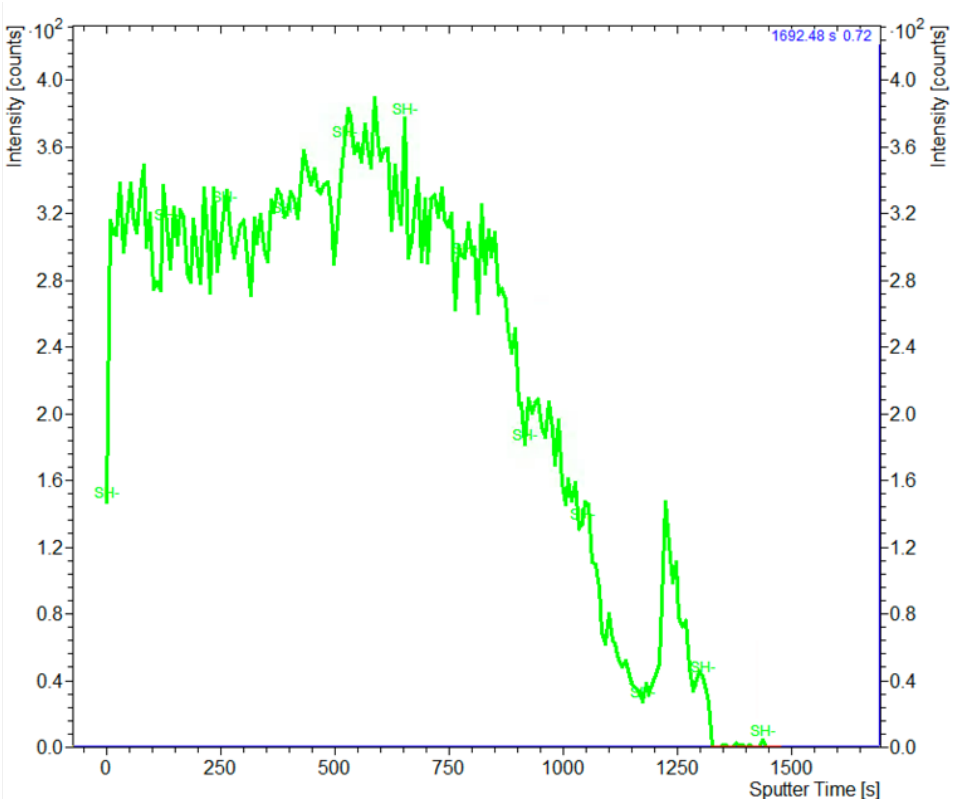


Figure 30. ToF-SIMS depth profile of European chemically untreated curly hair at negative polarity.

The analysis of the data in Figure 30 allowed to conclude that the sulfur content in the hair structure decreases along the fibre. It is possible to observe sulfur content can be considered stable until approximately 600 s, which may be associated to content in the cuticle (outer surface of hair). After that, the sulfur content drops as the beam reached the hair cortex, since sulfur content decreases from cuticle to cortex. After 1100 s sulfur content reaches another peak, which may indicate that another fibre is being analysed. A map of SH^- residue along the fibre was produced and the images of that analysis can be found in Figure 31.

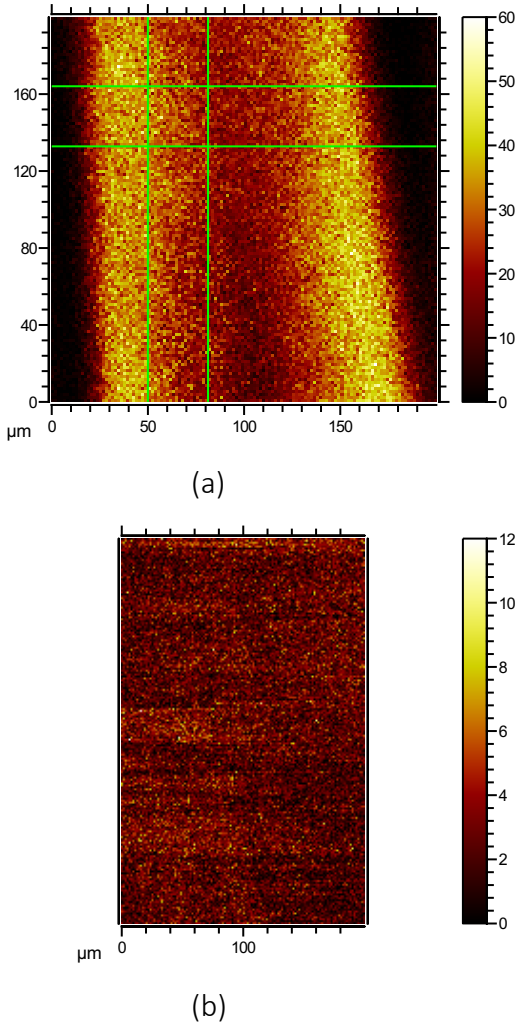


Figure 31. Image map of a single European chemically untreatedcurly hair fibre. (a) Total of SH^- residue throughout hair fibre, XY slice (cuticle of the fibre); (b) Total of SH^- residue throughout hair fibre, YZ slice (cross-section of the fibre – cuticle-cortex-cuticle). The bar represents the intensity (counts per ion) of SH^- residues, lower intensity (black) and maximum of intensity (yellow).

Figure 31 shows the distribution of SH^- from the cuticle to the cortex of the fibre, where is possible to conclude the limited content of sulfur in the middle of the fibre (cortex). The depth profile analysis of hair fibre treated with $[C_2C_1Im][OAc]$ was performed in same conditions as chemically untreated hair analysis. Hair fibres were highly damaged after IL treatment which is thought to have affected the results. Next, Figure 32 shows the depth profile of selected amino acid residues to study the hair's structure after treatment. In this discussion, only SH^- residue will be included due to the absence of sulfur in the ILs structure.

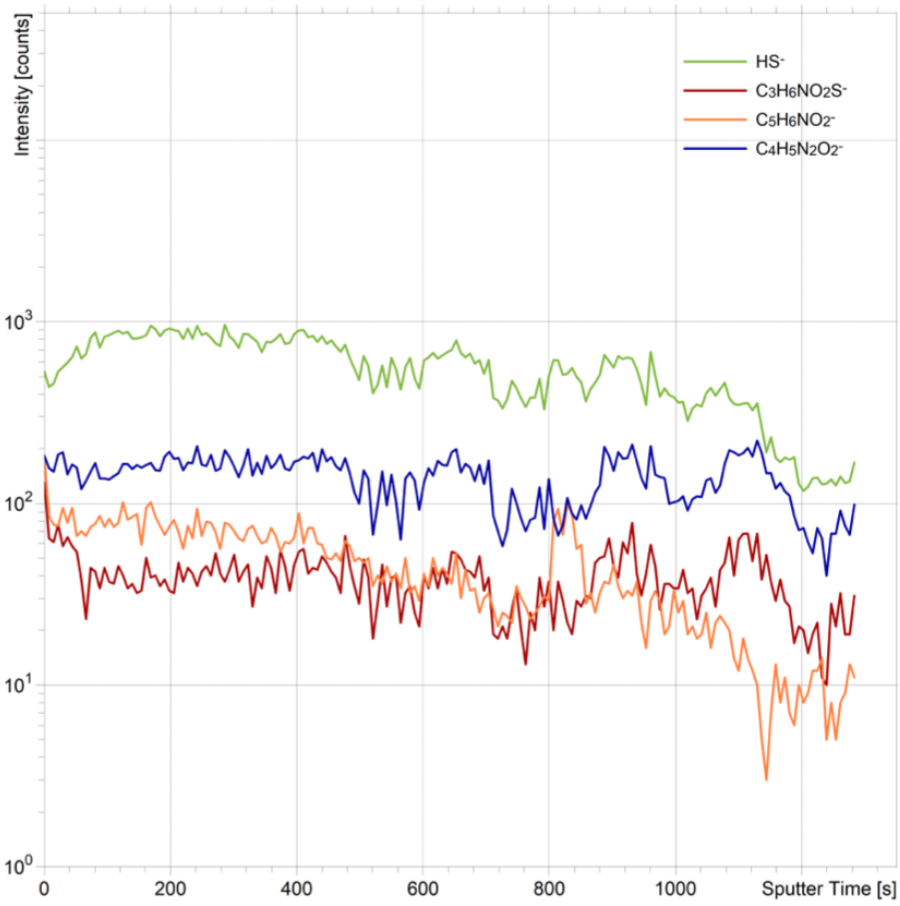
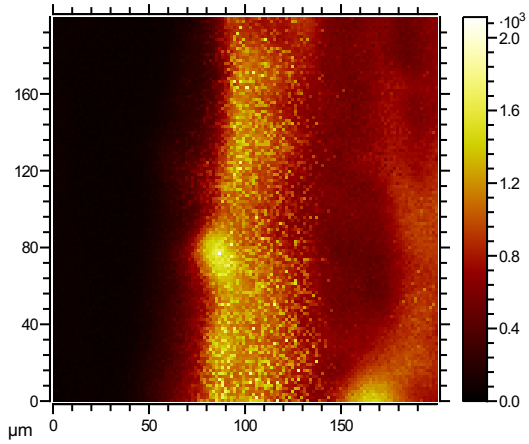


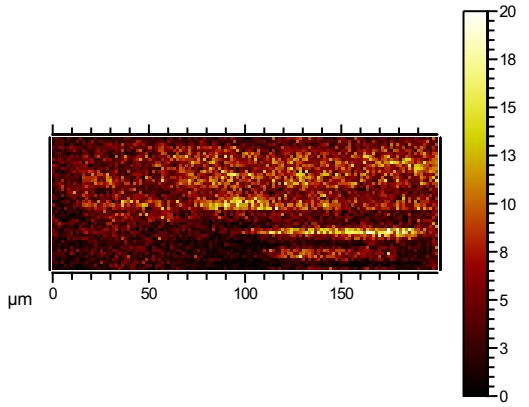
Figure 32. ToF-SIMS depth profile of hair fibre treated with $[C_2C_1Im][OAc]$ for 30 minutes at 100° C, negative polarity.

Once again, the analysis of these hair fibres was a challenge due to difficulty targeting only one fibre and due to the extremely damaged degree of the fibres after treatment with ILs.

According to Figure 32, no modification throughout the fibre were observed. Besides the noisy baseline, sulfur content was not seen to change during the analysis. Additionally, ToF-SIMS ion images were collected during analysis as shown in Figure 33.



(a)



(b)

Figure 33. Image map of a single hair fibre treated with $[C_2C_1Im][OAc]$ for 30 minutes at 100° C. (a) Total of SH^- residue throughout hair fibre, XY slice (cuticle of the fibre); (b) Total of SH^- residue throughout hair fibre, YZ slice (cross-section of the fibre – cuticle-cortex-cuticle). The bar represents the intensity (counts per ion) of SH^- residues, lower intensity (black) and maximum of intensity (yellow).

Figure 33 provides an overview of the highly damaged stage of the fibre, similarly an analysis of SH- residue on the YZ plane of the fibre was analysed. This plane is a cross-section of the fibre, and it is possible to identify the distribution of SH- residue throughout the fibre, which is not uniform. Yet, due to the fibre degradation it is not possible to conclude what has been changed in the structure of hair after IL treatment.

The same analysis was performed on hair fibres treated with $[C_2C_1Im][Me_2PO_4]$, Figure 34.

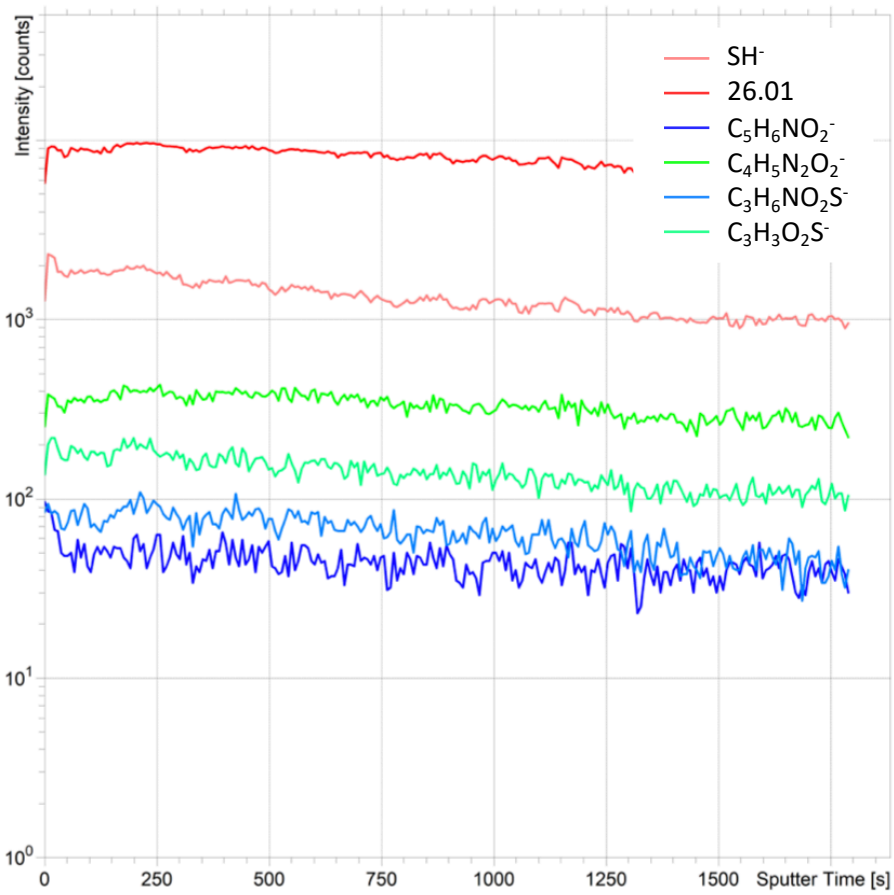
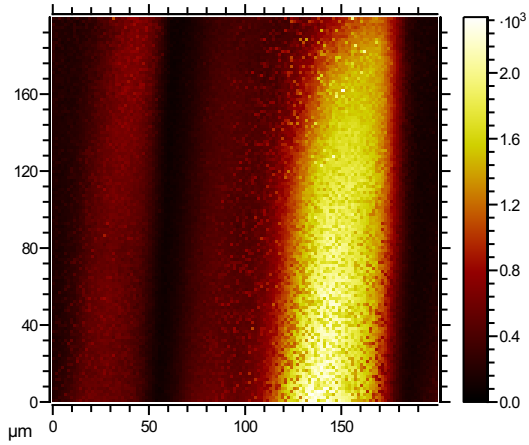
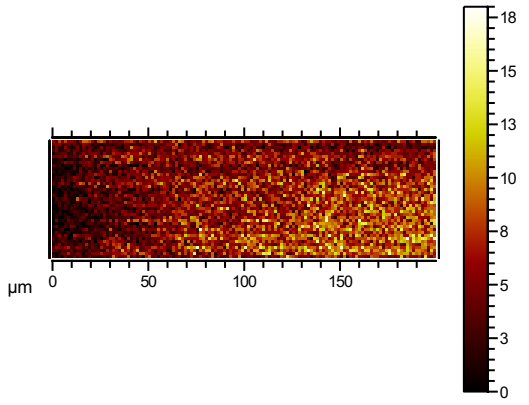


Figure 34. ToF-SIMS depth profile of hair fibre treated with $[C_2C_1Im][Me_2PO_4]$ for 30 minutes at 100° C, negative polarity.

Similarly to $[C_2C_1Im][OAc]$, depth profile of hair fibres treated with $[C_2C_1Im][Me_2PO_4]$ did not show any variation throughout the fibre. However, the noise decreased when compared to $[C_2C_1Im][OAc]$ depth profile analysis. The fibre treated with $[C_2C_1Im][Me_2PO_4]$ presented less damaged than the ones treated with acetate-based ILs, which may be the reason for a flatter baseline. Figure 35 shows a ToF-SIMS ion image where is possible to observe that the fibre structure was preserved after the treatment.



(a)



(b)

Figure 35. Image map of a single curly hair fibre treated with $[C_2C_1Im][Me_2PO_4]$ for 30 minutes at 100° C. (a) Total of SH^- residue throughout hair fibre, XY slice (cuticle of the fibre); (b) Total of SH^- residue throughout hair fibre, YZ slice (cross-section of the fibre – cuticle-cortex-cuticle). The bar represents the intensity (counts per ion) of SH^- residues, lower intensity (black) and maximum of intensity (yellow).

Similarly, the cross-section SH^- distribution was determined as presented in Figure 35, where it is possible to identify the higher count of SH^- on the right side of the image. As mentioned in section 1.2.1, the hair cuticle presents higher content of sulfur when compared to the cortex. Therefore, for the same time length of treatment (30 min at 100° C) the IL $[C_2C_1Im][Me_2PO_4]$ had less impact on the hair structure than $[C_2C_1Im][OAc]$. ToF-SIMS is a promising technique where more valuable information can be obtained. However, the target amino acids during this analysis should be fully understood, and thus further research is required.

4.2 ATR analysis on the impact of ILs on the structure of hair

As discussed in section 1.5.3.2, ATR-FTIR spectroscopy has been used to detect chemical treatments modifications on hair structure. Therefore, in this investigation ATR-FTIR was the technique selected to help understand the impact of the ILs in the hair fibre structure. According to Figure 8 in section 1.5.3.2, the analysis of a single hair fibre by ATR-FTIR is possible. Nevertheless, another important question needs to be raised, whether it will be possible to identify minor variations such as the disulfide and hydrogen bonds on hair structure with this technique. As referred in section 1.5.3.2, there is a specific band that should be an indicator that the disulfide bonds have been cleaved. The band 1040 cm^{-1} should be of more prominent and intense, as the band is the vibrational band of SO_3^- when cystine disulfide is converted to cysteic acid.[222,223]

In this current study European curly hair fibres were investigated, unless otherwise stated. Hair fibres were covered with ILs, either $[C_2C_1mim][OAc]$ or $[C_2C_1mim][Me_2PO_4]$, at room temperature and at 35° C to mimic the average bath water temperature for 24 hours. After this period, hair fibres were washed with water and shampoo to remove the IL left on the surface of the fibre and let them dry for 24 hours. Afterwards, the water solution containing shampoo/IL was disposed of in the appropriate chemical waste treatment.

The fibre treated with IL was analysed by ATR-FTIR to understand if the IL had an impact on the structure of the fibre. To better visualise these modifications, the spectrum of the treated hair fibre was compared with a chemically untreated hair fibre spectrum, as shown in Figure 36. The spectra correspond to the same hair fibre before and after IL treatment. To ease comparison, the spectra was normalised to the Amide I band (1690-1600 cm^{-1}). This way, the normalised spectra allow the comparison between fibres before and after the action of IL. Moreover, this eliminates the contact of the hair fibres with the ATR crystal, which does not represent an external factor of variation.

Figure 36 highlights the differences between spectra, however just by the analysis of these spectra it is not possible to conclude about variations as changes are very minute.

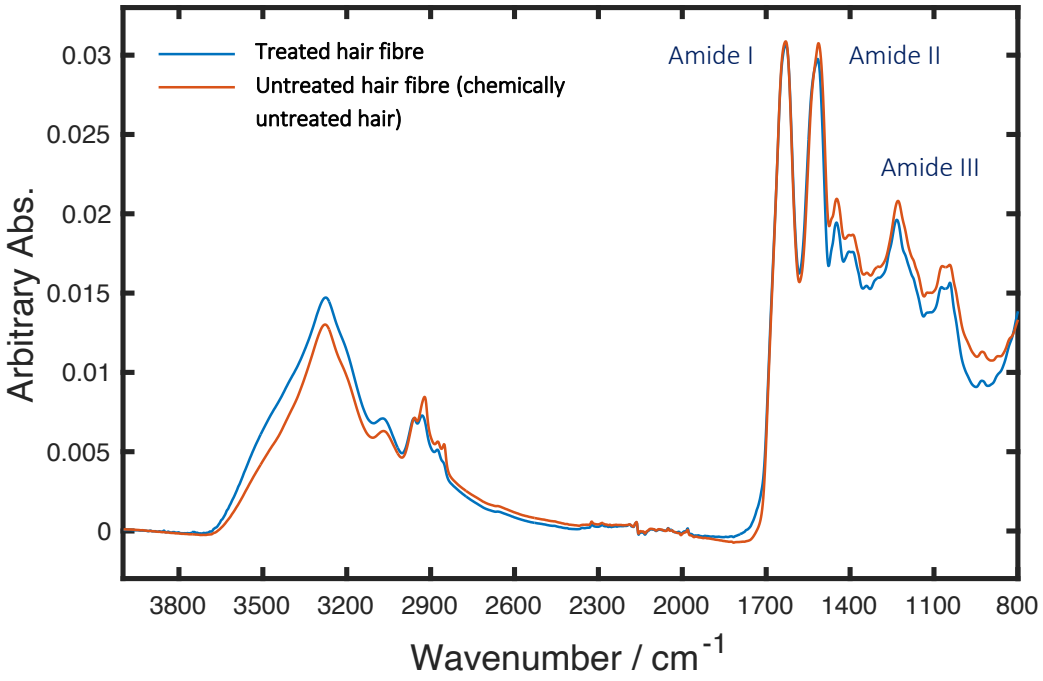


Figure 36. The comparison between untreated hair fibre (chemically untreated fibre) and after IL treatment. Intensities are normalised to Amide I band for comparison purposes. The spectra baselined 4000 to 3700 and 2400 to 1900.

The spectra are very similar, it seems to be an intensity variation, especially in the region 3500 to 2600 cm^{-1} and in the lower wavenumbers of the fingerprint region. Even when band 1040 cm^{-1} is compared, it's very difficult to find any modification.

At this stage, it is essential to understand the spectrum of hair fibre before jumping to conclusions regarding the modifications on the hair structure by the performance of ILs.

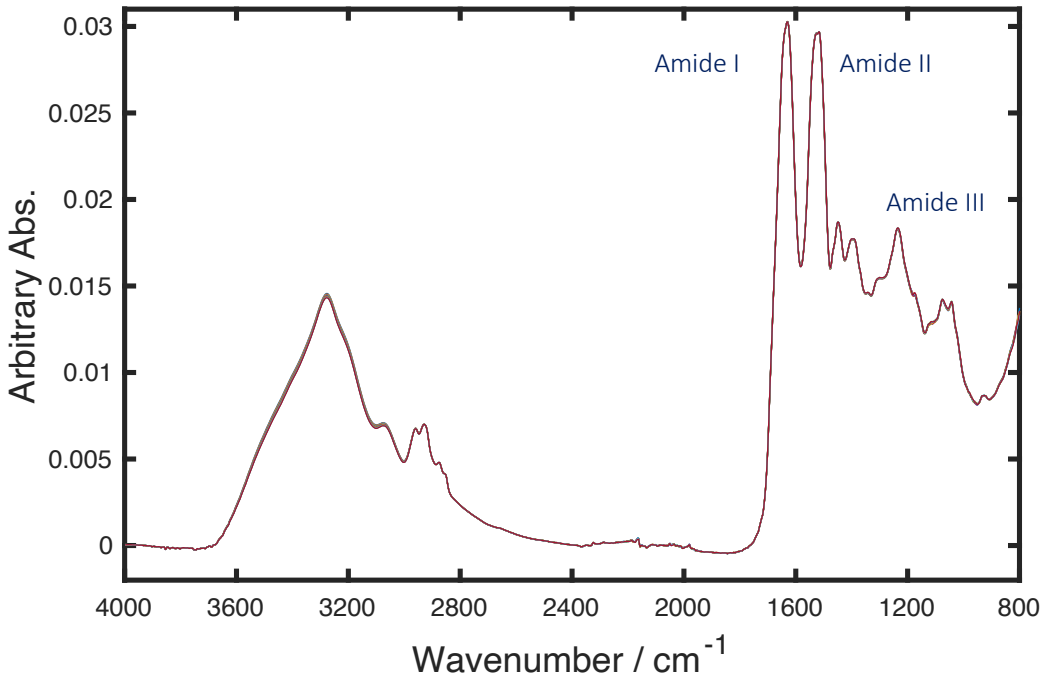
4.3 Natural variation of hair fibre

So far, it is possible to analyse hair fibre by ATR-FTIR, conversely any modification on the structure of hair is very difficult to be identified due to the complexity of human hair structure. At this point, it is not possible to distinguish whether the IL had an impact on the structure of hair or not. There are few factors to take into account, such as the complexity of the hair, the spot on the fibre where the spectrum was recorded. A question needs be addressed; it is important to investigate if the location of the analysis of the hair fibre has an impact on the results. Furthermore, it is key to identify if spectrum

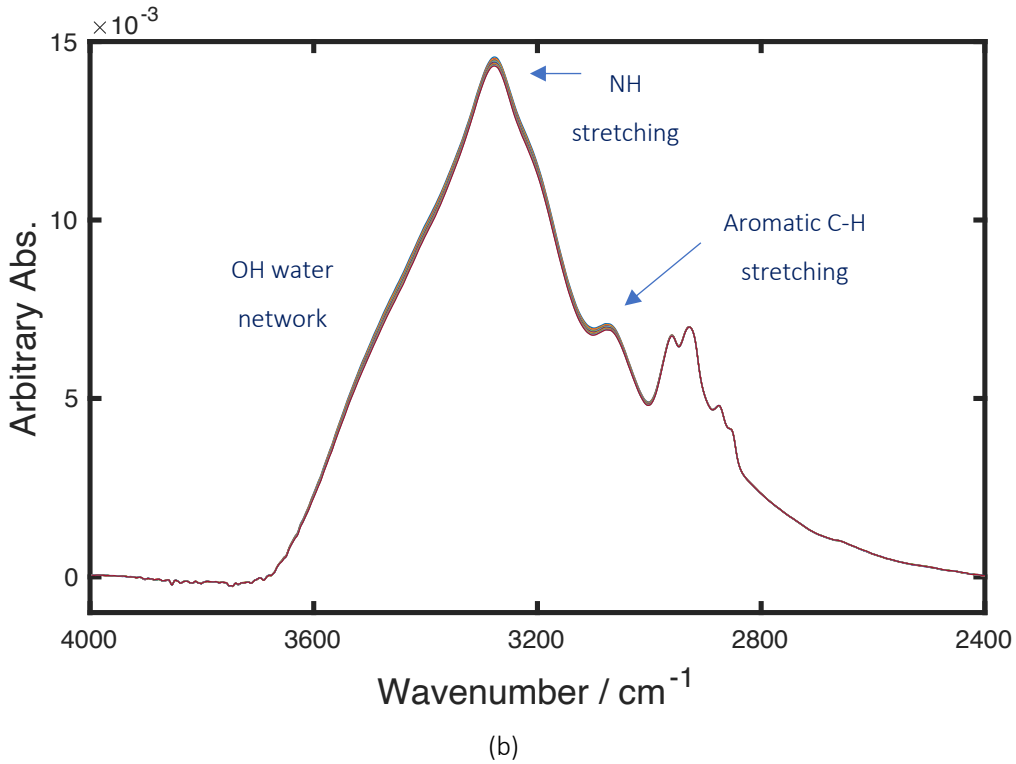
of the hair fibre vary from root to tip. To study all these possibilities, it is essential to know and study the hair fibre spectrum before any treatment.

Human hair structure is very complex, as discussed in subchapter 1.2.1, a natural variation along the fibre is expected. An additional factor to take into consideration is the hair spot under investigation since that area may not be the same before and after treatment. Consequently, even if the fibre examined was the same before and after the IL treatment, the spot would not be precisely the same, which would cause some variations on the spectrum.

The Figure 37 shows the spectra collected along 16 spots for the same fibre. The intensities were normalised to Amide I band for comparison purposes and the spectra baselined 4000 to 3700 and 2400 to 1900. Ideally, we should observe an overlapping of the spectra, but at the region from 3600 to 2800 cm^{-1} it's possible to conclude that there are variations, as well as the fingerprint region.



(a)



(b)

Figure 37. (a) Spectra collected along 16 spots for same chemically untreated hair fibre; (b) Detailed OH stretch region. Intensities are normalised to Amide I band for comparison purposes. The spectra baselined 4000 to 3700 and 2400 to 1900.

The variations observed in Figure 37, in the band 3500 cm^{-1} (OH water network), 3280 cm^{-1} (NH stretching), as well as 3200 to 3000 cm^{-1} (aromatic C-H stretching bands from Tyr, Phe and Trp groups) are very similar to the ones highlighted in Figure 36.

Hair fibres are not uniform along the fibre, in fact they are a combination of compact groups of cells within the follicle, from which originate the three main structures: cuticle, the outermost region that cover the core of the fibres; cortex, which comprise about 75% the hair volume and it is responsible for supporting the hair fibre; and medulla, the inner centre of the fibre, that can be present or not in hair.[199,299–302] So, a variation on fibres among gender, background and ethnicity is expected.[303]

Figure 37 raises a few questions regarding the natural variation on hair structure and the variation among different locations on the same fibre. The variation among spots for the same fibre could be overcome by marking the fibre to guarantee that before and after treatment the exact same spot would be analysed. However, another issue could arise from the variation on the contact with the ATR crystal that is enhanced by the ATR-FTIR armature, then the fibre may not be compressed the same way during each analysis. This

was investigated separately, and it is discussed in the Appendix section Distortion of hair fibres during ATR sampling, from this investigation it was possible to identify the most affected bands, such as OH bands (3500 cm^{-1}), N-H stretching (3280 cm^{-1}) and Amide I (1690-1600 cm^{-1}), Amide II (1575-1480 cm^{-1}).

4.3.1 Natural variation along hair fibre hair

Sixteen spots along the fibre were analysed to investigate the natural variation of hair. For the purpose of this study one spectrum was collected for each spot and then each spectrum was subtracted from the first one. This way, it is possible to evaluate the natural behaviour of the hair along the fibre.

Figure 38 shows the natural variation along the fibre, for better visualisation the spectra show a gradient of colour from deep blue (1st being analysed closer to the root) to yellow (last spot being analysed closer to the tip of the hair). Primarily, it is important to mention that the spectra of the natural variation along the hair fibre is not similar the spectra of the analysis of the impact of the ATR-FTIR armature pressure. After saying that, from now on all variations will only be associated to differences on human hair structure.

At higher wavenumbers, from top to bottom in the Figure 38, the spectra follow the sequential order from spot 1 to spot 7, where spots 6 and 7 are overlapping. The absorption bands at 3500 cm^{-1} (OH band) and 3280 cm^{-1} (N-H stretching) are decreasing intensity and moving towards higher wavenumbers. The N-H stretching, that is the prominent band at chemically untreated hair spectrum, is decreasing along the fibre which may suggest these interactions are changing along the fibre.

The band at 3050 cm^{-1} related to the absorption of C-H stretching is shifted to higher wavenumbers, this band is increasing for all spots although is decreasing intensity as we moved along the fibre from hair root to tip. The next absorption band at 3000-2700 cm^{-1} does not follow the same behaviour as the last two bands. The spots from 2 to 5 have the same behaviour, as the band decreases intensity. The last two spots show opposite behaviour, where the bands are increasing in their intensity. As mentioned before, hair fibres are biological material therefore the thickness of the fibre is not exactly the same along the fibre. So, an explanation for this behaviour can be related to the region

sampling at each spot, since the thickness along the fibre may be different and the region being sampled is different as well.

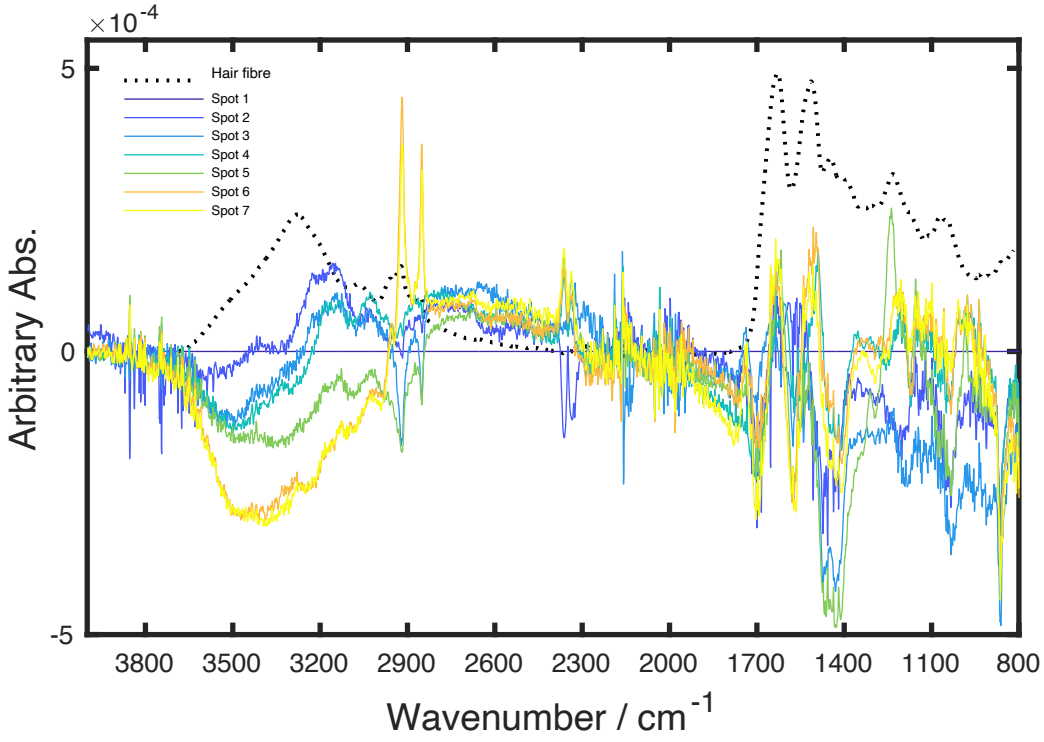


Figure 38. Natural variation of hair fibre along the fibre. Each spectrum corresponds to a spot, where each spot was subtracted to the first one. The first spot (deep blue spectrum) is the one closest to the root, being the 7th spot (yellow spectrum) the last one and near the tip of the hair; hair spectrum represented as dotted spectrum for comparison purposes.

In the fingerprint region, both Amide I and II, in Figure 39, are shifted towards lower wavenumbers. Despite the spikes related to water vapour during the analysis, the bands have an increased on the right side of the band that is related to β-structures, as mentioned before. Once again, the proportion among Amide bands has been changed, where Amide III seems to not change as much as Amide I and II, at least for the last four spots (4, 5, 6 and 7). The spot 5 shows the highest intensity for Amide III and does not show any shift for this band, while spots 4, 6 and 7 are slightly shifted to lower wavenumbers. The spots 2 and 3 show a different behaviour where the Amide III shows about the same proportions Amide I&II/Amide III as chemically untreated hair spectrum. From the analysis of this band, it's possible to identify that as we move towards the end of the fibre, the stability of the Amide III band may be changing.

The bands at 1445 and 1392 cm^{-1} show a decrease on its intensity, which was verified along the fibre but not in a specific order. Those bands are associated to CH_2 and CH_3 bending deformation, respectively.[230]

The last bands to be discussed on this section are 1071 and 1040 cm^{-1}, cystine monoxide stretch and cysteic acid stretch, respectively.[222–224] The fibre analysed by ATR-FTIR is chemically untreated hair (has not been treated before), but hair is damaged from natural weathering and some styling processes, such as drying or combing hair, that can also damage the fibre.[225] So, the appearance of these bands is not a surprise. The fibres follow a sequence from spot 2 to spot 7 (bottom to top in Figure 38) and a shift towards lower wavenumbers and an increased on the intensity of the fibre. The spot 2 and 3 has inverted on the sequence, however along the fibre these bands are more intense. That may suggest the end of the hair is more damaged by the natural weathering and some styling processes than the top of the hair, which may make some sense since the tip of hair has been exposed to these factors longer than the "newer" hair closer to the root.

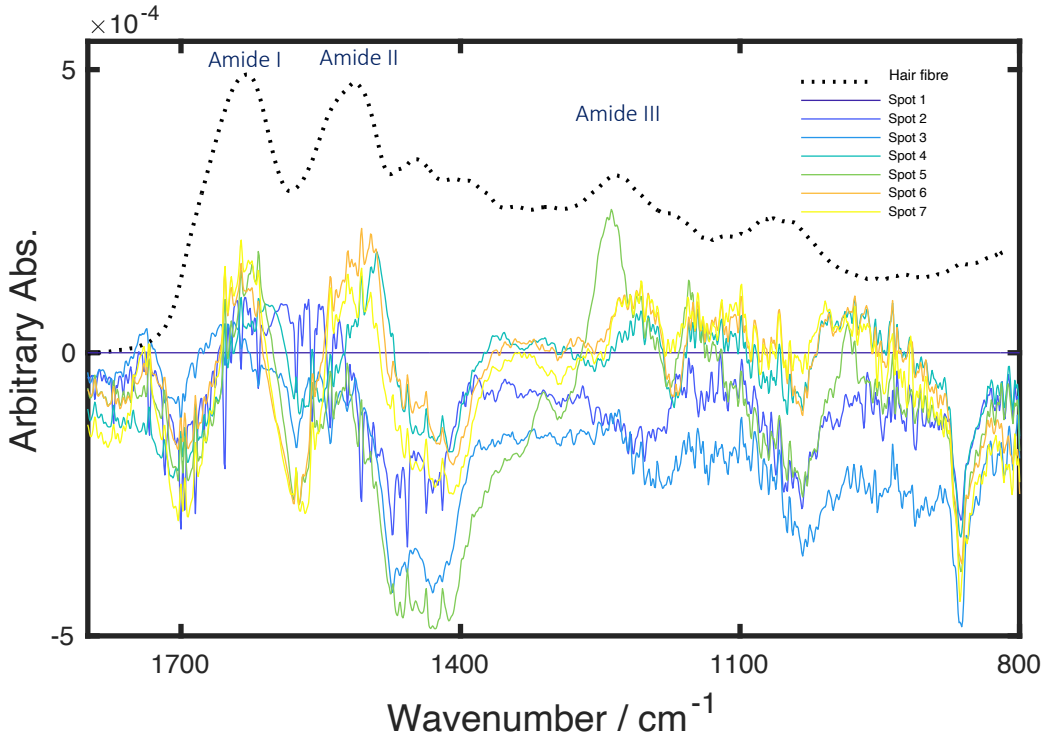


Figure 39. Fingerprint region of Natural variation of hair fibre along the fibre spectra. Each spectrum corresponds to a spot, where each spot was subtracted to the first one. The first spot (deep blue spectrum) is the one closest to the root, being the 7th spot (yellow spectrum) the last one and near the tip of the hair; hair spectrum represented as dotted spectrum for comparison purposes.

It was possible to determine some variations on the hair structure as we were moving along the hair fibre, some of them may be due to differences on the region being sampled or in some cases the changes are due to the natural weathering on the fibre. Also, from the analysis of the Amide I and II the fibre has shown an increase on the β-structure side of the band. Another interesting fact was the proportion Amide I and II regarding Amide III that changes, however that may be related once again to the region being sampled.

The variation along the fibre was discussed on this section 4.3.1 and, in the future, any modification on the structure of hair possibly can be easily identified and not confused with natural variations along the fibre.

The response of European curly hair fibres to pressure was studied, but it is important to understand if different hair types will be as affected as European curly hair. The next section 4.3.1.1 shows the behaviour of hair fibres from different backgrounds during ATR-FTIR analysis.

4.3.1.1 Natural variation among different hair fibres

In this study five hair types were analysed, European curly and straight, European blonde, Asian and Indian hair. In this investigation we want to understand if it is possible to detect variations on the structure of different hair types by ATR-FTIR. It is important to have in mind that the answer of different hair types to pressure was very similar for all hair types, as discussed in the Appendix section (see Pressure among different hair fibres).

Once again, the knowledge of what is changing among hair types will be very important during the determination of modifications of the hair structure. Subsequently, those modifications would not be mistaken by natural variation among hair types.

Each hair type was analysed very carefully, we tried to analyse the approximate same spots on the different hair fibres. On each spot a spectrum was collected and then compared with the spectra from other hair types.

Figure 40 illustrates the spectra of all hair types investigated in this study for a specific spot, as closer as possible to hair follicle. The data was baselined (first-order polynomial)

and normalised to Amide I. Variations were observed for all spectra with most of these variations being found at the fingerprint region, however interpretation of these spectra was not trivial. Therefore, in order to analyse the spectra, a mean spectrum of the five types of hair was obtained and subsequently each individual spectrum of each hair type was subtracted from this mean spectrum. This helped identified the variations and corresponding band positions among hair types, Figure 41.

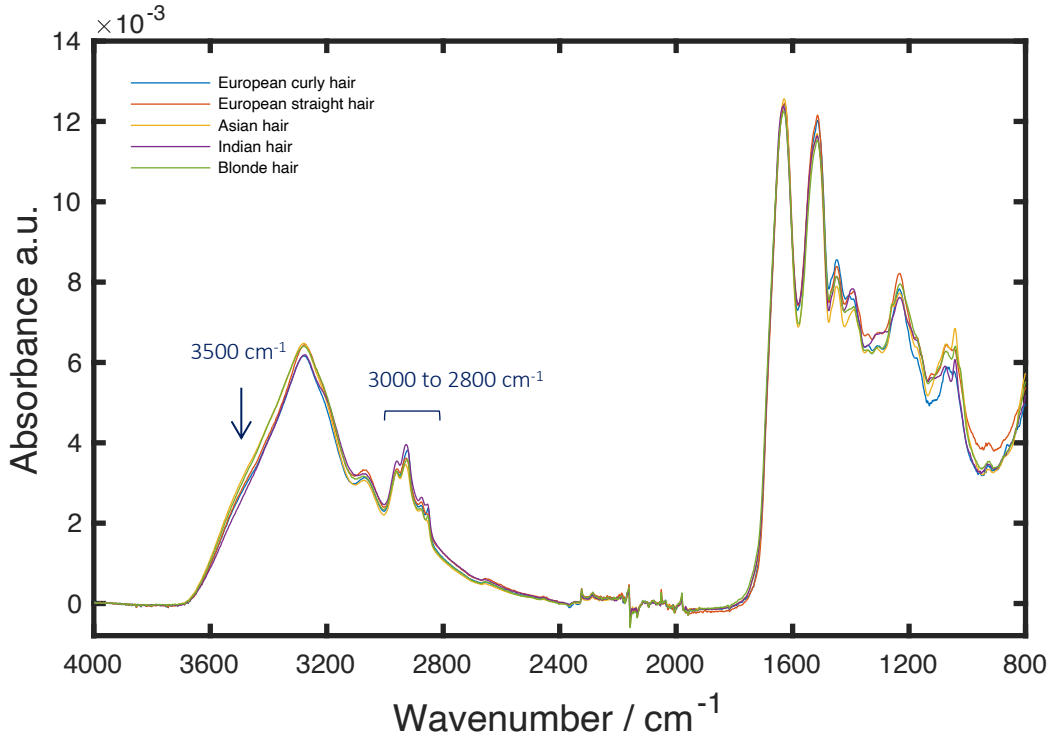


Figure 40. Spectra of all hair types. Blue: European curly hair; Orange: European straight hair; Yellow: Asian hair; Purple: Indian hair; Green: Blonde hair.

Figure 41 highlights the natural variation among hair types, the complexity of the spectra is evident. Nonetheless, there are some bands that can be highlighted and discussed. At higher wavenumbers the band at 3500 cm^{-1} and the absorption at 3000 to 2800 cm^{-1} show to be inversely proportional. The intensity of 3500 cm^{-1} decreases when the 3000 to 2800 cm^{-1} increases, that happen with European curly and Indian hair. The opposite behaviour was observed for European straight, Asian and blonde hair. Until now a relation between these two bands was not possible to confirm, since one is related to OH bonded water network and the other one to C-H stretching.

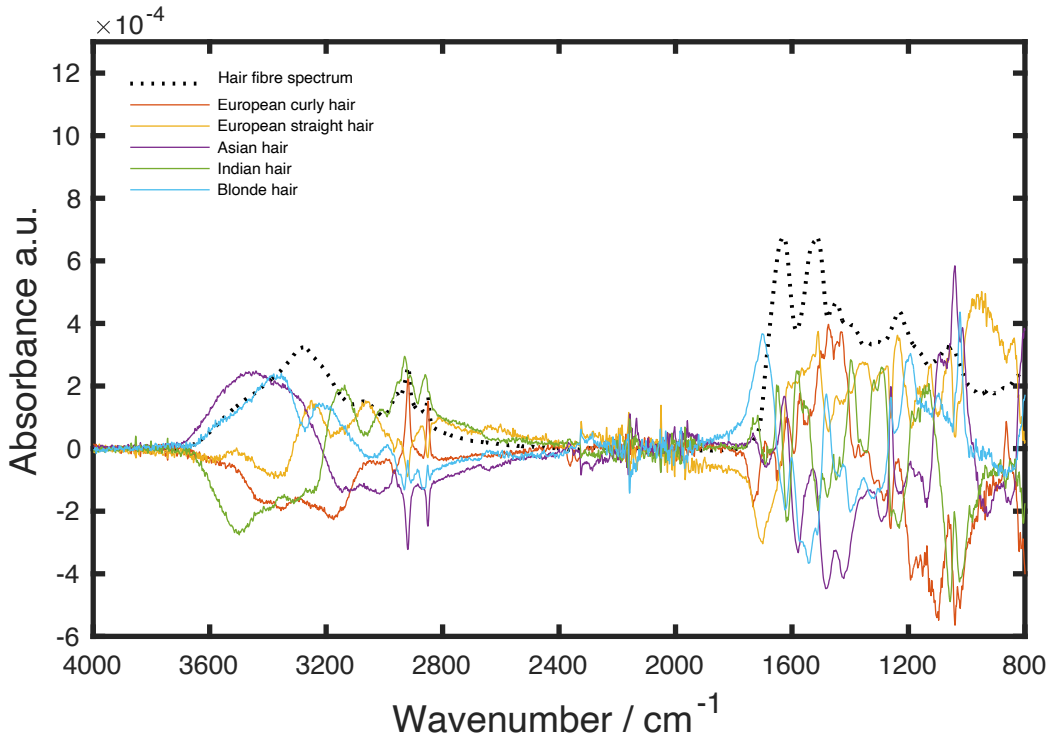


Figure 41. Study of the natural variation of hair from different background. Each spectrum corresponds to a different hair type. Each spectrum of each hair type was subtracted to the mean of the spectra of all hair types.

There are a lot of factors to have into account on the investigation of these variations, such as the amount of cortex that has been exposed or not, hair thickness and hair composition. The chemical composition of human hair depends on the race, gender, age of the individual and also the colour of hair.[303] Those are the factors that vary among hair types and the reason why the spectra is so complicated.

Regarding the Amide bands, the behaviour of all hair types is very similar, as shown in Figure 42. All hair types, beside European blonde hair, showed an increase of the right side of the Amine I band that is related to β-structure. The same just seems to be the same tendency at Amide II, however for European straight hair is very difficult to conclude about the behaviour of that band. Instead, Amide III is increasing for all hair types and once again the proportion Amide I&II/Amide III is very different from the original spectrum. That may suggest Amide III is the band that changes the most among hair types.

Finally, the band at the region from 1130 and 1000 cm^{-1} is not changing similarly for all hair types. As mentioned on subchapter 1.5.3.2, the band is related to oxidative damage

on the fibre. The band has three intensities related to different oxidations states of the cysteine acid. European curly, European straight and Indian hair followed the same behaviour where the middle band increases while the outside bands decrease. Asian hair shows the band also increasing; however, all the peaks of the band are increasing being the middle band the most intense one. European blonde hair only shows the peak at lower wavenumbers increasing. That may suggest that hair fibres show different oxidation of the cysteine acid, that may be the result of brushing, drying, and styling effects on the day-to-day basis.

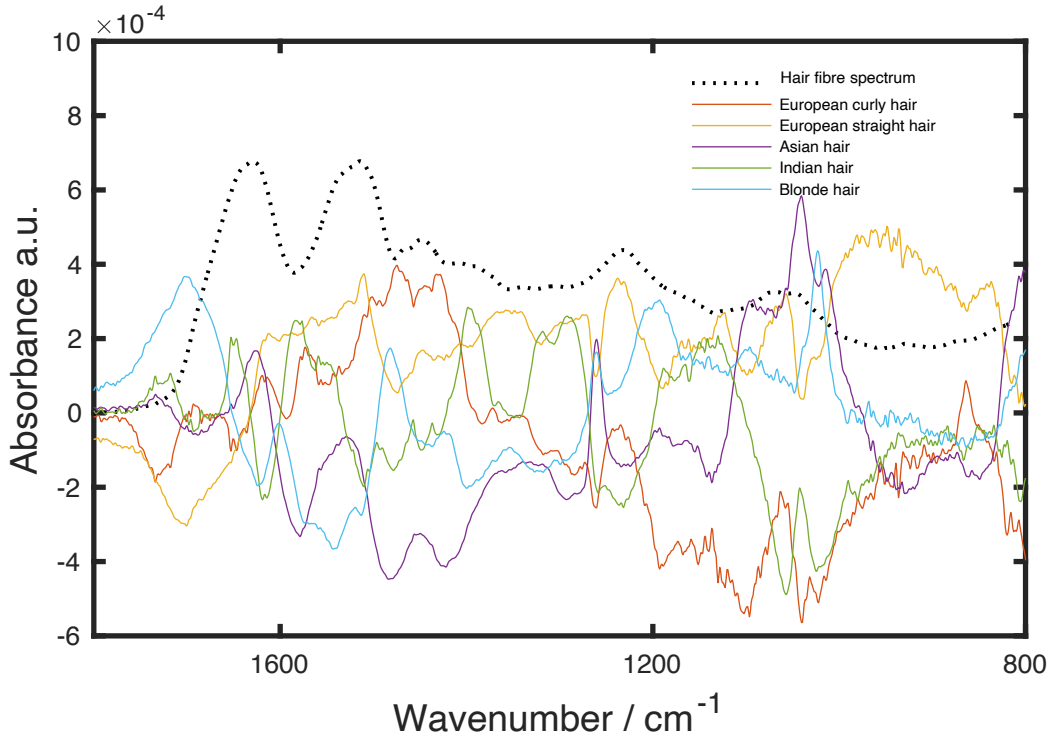


Figure 42. Fingerprint region of the study of the natural variation of hair from different background. Each spectrum corresponds to a different hair type. Each spectrum of each hair type was subtracted to the mean of the spectra of all hair types.

The study of the natural variation of hair fibres from different backgrounds by ATR-FTIR is not conclusive about what changes among the fibres. However, from Amide bands it is possible to conclude that the chemical composition of the fibres changes with race as suggested by literature.[303] Also, the section of sampling by ATR-FTIR may be different, because different hair types have different thicknesses and probably different ways to respond to the ATR-FTIR armature pressure.

4.4 Conclusions

The presented Chapter aimed to identify modifications on the structure of hair, after IL treatment. However, during this investigation questions were raised and addressed. The first section 4.1 aimed to investigate the impact of ILs on the structure of hair and for that, fibres were heated at 100° C with two different ILs, $[C_2C_1Im][OAc]$ and $[C_2C_1Im][Me_2PO_4]$. At the beginning of the partial dissolution was possible to observe the swelling of the fibre, after 45 min with $[C_2C_1Im][OAc]$ and after 90 min with $[C_2C_1Im][Me_2PO_4]$, as observed in Figure 25. In this study only partial dissolution was achieved, to be able to carry on with the investigation of the morphology and composition of the fibre after the impact of the IL. On the last stage of the partial dissolution was only possible to observe the cuticle of the fibre and the complete dissolution of the cortex, for both IL in this study. Later, the fibres were analysed by SEM to further characterise their morphology. SEM showed degradation of the fibre by $[C_2C_1Im][OAc]$, as observed in Figure 28. The sulfur content of the fibre was analysed and compared to the sulfur content of chemically untreated hair. The sulfur content of the fibre decreased after the treatment with $[C_2C_1Im][OAc]$. Also, a drastically decreased of sulfur content was observed on hair fibres treated with $[C_2C_1Im][Me_2PO_4]$. ToF-SIMS was the technique selected to investigate the modification on the structure of the fibre, due to the ability to do depth profile of the fibres. The residue SH^- was selected due to the absence of sulfur in the structure of the IL. According to ToF-SIMS analysis on fibres treated with $[C_2C_1Im][OAc]$, the content of sulfur decreased from cuticle to cortex, as expected. This is possible to be observed in Figure 30 and Figure 31, also the high damage of the fibre could be observed, Figure 35. As expected, fibres treated with $[C_2C_1Im][Me_2PO_4]$ did not show as damaged as fibres treated with acetate-based ionic liquid.

The second part of this study was the investigation of the natural variation of human hair, section 4.3. The first approach was the variation along the fibre and it was possible to conclude some variations are due to differences on the hair structure, but other ones may be related to the region being sampled and the depth of penetration has a big influence on the results. Also, the fibre might have different thicknesses along the hair and so the region being sampled may be different. The analysis of the fingerprint region

showed the proportion of Amide I & II/Amide III changed throughout the analysis, and the Amide III show an increased during the study. Both Amide I and II showed an increase of the right side of the band that usually is related to β-structures.

Some variations on the bands related to oxidation products of the cystine were detected, which suggested the tip of the hair is more damaged than the top of the hair by natural weathering and some styling methods.

The identification of the natural variation of hair from different backgrounds by ATR-FTIR showed to be not as conclusive as expected, section 4.2. There are a lot of variables changing along the spectra and a trend was not achieved, Figure 43. However, a few observations can be made. The Amide bands are the ones that changed the most in this investigation, which may be related to the chemical composition of different hair types. Once again, Amide III is the most affected band on all hair types. The analysis of human hair by ATR-FTIR is not as conclusive as expected.

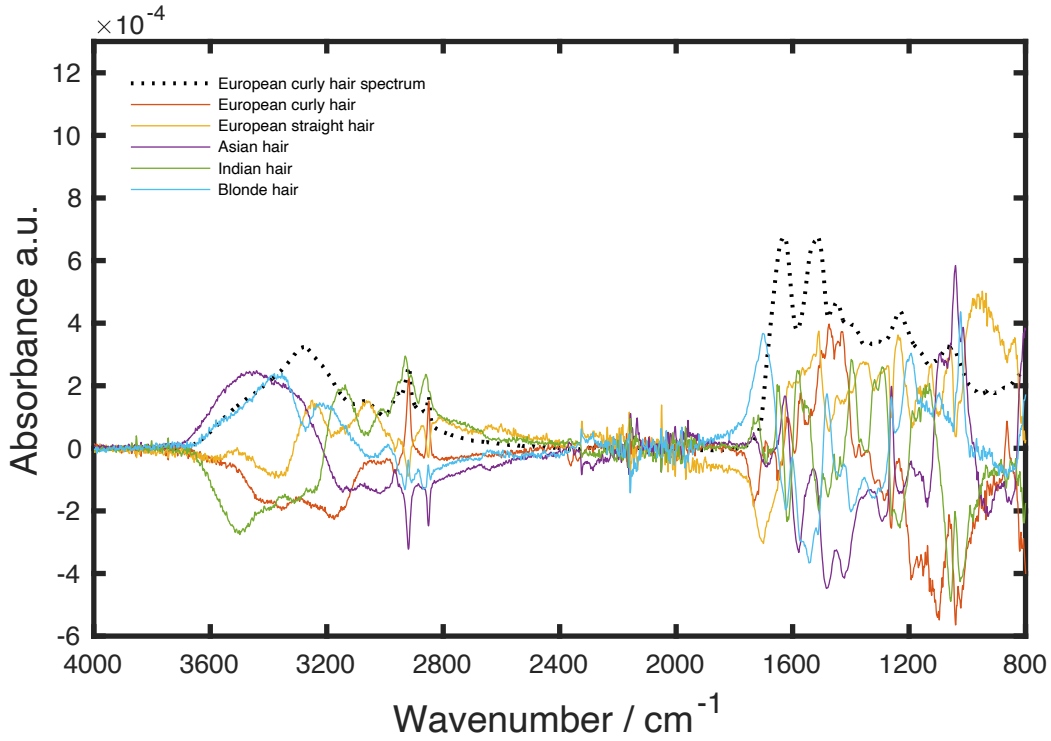


Figure 43. Study of the natural variation of hair from different background. Each spectrum corresponds to a different hair type. Each spectrum of each hair type was subtracted to the mean of the spectra of all hair types

The natural variation among hair types is very complex and using infrared spectroscopy as an analytical tool in this context proved to be very challenging. To fully understand the

natural structure of hair further techniques should be considered. Raman spectroscopy has been used to study specific bonds in the hair structure after cosmetic treatments, such as straightening, bleaching or thermal treatments. Raman spectroscopy might be a suitable alternative and complementary technique to evaluate the hair structure due to its sensitivity to different vibrational modes not detected by FTIR. Consequently, in the future, modifications by IL in the structure of hair should be identified using this technique. However, this technique can only be performed in albino hair/ grey hair. Moreover, Atomic Force Microscopy could be applied to determine any modification on the surface of hair after the IL treatment.

The conclusion of section 4.2 is that the ATR-FTIR might not be an invasive technique, however the morphology of the hair fibre has been altered and that can impact the analysis of the results. If this studied was not performed, some variations on the structure of hair might be claimed as chemical modifications by ILs when they are a consequence of the pressure applied by the ATR-FTIR armature.

Chapter 5 Experimental

5.1 Preparation of solvents

5.1.1 Methods of analysis

5.1.1.1 Nuclear Magnetic Resonance (NMR)

^{1}H, ^{13}C, ^{31}P and ^{19}F NMR spectra were recorded at room temperature on Bruker AV400 or AV(III)500 HD spectrometers, using $(CD_3)_2SO$ or $(CD_3)_2CO$ as solvent. NMR fids were processed in MestReNova (Mestrelab Research S.L. 2017).

5.1.1.2 Electrospray Ionisation Mass Spectrometry (ESI-MS)

ESI-MS was performed at Bucker MicroTOF 62 spectrometer and 3 mg of sample were prepared in methanol.

5.1.2 Ionic liquid synthesis

All ionic liquids, except $[C_2C_1Im][OAc]$ which was purchased from Sigma-Aldrich, were synthesised in our laboratories using standard methods reported in the literature. 1-methylimidazole (> 99%), 1-butylimidazole (> 98%), 1-octylimidazole (> 98%) and 1-butylpyrrolidine (98 %) were purchased from Sigma-Aldrich® and were used without further purification. All other chemical precursors such as sodium hydride (> 90%), bromoethane (≥ 99%), trimethylphosphate (97%), bis(trifluoromethane)sulfonimide (≥ 95%), 1-chlorobutane (99.5 %), dimethylsulfate (≥ 99%), methyl trifluoromethanesulfonate (≥ 98%), dipropylamine (99%), bis(2-ethylhexyl)amine (99 %), 1,1,3,3-tetramethylguanidine (99%), acetic acid (≥ 99.7%) were purchased from Sigma-Aldrich. Other solvents for these syntheses were obtained from commercial suppliers

and used without additional purification, unless otherwise stated. The water used in this study was Millipore Milli-Q 18 MΩ ultrapure. All solvents were analytical reagent grade with exception to anhydrous solvents(≥ 99.7%).

All compounds were dried *in vacuo* ($p \leq 10^{-3}$ mbar) at 50° C and stored under argon before being characterised by ^{1}H, ^{13}C, ^{31}P and ^{19}F NMR when appropriate (recorded at room temperature on Bruker AV400 or AV(III)500 HD spectrometers); chemical shifts (δ) are expressed in parts per million (ppm) with reference to residual traces of protonated solvents in commercial NMR solvents; protonated dimethyl sulfoxide (δ_H 2.50) and $(CD_3)_2SO$ (δ_C 77.0), and protonated acetone (δ_H 2.05) and $(CD_3)_2CO$ (δ_C 29.84 and 206.26).

Coupling constants (*J*) are given in Hz and multiplicities were labelled singlet (s), doublet (d), triplet (t), q (quartet), quint (quintet), sext (sextet), dd (double doublet) and m (multiplet). NMR FIDs were processed in MestReNova (Mestrelab Research S.L. 2017).

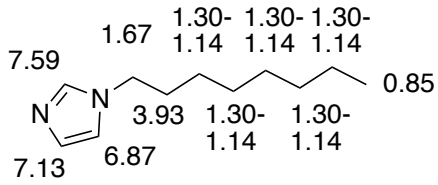
^{13}C-NMR and ^{31}P-NMR or ^{19}F-NMR chemical shifts are represented together in the compound structure.

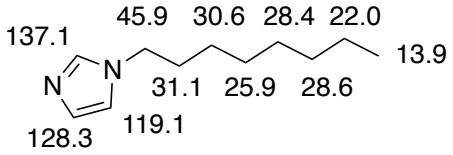
Note: ^{19}F, ^{31}P and ^{13}C chemical shifts are represented together in the compound structure when applicable.

Further characterisation by ESI-MS (Bruker MicroTOF 62 spectrometer) and DSC (TA-Q2000) were also included.

5.1.2.1 Imidazolium based Ionic Liquids

5.1.2.1.1 1-octylimidazole. [304]





Imidazole (15.1000 g, 0.2220 mol) was dissolved in dry THF (200 mL), under an inert Ar atmosphere. Sodium hydride (8.8700 g, 0.2220 mol) was slowly added. The mixture was stirred for 24 hours at room temperature. The mixture was stirred for 24 hours at room temperature. 1-bromooctane (42.9 g, 222 mmol) was dissolved in dry THF (~ 1:1 v/v) and the resulting solution added dropwise to the cooled (0° C) sodium imidazolate solution. After 2 hours, the mixture was heated to reflux and stirred for 48 hours. The mixture was cooled and filtered to remove insoluble by products, solvent was evaporated at 40° C at 357 mbar.

1-Octylimidazole was recovered to yield a colourless liquid (33.3 g, 83% yield).

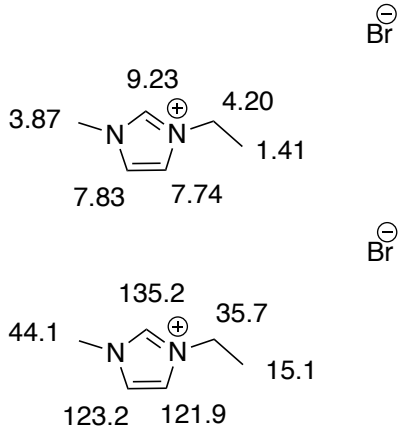
^{1}H NMR (400 MHz, $(CD_3)_2SO$): δ ppm 7.59 (dd, *J*=3.5 Hz,1H), 7.13 (dd, *J*=3.5 Hz, 1H), 6.87 (dd, *J*=3.5 Hz, 1H), 3.93 (*t*, *J*=7.5H, 2H), 1.67 (quint, *J*=2.5, 2H), 1.30 – 1.14 (m, 10H), 0.85 (*t*, *J*=7.5, 3H);

^{13}C NMR (101 MHz, $(CD_3)_2SO$): δ ppm 137.1, 128.3, 119.1, 45.9, 31.1, 30.6, 28.6, 28.4, 25.9, 22.0 and 13.9.

ESI-MS (+ve) [$C_{11}H_{20}N_2$]: calc 180.1626, found 180.1703

Data in agreement with literature values.[305]

5.1.2.1.2 1-ethyl-3-methylimidazolium bromide, $[C_2C_1Im]Br$.[306]



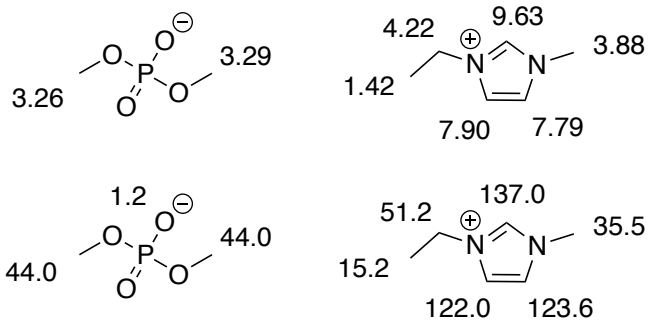
1-butylimidazole (4.3000 g, 0.0520 mol) was dissolved in 10 mL of acetonitrile and added dropwise to the cooled (0° C) to bromoethane (9.7800 g, 0.0700 mol). Afterward, the reaction was stirred for 48 hours under reflux and under an inert Ar atmosphere.
The solvent was evaporated at reduced pressure and then the product was recrystallized from acetonitrile/ ethyl acetate. After this process the IL was dried *in vacuo* at 70° C. The IL was recovered to yield a white solid (8.75 g, 87.5% yield).

^{1}H NMR (400 MHz, $(CD_3)_2SO$): δ ppm 9.23 (dd, *J*=3.5 Hz, 1H), 7.83 (dd, *J*=3.5 Hz, 1H), 7.74 (dd, *J*=3.5 Hz, 1H), 4.20 (q, *J*=2.5 Hz, 2H), 3.87 (3H, s) and 1.41 (t, *J*=7.5 Hz, 3H).

^{13}C NMR (101 MHz, $(CD_3)_2SO$): δ 135.2, 123.2, 121.9, 44.1, 35.7 and 15.1;

ESI-MS (+ve) $[C_6H_{11}N_2]$: calc 111.0915, found 111.0924;
Data in agreement with literature values.[307]

5.1.2.1.3 1-ethyl-3-methylimidazolium dimethylphosphate, $[C_2C_1Im][Me_2PO_4]$.[137]



1-ethylimidazole (6.1000 g, 0.0640 mol) was dissolved in 10 mL of acetonitrile and added dropwise to the cooled (0° C) to trimethylphosphate (9.7800 g, 0.0700 mol). Afterward, the reaction was stirred for 20 hours under reflux and under an inert Ar atmosphere. The solvent was evaporated at reduced pressure and then the product was recrystallized from acetonitrile/ ethyl acetate. After this process the IL was dried *in vacuo* at 60° C. 1-ethyl-3-methylimidazolium dimethylphosphate was recovered to yield a yellowish liquid (12.50 g, 83% yield).

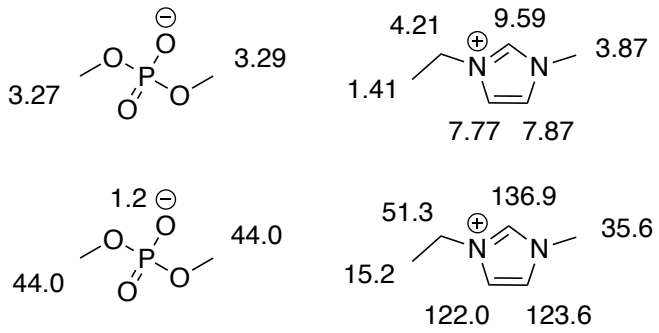
^{1}H NMR (400 MHz, $(CD_3)_2SO$): δ ppm 9.63 (dd, *J*=3.5 Hz, 1H), 7.79 (dd, *J*=3.5 Hz, 1H), 7.90 (dd, *J*=3.5 Hz, 1H), 4.22 (q, *J*=2.5 Hz, 2H), 3.88 (3H, s), 3.29 (3H, s), 3.26 (3H, s) and 1.42 (t, *J*=7.5 Hz, 3H).

^{13}C NMR (101 MHz, $(CD_3)_2SO$): δ 137.0, 123.6, 122.0, 51.2, 44.0, 35.5 and 15.2;

^{31}P NMR (202 MHz, $(CD_3)_2SO$): δ ppm 1.2.

ESI-MS (+ve) $[C_6H_{11}N_2]$: calc 111.0923, found 111.0936;
ESI-MS (-ve) $[C_2H_6O_4P_1]$: calc 125.0008, found 125.0007.
Data in agreement with literature values.[308]

5.1.2.1.4 1-ethyl-3-methylimidazolium dimethylphosphate, $[C_2C_1Im][Me_2PO_4]$.[137]



1-ethyl-3-methylimidazolium dimethylphosphate $[C_2C_1Im][Me_2PO_4]$, was synthesised assisted by Microwave.

Trimethylphosphate (6.5500 g, 0.0465 mol) was added to 1-ethylimidazole (4.0900 g, 0.0425 mol) at 100° C. The reaction was carried out at 100 psi and a power of 100 W. The reaction took 3 hours to be complete at these conditions. After reaction, the mixture was washed with diethyl ether (2x50 mL) to remove any excess of the trimethylphosphate. The recovery liquid was dried *in vacuo* at 80°C for 24hours (7.24 g, yield 73%).

^{1}H NMR (400 MHz, $(CD_3)_2SO$): δ ppm 9.59 (dd, *J*=3.5 Hz, 1H), 7.87 (dd, *J*=3.5 Hz, 1H), 7.77 (dd, *J*=3.5 Hz, 1H), 4.21 (q, *J*=2.5 Hz, 2H), 3.87 (3H, s), 3.29 (3H, s), 3.27 (3H, s) and 1.41 (t, *J*=7.5 Hz, 3H).

^{13}C NMR (101 MHz, $(CD_3)_2SO$): δ 136.9, 123.6, 122.0, 51.3, 44.0, and 15.2;

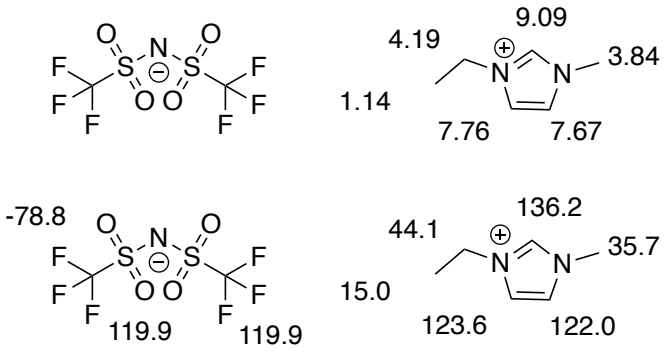
^{31}P NMR (202 MHz, $(CD_3)_2SO$): δ ppm 1.2.

ESI-MS (+ve) $[C_6H_{11}N_2]$: calc 111.0917, found 111.0924;

ESI-MS (-ve) $[C_2H_6O_4P_1]$: calc 125.0009, found 125.0008.

Data in agreement with literature values.[308]

5.1.2.1.5 1-ethyl-3-methylimidazolium bis(trifluoromethanesulfonyl)imide,[C_2C_1Im][NTf_2].[309]



To a solution of 1-ethyl-1-methylimidazolium bromide (4.8900 g, 0.0260 mol) in 10 mL of water, a solution of lithium bis(trifluoromethane)sulfonimide (7.3400 g, 0.0260 mol) in 25 mL of water was added dropwise. The reaction was stirred for 24 hours at room temperature and under an inert Ar atmosphere. Dichloromethane (10 mL) was added and the organic layer separated and washed with water (5x100 mL). The solvent was evaporated at 40° C at 100 mbar. The solvent was removed, and the product was dried *in vacuo* at 50° C to yield a yellowish liquid (7.53 g, 75%).

^{1}H NMR (400 MHz, $(CD_3)_2SO$): δ ppm 9.09 (dd, *J*=3.5, 1H), 7.76 (dd, *J*=3.5, 1H), 7.67 (dd, *J*=3.5,1H), 4.19 (q, *J*=2.5, 2H), 3.84 (s, 3H);

^{13}C NMR (101 MHz, $(CD_3)_2SO$) δ 136.2, 123.6, 122.0, 119.9 (q, J_{C-F}=322 Hz,1C), 44.1, 35.7, and 15.0;

^{19}F NMR (376 MHz, $(CD_3)_2SO$): δ ppm -78.8.

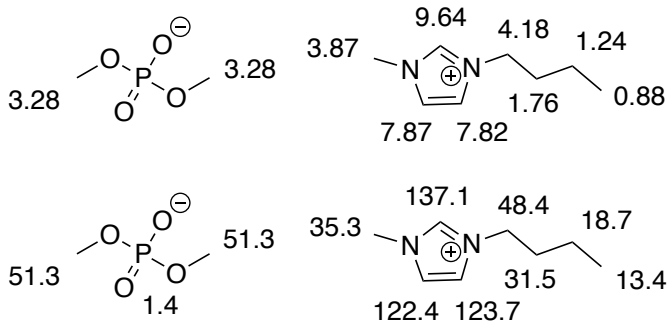
ESI-MS (+ve) [$C_6H_{11}N_2$]: calc 111.0917, found 111.0926;

ESI-MS (-ve) [$C_2F_6NO_4S_2$]: calc 279.9173, found 279.9187.

The IL was analysed by Ion Chromatography-Mass Spectroscopy and bromide anion values were under the detection limit.

Data in agreement with literature values.[310,311]

5.1.2.1.6 1-butyl-3-methylimidazolium dimethylphosphate, $[C_4C_1Im][Me_2PO_4]$.[312]



1-butylimidazole (7.0500 g, 0.0570 mol) was dissolved in 20 mL of acetonitrile and added dropwise to the cooled (0° C) to trimethylphosphate (8.7500 g, 0.0630 mol). Afterward, the reaction was stirred for 20 hours under reflux and under an inert Ar atmosphere. The solvent was evaporated at reduced pressure and then the product was recrystallized from acetonitrile/ ethyl acetate. After this process the IL was dried *in vacuo* at 60° C. The IL was recovered to yield a yellowish liquid (14.00 g, 93 % yield).

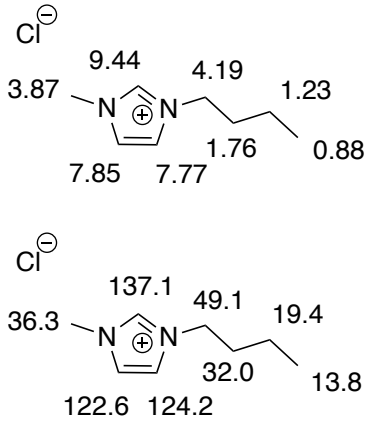
^{1}H NMR (500 MHz, $(CD_3)_2SO$): δ ppm 9.57 (dd, *J*=3.5, 1H), 7.85 (dd, *J*=3.5, 1H), 7.78 (dd, *J*=3.5, 1H), 4.18 (t, *J*=7.5, 2H), 3.87 (s, 3H), 3.27 (s, 3H), 3.25 (s, 3H), 1.76 (quint, *J*=2.5, 2H), 1.25 (sext, *J*=7.5, 2H) and 0.89 (t, *J*=7.5, 3H);

^{13}C NMR (500 MHz, $(CD_3)_2SO$): δ ppm 137.2, 123.6, 122.3, 51.2, 48.4, 35.6, 31.4, 18.8 and 13.3;

^{31}P NMR (202 MHz, $(CD_3)_2SO$): δ ppm 1.4.

ESI-MS (+ve) [$C_8H_{15}N_2$]: calc 139.1230, found 139.1236;
ESI-MS (-ve) [$C_2H_6O_4P_1$]: calc 125.0009, found 125.0006.
Data in agreement with literature values.[313]

5.1.2.1.7 1-butyl-3-methylimidazolium chloride, $[C_4C_1Im]Cl$.[259]



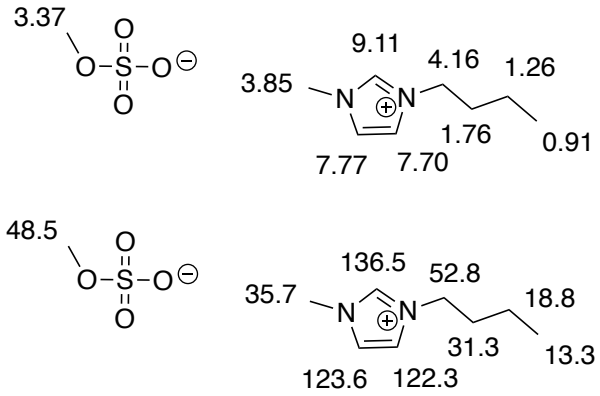
1-methylimidazole (4.7000 g, 0.0570 mol) was dissolved in acetonitrile (30 mL) and 1-chlorobutane (5.8300 g, 0.0630 mol) was added dropwise, under an inert Ar atmosphere. The mixture was stirred in reflux for 72-96 hours. The mixture was allowed to warm up at room temperature. The solvent removed at reduced pressure and recrystallized from acetonitrile/ ethyl acetate. The IL was dried *in vacuo* for 24 hours at 60° C. 1-butyl-3-methylimidazolium chloride was recovered to yield a yellowish powder (8.80 g, 88%).

^{1}H NMR (400 MHz, $CDCl_3$): δ ppm 8.92 (dd, *J*=3.5, 1H), 7.92 (dd, *J*=3.5, 1H), 7.75 (dd, *J*=3.5, 1H), 5.01 (t, *J*=7.5, 2H), 3.73 (s, 3H), 2.01 (quint, *J*=2.5, 2H), 1.36 (sext, *J*=7.5, 2H) and 0.92 (t, *J*=7.5, 3H);

^{13}C NMR (101 MHz, $CDCl_3$): δ ppm 137.0, 122.8, 123.0, 54.2, 37.1, 32.3, 20.7 and 13.9

ESI-MS (+ve) $[C_8H_{15}N_2]$: calc 139.1235, found 139.1231;
Data in agreement with literature values.[136,314]

5.1.2.1.8 1-butyl-3-methylimidazolium methylsulphate, $[C_4C_1Im][MeSO_4]$.[315]



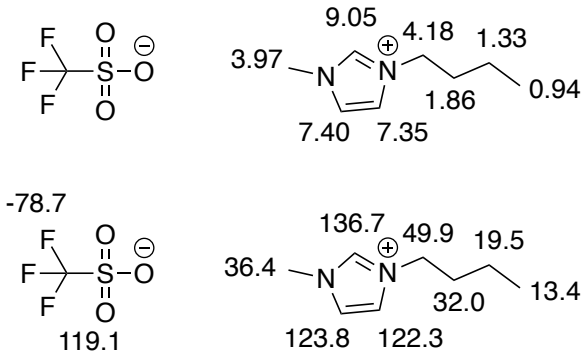
The 1-butylimidazole (4.9600 g, 0.0400 mol) was dissolved in acetonitrile (10 mL) in a flask with a condenser. Afterward, dimethyl sulfate (5.2900 g, 0.0420 mol) was added dropwise to the solution. The reaction was refluxed for 72 hours under an inert Ar atmosphere. After removed the solvent at reduced pressure, the mixture was recrystallized from acetonitrile/ ethyl acetate and IL dried *in vacuo* at 50° C. the IL was recovered to yield a liquid (7.77 g, 78%).

^{1}H NMR (400 MHz, $CDCl_3$): δ ppm 9.11 (dd, *J*=3.5, 1H), 7.77 (dd, *J*=3.5, 1H), 7.70 (dd, *J*=3.5, 1H), 4.16 (t, *J*=7.5, 2H), 3.85 (s, 3H), 1.76 (quint, *J*=2.5, 2H), 1.26 (sext, *J*=7.5, 2H) and 0.91 (t, *J*=7.5, 3H);

^{13}C NMR (101 MHz, $CDCl_3$): δ ppm 136.5, 123.6, 122.3, 52.8, 35.7, 31.3, 18.8 and 13.3

ESI-MS (+ve) $[C_8H_{15}N_2]$: calc 139.1244, found 139.1234;
Data in agreement with literature values.[260,316,317]

5.1.2.1.9 1-butyl-3-methylimidazolium trifluoromethanesulfonate, $[C_4C_1Im][CF_3SO_3]$.[318]



Methyl trifluoromethanesulfonate (3.4500 g, 0.0210 mol) was added dropwise to the cooled (0° C) into 1-butylimidazole (2.5800 g, 0.0208 mol) and magnetically stirred during 14 hours, under an inert Ar atmosphere. The stirring was continued for 3 hours at 25° C to complete the reaction.

The excess of methyl trifluoromethanesulfonate was removed, and the product was dried *in vacuo* at 82° C to yield a yellowish liquid (5.83 g, 97%).

^{1}H NMR (400 MHz, $CDCl_3$): δ ppm 9.05 (dd, *J*=3.5, 1H), 7.40 (dd, *J*=3.5, 1H), 7.35 (dd, *J*=3.5, 1H), 4.18 (t, *J*=7.5, 2H), 3.97 (s, 3H), 1.86 (quint, *J*=2.5, 2H), 1.33 (sext, *J*=7.5, 2H) and 0.94 (t, *J*=7.5, 3H);

^{13}C NMR (101 MHz, $CDCl_3$): δ ppm 136.7, 123.8, 122.3, 49.9, 36.4, 32.0, 19.5 and 13.4;

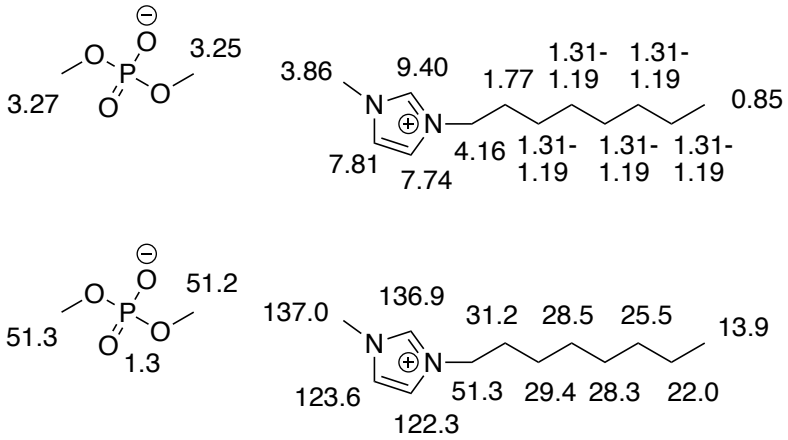
^{19}F NMR (376 MHz, $CDCl_3$): δ ppm -78.7.

ESI-MS (+ve) $[C_8H_{15}N_2]$: calc 139.1244, found 139.1234;

ESI-MS (-ve) $[C_1F_3O_3S]$: calc 148.9522, found 148.9611;

Data in agreement with literature values.[319]

5.1.2.1.10 1-octyl-3-methylimidazolium dimethylphosphate, $[C_8C_1Im][Me_2PO_4]$.[312]



Trimethylphosphate (4.8100 g, 0.3400 mol) was added to 1-octylimidazole (5.6300 g, 0.3100 mol) at room temperature under an inert Ar atmosphere. The reaction was stirred at 80° C for 48 hours. Dichloromethane (10 mL) was added and the organic layer separated and washed with diethyl ether (2x40 mL). The solvent was removed, and the product was dried *in vacuo* for 24 hours at 60° C. $[C_8C_1Im][Me_2PO_4]$ to yield a viscous pale yellow liquid (8.53 g, 85%).

^{1}H NMR (400 MHz, $(CD_3)_2SO$): δ ppm 9.40 (dd, *J*=3.5, 1H,), 7.81 (dd, *J*=3.5, 1H,), 7.74 (dd, *J*=3.5, 1H,), 4.16 (t, *J*=7.5, 2H), 3.86 (s, 3H), 3.27 (s, 3H), 3.25 (s, 3H), 1.77 (quint, *J*=7.5, 2H), 1.31-1.19 (m, 10H) and 0.85(t, *J*=7.5, 3H).

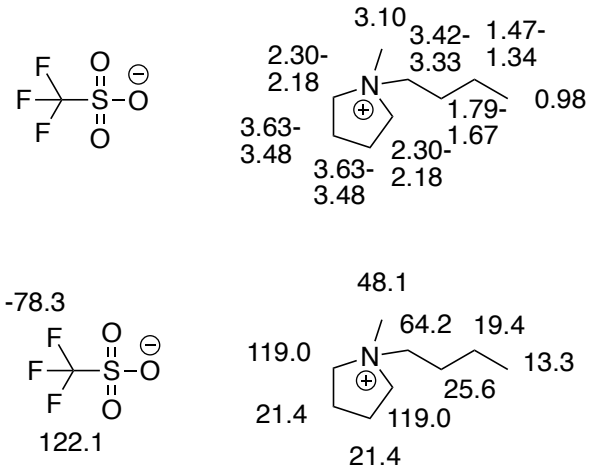
^{13}C NMR (101 MHz, $(CD_3)_2SO$): δ ppm 136.91, 123.57, 122.25, 51.26, 51.20, 48.69, 35.65, 31.15, 29.41, 28.47, 28.34, 25.50, 22.04, 13.92;

^{31}P NMR (202 MHz, $(CD_3)_2SO$): δ ppm 1.3.

ESI-MS (+ve) $[C_{12}H_{23}N_2]$: calc 195.1856, found 195.1858;
ESI-MS (-ve) $[C_2H_6O_4P_1]$: calc 125.0009, found 125.0008.
Data in agreement with literature values.[320]

5.1.2.2 Pyrrolidinium Ionic Liquids

5.1.2.2.1 1-butyl-1-methylpyrrolidinium trifluoromethanesulfonate, $[C_4C_1Pyrr][CF_3SO_3]$.[318]



Methyl trifluoromethanesulfonate (5.6900 g, 0.3500 mol) was added dropwise to the cooled (0° C) into 1-butylpyrrolidine (4.3700 g, 0.3400 mol). The mixture was stirred over a period of 24 hours under an inert Ar atmosphere. The mixture was stirred for 3 hours at 25° C to complete reaction.

The excess of methyl trifluoromethanesulfonate was removed, and the product was dried *in vacuo* at 82° C to yield a yellowish liquid (8.76 g, 87.6%).

^{1}H NMR (400 MHz, $CDCl_3$): δ ppm 3.63-3.48 (m, 4H), 3.42-3.33 (m, 2H), 3.10 (s, 3H,), 2.30-2.18 (m, 4H), 1.79-1.67 (m, 2H), 1.47-1.34 (m, 2H) and 0.98 (t, *J*=7.0, 3H).

^{13}C NMR (101 MHz, $CDCl_3$): δ ppm 122.1, 119.0, 64.2, 48.1, 25.6, 21.4, 19.4 and 13.3

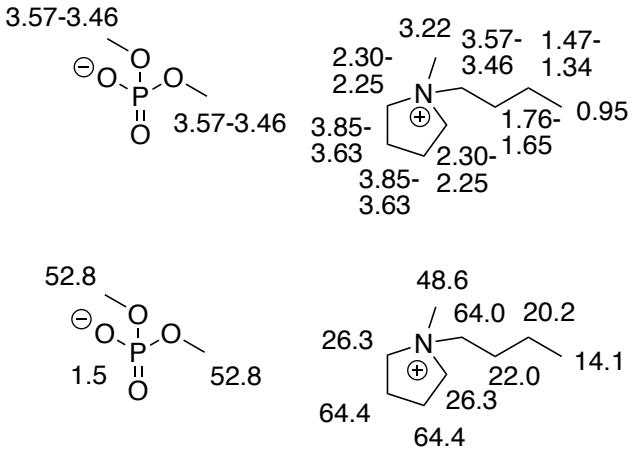
^{19}F NMR (376 MHz, $CDCl_3$): δ ppm -78.3.

ESI-MS (+ve) $[C_9H_{20}N]$: calc 142.1575, found 142.1599;

ESI-MS (-ve) $[CF_3O_3S]$: calc 148.9565, found 148.8566.

Data in agreement with literature values.[321,322]

5.1.2.2.2 1-butyl-1-methylpyrrolidinium dimethylphosphate, $[C_4C_1Pyrr][Me_2PO_4]$.[136]



To a solution of 1-butylpyrrolidine (5.5200 g, 0.4300 mol) in toluene (10 mL), trimethylphosphate (5.2400 g, 0.3700 mol) was added dropwise. The mixture was stirred at 80° C for 24 hours under an inert Ar atmosphere. The remaining solvent was evaporated. The crude was re-dissolved in a minimal amount of acetonitrile, then washed with diethyl ether and dried *in vacuo* at 50° C to yield a yellowish viscous liquid. (8.93 g, 89.3%)

^{1}H NMR (400 MHz, $CDCl_3$): δ ppm 3.85-3.63 (m, 4H), 3.57-3.46 (m, 8H), 3.22 (s, 3H,), 2.30-2.15 (m, 4H), 1.76-1.65 (m, 2H), 1.47-1.34 (m, 2H) and 0.95 (t, *J*=7.0, 3H).

^{13}C NMR (101 MHz, $CDCl_3$): δ ppm 64.4, 64.0, 52.8, 48.6, 26.3, 22.0, 20.2 and 14.1

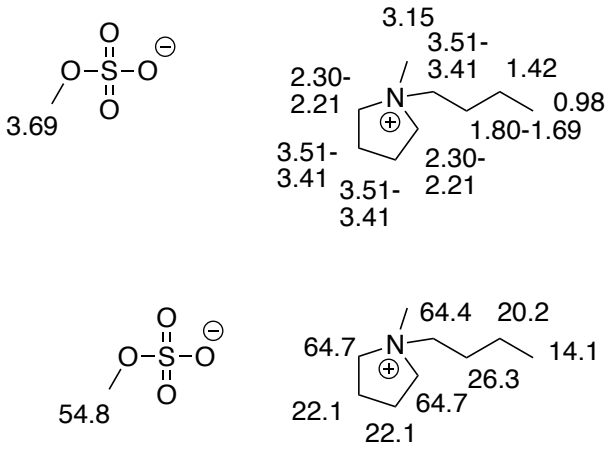
^{31}P NMR (202 MHz, $CDCl_3$): δ ppm 1.5.

ESI-MS (+ve) [$C_9H_{20}N$]: calc 142.1590, found 142.1589;

ESI-MS (-ve) [$C_2H_6O_4P$]: calc 125.0009, found 125.0008.

Data in agreement with literature values.[136]

5.1.2.2.3 1-butyl-1-methylpyrrolidinium methylsulfate, $[C_4C_1Pyrr][MeSO_4]$.[280]



Dimethyl sulfate (5.2300 g, 0.4100 mmol) was added dropwise to the cooled (0° C) to a solution of 1-butylpirrolidine (5.0200 g, 0.3900 mmol) in 25 mL of toluene. The reaction mixture was stirred at room temperature for 4 hours, under an inert Ar atmosphere.
After the reaction stopped, the upper organic phase of the resulting mixture was decanted, and the lower IL phase was washed with ethyl acetate (4x10 mL). After the last washing, the remaining ethyl acetate was removed under reduced pressure. The IL was dried *in vacuo* at 70° C to yield a yellowish liquid (8.12 g, 81.2%).

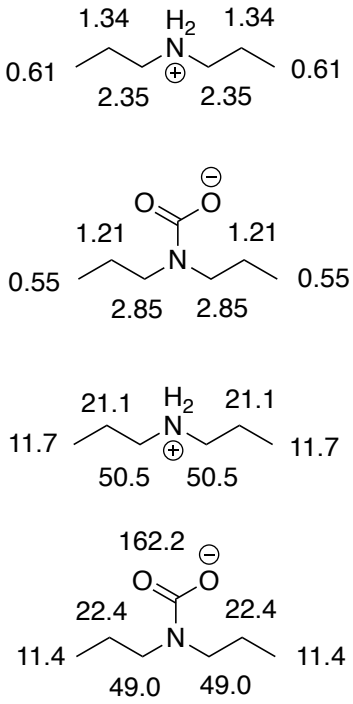
^{1}H NMR (400 MHz, $CDCl_3$): δ ppm 3.69 (s, 3H,), 3.51-3.41 (m, 4H), 3.15 (s, 3H,), 2.30-2.21 (m, 4H), 1.80-1.69 (m, 2H), 1.42 (sext, *J=7.0,* 2H) and 0.98 (t, *J*=7.0, 3H).

^{13}C NMR (101 MHz, $CDCl_3$): δ ppm 64.7, 64.4, 54.8, 48.7, 26.3, 22.1, 20.2 and 14.1

ESI-MS (+ve) $[C_9H_{20}N]$: calc 142.1678, found 142.1692;
Data in agreement with literature values.[280]

5.1.2.3 Distillable ILs

5.1.2.3.1 *N,N*-dipropylammonium *N',N'*-dipropylcarbamate, DPCARB.[323]

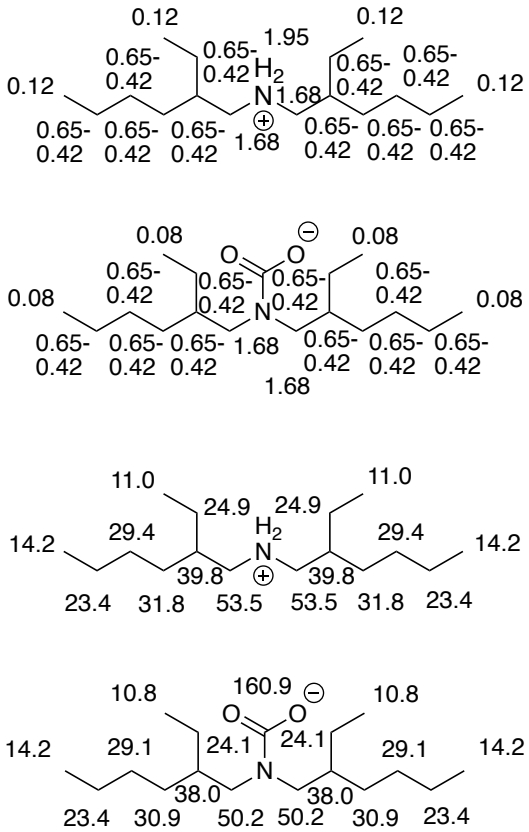


The synthesis of *N,N*-dipropylammonium *N',N'*-dipropylcarbamate, DPCARB, involved the mixture of dipropylamine (20.0000 g, 0.200 mol) with dry ice (4.35 g, 0.990 mol) at a 2:1 M ratio. Small pieces of dry ice were added into amine in a round bottom flask, which was placed in an ice bath. A stopper was immediately inserted to prevent any vapour from escaping. However, a needle was used in order to release some pressure. The contents were stirred until the dry ice is fully dissolved. The product was obtained as a transparent liquid.

^{1}H NMR (500 MHz, $(CD_3)_2CO$): δ ppm 2.85 (t, *J*=7.5, 4H), 2.35 (t, *J*=7.5, 4H), 1.34 (sext, *J*=7.5, 4H), 1.21 (sext, *J*=7.5, 4H), 0.61 (t, *J*=7.5, 6H) and 0.55 (sext, *J*=7.5, 6H);

^{13}C NMR (126 MHz, $(CD_3)_2CO$): δ ppm 162.2, 50.5, 49.0, 22.4, 21.1, 11.7 and 11.4.
Data in agreement with literature values.[323]

5.1.2.3.2 Bis(2-ethylhexyl)ammonium bis(2-ethylhexyl)carbamate, DBCARB.[323]



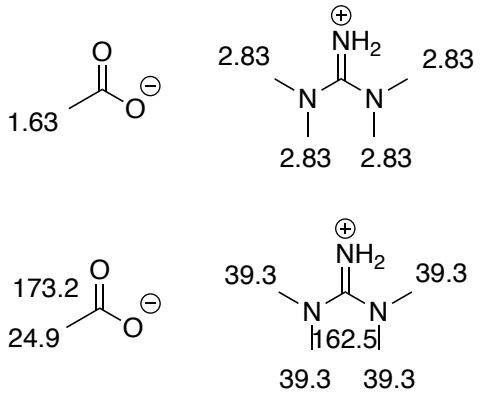
The synthesis of bis(2-ethylhexyl)ammonium bis(2-ethylhexyl)carbamate, DBCARB, involved the mixture of bis(2-ethylhexyl)amine (20.0000 g, 0.0830 mol) with dry ice (1.8200 g, 0.0410 mol) at a 2:1 M ratio. Small pieces of dry ice were added into amine in a round bottom flask, which was placed in an ice bath. A stopper was immediately inserted to prevent any vapour from escaping. However, a needle was used to release some pressure. The contents were stirred until the dry ice is fully dissolved. The product was obtained as a transparent liquid.

^{1}H NMR (500 MHz, $(CD_3)_2CO$): δ ppm 0.08 (t, *J*=7.5, 12H), 0.12 (t, *J*=7.5, 12H), 0.65-0.42 (m, 36H), 1.68 (d, *J*=5, 8H) and 1.95 (s, 2H);

^{13}C NMR (126 MHz, $(CD_3)_2CO$): δ ppm 160.9, 53.5, 50.2, 39.8, 38.0, 31.8, 30.9, 29.4, 29.1, 24.9, 24.1, 23.4, 14.2, 11.0 and 10.8.

Data in agreement with literature values.[323]

5.1.2.3.3 1,1,3,3-tetramethylguanidinium acetate, [TMGH][OAc]. [294]



The 1,1,3,3-tetramethylguanidinium acetate, [TMGH][OAc], was synthesised by the mixture 1,1,3,3-tetramethylguanidine (20.0000 g, 0.1700 mol) with acetic acid (10.4000 g, 0.1700 mmol) at a 1:1 M ratio. The product was obtained as a solid.

^{1}H NMR (500 MHz, $(CD_3)_2SO$): δ ppm 2.83 (s, 12H) and 1.63 (s, 3H);

^{13}C NMR (101 MHz, $(CD_3)_2SO$): δ ppm 173.2, 162.5, 39.3 and 24.9.

ESI-MS (+ve) [$C_5H_{14}N_3$]: calc 116.1182, found 116.1191;
Data in agreement with literature values.[294]

5.1.3 Water content of IL

It is well known that the presence of water has a substantial impact on the dissolution methods.[108,324–326] For that purpose, all the ILs were analysed by Karl Fischer beforehand. The measure was performed in Model CA-200 Series Karl Fischer Analysers for Low Level Moisture Detection Mitsubishi.

Table 24. Ionic Liquids moisture.

Ionic liquid	Sample w(g)	Water content w(µg)
$[C_2C_1Im][OAc]$	0.0522	20.2
$[C_2C_1Im]Br$	0.0418	21.8
$[C_2C_1Im][Me_2PO_4]$	0.0374	31.0
$[C_4C_1Im][OAc]$	0.0423	33.8
$[C_4C_1Im][Me_2PO_4]$	0.0673	36.1
$[C_4C_1Im]Cl$	0.0340	22.7
$[C_4C_1Im][CH_3O_4S]$	0.0551	3.1
$[C_4C_1Im][CF_3SO_3]$	0.0429	25.1
$[C_8C_1Im][Me_2PO_4]$	0.0322	40.6
$[C_4C_1Pyrr][CF_3SO_3]$	0.0726	20.2
$[C_4C_1Pyrr][Me_2PO_4]$	0.0318	30.7
$[C_4C_1Pyrr][Me_2SO_4]$	0.0398	9.9

5.2 Keratin process

5.2.1 Pre-treatment

All hair samples tested in this Thesis were obtained from Banbury Postiche Limited. The samples were used on their original length (15 cm) for dissolution and they were kept in sealed bags at room temperature.

The hair samples were washed with 5 g of a standard shampoo provided by Unilever and air-dried for at least 24 hours. This step pretends eliminate any contamination of the hair fibres. After the fibres were air-dried for at least 24 hours, they were tested on dissolution.

5.2.2 Dissolution method

The dissolution of hair was tested at different ratios, maintaining the mass of IL constant at 0.77 g. The hair mass varied from 0.0800 g, 0.1000 g, 0.1500 g, 0.2000 g, 0.2500 g and 0.3000 g.

To an empty vial, the hair fibres were weighed and 0.77 g of IL was added. Each hair:IL wt% ratio was repeated three times. The vials were placed into a sand bath at 100° C since sand conducts heat evenly to all sides of the vials. The dissolution was considered completed when it was no longer possible to observe hair fragments. After dissolution, by visual observation, vials were removed from the bath and allow to cool down.

5.3 Regeneration process of recovered material

After dissolution, the recovered material (recovered keratin) was regenerated from the ILs solution by the addition of 6 mL of water at room temperature, separated by centrifugation for 10 minutes at 7500 rpm. The water-soluble fraction was decanted and kept inside a round bottom flask. This process was repeated one more time. 5 mL of ethanol was added to the recovered material and mixed on a vortex to help to remove any IL left. The mixture was separated by centrifugation for 5 minutes at 7500 rpm. After that, recovered material was dried at 70° C for 24 hours. The water-soluble fraction after the regeneration process presented a brown colour, which may indicate that there is some hair material left on the water-soluble fraction trapped with IL. The dissolution samples prepared for dissolution studies are listed below.

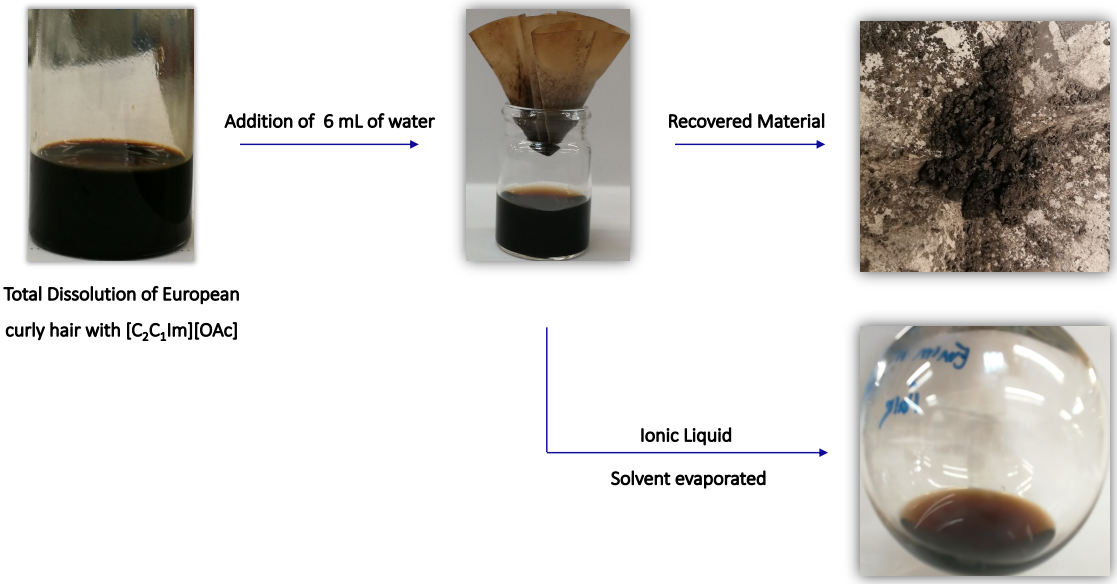


Figure 44. Schematics of the regeneration process after dissolution of hair.

Table 25. Samples prepared for the dissolution of hair from different ethnicities backgrounds performed with $[C_2C_1Im][OAc]$.

					Average	STDEV	Average	STDEV
Hair type	Hair w(g)	IL w(g)	Time (hours)	Recovered material w(g)	Time (hours)	Time (hours)	Recovered material (g)	Recovered material (g)
	0.0833	0.7788	8	0.0230				
	0.0819	0.7765	15	0.1040	11	3	0.045	0.0311
	0.0817	0.7724	12	0.0670				
	0.1034	0.7769	11	0.0237				
	0.1169	0.7818	18	0.0354	21	4	0.0295	0.0083
	0.1018	0.7772	35*	0.0606				
Curly	0.1575	0.7716	14*	0.0304				
	0.1509	0.7744	35	0.1105*	28	1	0.0502	0.0398
	0.1549	0.7715	35	0.0701				
	0.2037	0.7701	32*	0.1269*				
	0.2007	0.7704	93	0.0163	73	0	0.0161	0.0003
	0.2079	0.7744	93	0.0159				
	0.2519	0.7789	34	0.1266	115	0	0.0751	

	0.2544	0.7795	156	0.0235				0.0729
	0.2475	0.775	156	**				
	0.3082	0.7787	140	0.0903				
	0.3121	0.7791	138	0.0233	139	1	0.0233	0.0474
	0.3076	0.7758	201	**				
Straight	0.0831	0.7794	23	0.0418				
	0.0848	0.7826	12	0.0582	17	6	0.0689	0.0116
	0.0899	0.7733	18	0.1068				
	0.1079	0.7785	24	0.0455				
	0.1075	0.7738	15	0.0974	18	5	0.0763	0.0081
	0.1115	0.7729	15	0.0860				
	0.1621	0.7735	24	0.0052				
	0.1588	0.7741	25	0.0768	25	2	0.0499	0.0390
	0.1601	0.7736	27	0.0678				
	0.2111	0.7712	26	0.0948				
	0.2055	0.7752	35	0.1717	31	5	0.1276	0.0397
	0.2176	0.7786	32	0.1163				
	0.255	0.7741	58	0.0919				
	0.2694	0.7716	93	0.0257	76	25	0.0614	0.0334
	0.2844	0.7738	195	0.0666				
	0.3074	0.7758	197*	0.1857				
	0.2959	0.7715	99	0.0764	96	4	0.0983	0.0308
	0.3001	0.776	93	0.0329				
Blonde	0.0832	0.7714	18	**				
	0.0902	0.7803	20	0.0383	19	1	0.0428	0.0064
	0.0878	0.7702	20	0.0473				
	0.1049	0.7885	24	**	24	0	0.0573	
	0.1055	0.7733	24	0.0573				
	0.1655	0.7866	43	0.1084				
	0.1529	0.773	43	0.0185	43	0	0.1187	0.0146
	0.1546	0.7868	43	0.129				
	0.2004	0.7687	72	0.0036				
	0.2035	0.7717	72	**	72	0	0.0389	0.0499
	0.205	0.7802	72	0.0741				

	0.2508	0.7758	112	0.0922				
	0.2513	0.7702	112	0.0299	112	0	0.0648	0.0318
	0.2534	0.7707	112	0.0722				
	0.087	0.77	10	0.0255				
	0.0886	0.7953	11	**	11	1	0.0193	0.0088
	0.0801	0.7745	10	0.013				
	0.109	0.7702	13	0.0262				
	0.1001	0.7711	11	0.0009*	12	1	0.0307	0.0064
	0.103	0.7778	11	0.0352				
	0.1609	0.7831	48	0.038				
Asian	0.1512	0.7723	48	0.0241	48	0	0.0458	0.0265
	0.1529	0.7726	48	0.0754				
	0.2166	0.7717	72	0.0701				
	0.2047	0.7716	72	0.0038	72	0	0.0283	0.0364
	0.2099	0.7713	72	0.0111				
	0.2526	0.7749	360	0.0407				
	0.2546	0.7917	360	0.0942	360	6	0.0730	0.0284
	0.2582	0.7725	350	0.084				

*values discarded due to be outliers.

** *Measurement corrupted*

Table 26. Samples prepared for the dissolution of European curly hair performed with $[C_4C_1Im][OAc]$.

				Average	STDEV	Average	STDEV
Hair w(g)	IL w(g)	Time (hours)	Recovered material W(g)	Time (hours)	Time (hours)	Recovered material w(g)	Recovered material w(g)
0.0807	0.7707	14	0.0240				
0.0811	0.7788	14	0.0176	14	7	0.0208	0.0045
0.0825	0.7721	26*	0.0528*				
0.1121	0.771	23	0.0447				
0.1067	0.7732	32	0.0531	25	6	0.0489	0.0059
0.1098	0.7745	21	0.0113*				

0.1534	0.78	28	0.0608				
0.1606	0.7763	26	0.0541	27	9	0.0574	0.0047
0.1525	0.7754	43*	0.0318*				

*values discarded due to be outliers.

Table 27. Samples prepared for the dissolution of European curly hair performed with $[C_2C_1Im][Me_2PO_4]$.

Hair w(g)	IL w(g)	Time (hours)	Recovered material w(g)	Average Time (hours)	STDEV Time (hours)	Average Recovered material w(g)	STDEV Recovered material w(g)
0.0807	0.772	111	0.0396				
0.0846	0.7752	115	0.0312	112	3	0.0354	0.0059
0.0857	0.7755	110	0.008*				
0.1039	0.7717	164	0.0654				
0.1053	0.7754	180	0.0532	171	8	0.0558	0.0086
0.1099	0.7721	168	0.0488				
0.1509	0.7722	195	0.1109				
0.1567	0.772	250	0.1009	194	32	0.0998	0.0116
0.1476	0.7703	193	0.0877				
0.206	0.7702	198	0.1136				
0.1972	0.7712	360	0.1055	199	93	0.1028	0.0124
0.2087	0.7801	200	0.0893				
0.2639	0.7722	200	0.1109				
0.2577	0.7765	205	0.1215	218	28	0.1162	0.0075
0.2532	0.7782	250	0.0076*				
0.3149	0.7728	216	0.1391				
0.3088	0.7712	300	0.1076	213	50	0.0855	0.0674
0.3043	0.7723	210	0.0098				

*values discarded due to be outliers.

Table 28. Samples prepared for the dissolution of European curly hair performed with $[C_4C_1Im][Me_2PO_4]$.

Hair w(g)	IL w(g)	Time (hours)	Recovered material w(g)	Average Time (hours)	STDEV Time (hours)	Average Recovered material w(g)	STDEV Recovered material w(g)
0.0819	0.7787	147	0.0428				
0.0836	0.7717	140	0.0522	179	5	0.0447	0.0068
0.0804	0.7719	250	0.0391				
0.1011	0.7781	199	**				
0.1055	0.7765	200	**	201	3		
0.1101	0.7721	205	**				
0.1518	0.7704	219	**				
0.1511	0.7710	220	**	230	1		
0.1566	0.7708	250	**				

** *Measurement corrupted*

5.3.1 Dissolution assisted by microwave radiation

The dissolution assisted by microwave was tested with 0.1500 g of hair and two ILs $[C_2C_1Im][OAc]$ and $[C_2C_1Im][Me_2PO_4]$ (0.7700 g). The hair was placed inside a microwave flask with a magnetic stirring bar and IL. The dissolution with $[C_2C_1Im][OAc]$ was performed at 10 W of power at 87° C, maximum temperature reached during the experiment, for 5 minutes. The dissolution of hair with $[C_2C_1Im][Me_2PO_4]$ was performed at 10 W of power, maximum temperature reached was 87° C, for 10 min. To improve the mixing and temperature gradients, triangular shape stirring bars were used.

After the total dissolution, by visual observation, the dissolution was allowed to cool to room temperature to then process with the regeneration process.

5.4 Instrumentation

After the regeneration process, it was noticed that the IL solution showed a brownish colour, Figure 13. This is may be due to hair material left in the IL solution. To recover the material left in solution several attempts were made. To IL solution (water-soluble fraction) a solvent with different polarity was added in order to precipitate the material. The solvents tested in this procedure were, chloroform, ethyl acetate, diethyl ether, and hexane. After drying, to remove the excess water, after the regeneration process ILs were analysed by ATR-FTIR to detect any material left. During this analysis only IL peaks were possible to detect.

The IL solution was analysed by ToF-SIMS, but due to the small window of m/z the fragments detected were similar to IL fragmentation, which makes it difficult to distinguish hair material fragments from IL fragments.

5.4.1 Thermogravimetric analysis (TGA)

5.4.1.1 Analysis of the recovered hair material

Approximately 0.0400 g of sample was heated, in a platinum sample pan, from 40° C to 600° C under a dynamic air atmosphere at a heating rate of 5° C/min. TGA instrument used in these analyses was TA Instruments Discovery.

5.4.1.2 Analysis of the precipitate from IL water-soluble fraction

The thermal stability of precipitate from water-soluble fraction (water used to precipitate keratin from the IL) was further analysed via thermogravimetric analysis (TGA). Approximately 0.0200 g of sample was heated, in a platinum high temperature sample pan, from 40 to 600° C under a dynamic air atmosphere at a heating rate of 5° C/min.

5.4.2 FTIR spectroscopy: Attenuated Total Reflectance (ATR)

Attenuated total reflectance infrared spectroscopy (ATR-FTIR) was recorded using a FT-IR Bruker Vertex system with a diamond micro-Attenuated total reflectance crystal and a liquid nitrogen cooled LN-MCT detector. Spectra were recorded in the 400 to 4000 cm^{-1} range. The spectra were collected with a resolution of 2 cm^{-1} with 32 scans.

5.4.3 FTIR spectroscopy

FT-IR was recorded using a FT-IR Bruker using KBr disc. Spectra were recorded in the 400 to 4000 cm^{-1} range. Analysis performed by Doctor Coby Clarke.

5.4.4 Scanning Electron Microscopy (SEM)

5.4.4.1 Analysis of the recovered hair material

The Scanning electron microscopy was used to identify the morphology of the recovered material. Samples were placed on carbon tape and coated with platinum. The analysis was led on JEOL JSM-6490LV, the magnification varied from x65 to x85, a 10 kV accelerating voltage and working distance of 10 mm.

The recovered material was also analysed by SEM with EDX detector attached to provide elemental identification and semi-quantitative compositional information where necessary.

5.4.4.2 Analysis of the treated hair fibres

The Scanning electron microscopy was used to identify morphological changes on the surface of hair fibres after the ATR-FTIR analysis. The fibres were placed on carbon tape and coated with platinum. The analysis was led on JEOL JSM-6490LV, the magnification

ranged from x50 to x300 in order to obtain the best results a 10 kV accelerating voltage and a working distance of 9 mm.

The modified fibres were also analysed by SEM with EDX detector attached to provide elemental identification and semi-quantitative compositional information where necessary. The magnification varied from x65 to x85, a 10 kV accelerating voltage and working distance of 10 mm.

5.4.5 Time of Flight (ToF) Mass Spectrometer Coupled with Matrix Assisted Laser Desorption Ionization (MALDI)

5.4.5.1 Analysis of the recovered hair material

The Time of Flight (TOF) mass spectrometer coupled with Matrix Assisted Laser Desorption Ionization (MALDI) was recorded with Bruker Autoflex. This technique allows the analysis of large organic molecules and biomolecules, which was the case of our recovered material samples and chemically untreatedhair.

Preparation of the MALDI matrix

A solution of sinapinic acid was prepared, 0.0050 g of sinapinic acid was dissolved in 0.5 mL of 30% acetonitrile, 70% proteomics grade water and 0.1% trifluoroacetic acid (TFA). After that the solution was mixed vigorously on a vortex. 5 μL of matrix was added to the sample placed on the steel MALDI plate.

The data was collected in Positive MS reflector mode for the mass-to-charge ratio (m/z) 20 to 210 kDa. The system used a laser source with a wavelength of 355 nm, the detection algorithm was used to centroid de data.

5.4.5.2 Analysis of the treated hair fibres

The Time of Flight Secondary Ion Mass Spectrometry (ToF-SIMS) measurement were performed with an ION-TOF IV spectrometer. The depth profile analysis of chemically untreated hair was performed with negative polarity, the primary ion source was

bismuth cluster ion (Bi_3^+) and their sputter ion source was argon gas cluster ion with 20 000 eV energy (Ar_{1900}^+). Chemically untreated European straight hair was placed aligned to the beam axis of the primary ion and the sputter ion beam was located in an orthogonal direction to it.

The surface analysis of ILs during and after total dissolution of hair were also analysed by ToF-SIMS, as well as, the recovered material from the European curly hair dissolution with $[C_2C_1Im][OAc]$. The surface analysis of these compounds was performed in both positive and negative polarity using Bi_3^+ ion beam with 25000 eV of energy with a field of view (FoV) of 150 x 150 μm and rastered in random mode, 256 by 256 pixels.

5.4.6 Mass spectrometry

5.4.6.1 Analysis of the ionic liquids

ESI-MS was performed at Bruker MicroTOF 62 spectrometer and 0.0030 g of sample were prepared in acetonitrile.

5.4.7 Polarised light microscopy

The dissolution of a single fibre followed by microscopy analysis was recorded with BX51P polarizing microscope. The fibres were analysed with bottom light with 20 % intensity.

Chapter 6 Conclusions and Future work

The various studies in this Thesis have shown that the successful dissolution of hair with ILs is possible as is the consequent recovery of the material after the dissolution.

The study in Chapter 2 was designed to determine the effect of the anion and cation of ILs on the dissolution of hair. This study has shown that the dissolution of hair is possible when 1-butyl-3-methylimidazolium cation is coupled with [OAc], [Me_2PO_4] and Cl. Furthermore, the cation made no significant difference to the dissolution of hair when imidazolium and pyrrolidinium cations where investigated. However, the aliphatic side chain of the cation has an impact on the performance of the IL on the dissolution of hair due to the increase of the viscosity of the IL. The results of this investigation show that [C_2C_1Im][OAc] has the fastest dissolution rate (see Figure 11), which might indicate that acetate anion can easily penetrate the structure of hair, from the cuticle cells to the cortex. What stands out from this investigation is the time required to dissolve hair with ILs with conventional heating methods, consequently it was possible to decrease the time of dissolution with the use of microwave radiation, Table 10. Finally, it was possible to conclude that the nature of the hair has no impact on its dissolution with ILs. One of the more significant finding to emerge from this study is that it is possible to dissolve hair with ILs.

Moreover, in Chapter 3, a study in this Thesis shown the recovery of material from the dissolution of hair with ILs is possible. This study has found that generally is possible to recover material from the dissolution, additionally the dissolution of hair with [C_2C_1Im][OAc] showed lower results for recovered material weights when compared with dimethylphosphate-based IL. It was also found that as the initial mass of dissolved hair increased the recovered material weight decreased. This could be due to experimental errors, but it could also be related to the mechanism of dissolution of different ILs. One hypothesis can be the way that acetate anion cleaves hydrogen and disulfide bonds and the affinity of these particles to IL phase, which results in less recovered material as the

majority has been retained within the IL. Additional theoretical or computational analysis with different anions and cations would offer additional information on how ILs disrupt the structure of hair and the affinity of hair to IL phase.[261] During the regeneration process of recovered material, it was observed the formation of a precipitate layer in the water-soluble fraction. The thermal profile of the precipitate was identical to the chemically untreated hair profile, it is important to mention that this was observed in the regeneration process of all hair types from the dissolution with $[C_2C_1Im][OAc]$. Considerably more work will need to be done to characterise the water-soluble fraction, sodium dodecyl sulphate-polyacrylamide gel electrophoresis (SDS-PAGE) with a standard marker could be used to characterise and identify proteins in the water-soluble fraction.[133] On the other hand, recovered material and precipitate from the water-soluble fraction from dissolution with $[C_2C_1Im][Me_2PO_4]$ presented similar behaviour, however they had a different thermal profile from chemically untreated hair. This might indicate the presence of IL in the recovered material from conventional heating dissolution. In order to better comprehend this issue a dissolution of hair with a comparison mixture of $[C_2C_1Im][Me_2PO_4]$ diluted with $[C_2C_1Im][OAc]$ could be performed. The TG profile of the recovered material from this dissolution would reveal the complexity of the interactions, furthermore the quantification of $[OAc]^-$ and $[Me_2PO_4]^-$ modification on the structure of hair would be possible. Additionally, X-Ray Photoelectron Spectroscopy (XPS) would show residual phosphorous in the structure of hair.

Finally, MALDI analysis on recovered material allowed the identification of keratins, in this investigation only keratins present in hair's cortex/medulla were considered. This technique is very promising, however more investigation on the sample preparation need to be further investigated. Due to the difficulties on the recovery process of the dissolution of hair with imidazolium based ILs, distillable ILs were investigated to improve the recovery method. However, in this study the dissolution of hair was not achieved. A further study could assess the long-term effects of distillable ILs on the structure of hair. An alternative to the current used distillable ILs could be dimethylammonium formate [DMEA][HCOO] as has been reported to dissolve up to 63% of feather keratin.[110]

In Chapter 4, the impact of ILs on the structure of hair was investigated and it was possible to observe the swelling of the fibre, following by the total dissolution of the

cortex. SEM analysis on these fibres shown the sulfur content decrease drastically when compared to chemically untreated hair fibres. Similarly, ToF-SIM analysis highlighted the damage of the fibre treated with $[C_2C_1Im][OAc]$, yet as expected, fibres treated with $[C_2C_1Im][Me_2PO_4]$ did not show as damaged as fibres treated with acetate-based ionic liquid.

Both $[C_2C_1Im][OAc]$ and $[C_2C_1Im][Me_2PO_4]$ are able to dissolve hair, however $[C_2C_1Im][OAc]$ has the disadvantage of complex synthesis process and high price which limits its industrial application.[327] While $[C_2C_1Im][Me_2PO_4]$ is easily synthesised and lower price.[137]

In Chapter 4 the natural variation of hair was investigated by ATR-FTIR, this study has shown that some variations on spectrum may be due to differences on the structure of hair, but others may be related to the region being sampled. This can be related to the thickness of the fibre along the hair and so the region being sampled may be different. Some variations on the bands related to oxidation products of the cystine were detected, which suggested the tip of the hair is more damaged than the top of the hair by natural weathering and some styling methods. The analysis of hair with infrared spectroscopy has proven to be very challenging and very complex, for that reason Raman spectroscopy might be a suitable alternative and complementary technique to evaluate the hair structure due to its sensitivity to different vibrational modes not detected by FTIR. However, this investigation can only be performed with albino/grey hair. Additionally, Atomic Force Microscopy could be applied to determine any modification on the surface of hair after the IL treatment.

References

1 Material District, Human hair rope, https://materialdistrict.com/material/human-hair-rope/#moved, (accessed 20 January 2010).

2 Molika Ashford, What Happens Inside a Landfill?, https://www.livescience.com/32786-what-happens-inside-a-landfill.html, (accessed 6 June 2021).

3 A. Chamas, H. Moon, J. Zheng, Y. Qiu, T. Tabassum, J. H. Jang, M. Abu-Omar, S. L. Scott and S. Suh, *ACS Sustain. Chem. Eng.*, 2020, **8**, 3494–3511.

4 M. Brebu and I. Spiridon, *J. Anal. Appl. Pyrolysis*, 2011, **91**, 288–295.

5 A. Gupta, *J. Waste Manag.*, 2014, **2014**, 1–17.

6 Schwarzkof, Hair Dictionary: Important Facts about Hair, https://www.schwarzkopf.co.uk/en/hairstyling/tipsandtricks/hair_dictionary.html, (accessed 10 August 2019).

7 L. N. Jones and D. E. Rivett, *Micron*, 1997, **28**, 469–485.

8 L. Coderch, S. Méndez, C. Barba, R. Pons, M. Martí and J. L. Parra, *Chem. Phys. Lipids*, 2008, **155**, 1–6.

9 L. Kreplak, F. Briki, Y. Duvault, J. Doucet, C. Merigoux, F. Leroy, J. L. Lévêque, L. Miller, G. L. Carr, G. P. Williams and P. Dumas, *Int. J. Cosmet. Sci.*, 2001, **23**, 369–374.

10 N. Keiichi, N. Minako, I. Yasunori, K. Yoshio and F. Makoto, *J. Japanese Cosmet. Sci. Soc.*, 1989, **13**, 134–139.

11 C. Barba, M. Martí, J. Carilla, A. M. Manich and L. Coderch, *Thermochim. Acta*, 2013, **552**, 70–76.

12 L. Coderch, M. A. Oliver, V. Martínez, A. M. Manich, L. Rubio and M. Martí, *Ski. Res. Technol.*, 2017, **23**, 479–485.

13 M. Picardo, M. Ottaviani, E. Camera and A. Mastrofrancesco, *Dermatoendocrinol.*, 2009, **1**, 68–71.

14 A. Franbourg, P. Hallegot, F. Baltenneck, C. Toutain and F. Leroy, *J. Am. Acad. Dermatol.*, 2003, **48**, 115–119.

15 L. J. Wolfram, *J. Am. Acad. Dermatol.*, 2003, **48**, 106–114.

16 N. H. Leon, *J. Soc. Cosmet. Chem.*, 1972, **23**, 427–445.

17 A. P. Negri, H. J. Cornell and D. E. Rivett, *J. Soc. Dye. Colour.*, 1993, **109**, 296–301.

18 J. A. Swift, *J. Cosmet. Sci.*, 1999, **50**, 23–47.

19 D. E. Rivett, C. W. Ward, L. M. Beikin, J. A. M. Ramshaw and J. F. K. Wilshire, *The Lennox Legacy : the History of the CSIRO Laboratory at 343 Royal Parade Parkville.*, CSIRO Publishing, Collingwood, 1996.

20 M. Feughelman, *Mechanical properties and structure of alpha-keratin fibres : wool, human hair, and related fibres*, UNSW Press, Sydney, 1997.

21 S. D. O'Connor, K. L. Komisarek and J. D. Baldeschwieler, *J. Invest. Dermatol.*, 1995, **105**, 96–99.

22 C. R. Robbins, in *Chemical and Physical Behavior of Human Hair*, Springer, New York, 2012, pp. 105–176.

23 D. I. H. Zhan, F.-J. Wortmann and H. Höcker, *Chemie unserer Zeit*, 1997, **31**, 280–290.

24 M. A. Rogers, L. Langbein, S. Praetzel-Wunder, H. Winter and J. Schweizer, *Int. Rev. Cytol.*, 2006, **251**, 209–263.

25 D. W. Deedrick and S. L. Koch, *Forensic Sci. Commun.*, 2008, **6**, 1–44.

26 R. Matsunaga, R. Abe, D. Ishii, S. ichi Watanabe, M. Kiyoshi, B. Nöcker, M. Tsuchiya and K. Tsumoto, *J. Struct. Biol.*, 2013, **183**, 484–494.

27 J. W. S. Hearle, *Int. J. Biol. Macromol.*, 2000, **27**, 123–138.

28 S. E. Medland, D. R. Nyholt, J. N. Painter, B. P. McEvoy, A. F. McRae, G. Zhu, S. D. Gordon, M. A. R. Ferreira, M. J. Wright, A. K. Henders, M. J. Campbell, D. L. Duffy, N. K. Hansell, S. Macgregor, W. S. Slutske, A. C. Heath, G. W. Montgomery and N. G. Martin, *Am. J. Hum. Genet.*, 2009, **85**, 750–755.

29 I. J. Rodney, O. C. Onwudiwe, V. D. Callender and R. M. Halder, *J. Drugs Dermatology*, 2013, **12**, 420–427.

30 S. Thibaut, O. Gaillard, P. Bouhanna, D. W. Cannell and B. A. Bernard, *Br. J. Dermatol.*, 2005, **152**, 632–638.

31 S. Breakspear, J. R. Smith and G. Luengo, *J. Struct. Biol.*, 2005, **149**, 235–242.

32 S. Thibaut and B. A. Bernard, *Int. J. Dermatol.*, 2005, **44**, 2–3.

33 Ashish, Why Do Some People Have Curly Hair While Others Have Straight Hair? » Science ABC, https://www.scienceabc.com/humans/why-do-some-people-have-

curly-hair-while-others-have-straight-hair.html, (accessed 22 January 2020).

34 F.-C. Yang, Y. Zhang and M. C. Rheinstädter, *PeerJ*, 2014, **2**, 1–19.

35 N. P. Khumalo, J. Stone, F. Gumedze, E. McGrath, M. R. Ngwanya and D. de Berker, *J. Am. Acad. Dermatol.*, 2010, **62**, 402–408.

36 S. Thibaut, P. Barbarat, F. Leroy and B. A. Bernard, *Int. J. Dermatol.*, 2007, **46**, 7–10.

37 W. G. Bryson, D. P. Harland, J. P. Caldwell, J. A. Vernon, R. J. Walls, J. L. Woods, S. Nagase, T. Itou and K. Koike, *J. Struct. Biol.*, 2009, **166**, 46–58.

38 C. F. Cruz, C. Costa, A. C. Gomes, T. Matamá and A. Cavaco-Paulo, *Cosmetics*, 2016, **3**, 26.

39 C. Nappe and M. Kermici, *J. Soc. Cosmet. Chem.*, 1988, **40**, 91–99.

40 L. J. Wolfram, *The Reactivity of Human Hair. A Review*, Springer Berlin Heidelberg, 1981.

41 E. Vijayalakshmi, Hair pollution hits Karnataka, https://www.downtoearth.org.in/news/in-disitressi-13180, (accessed 19 March 2020).

42 J. Turner, *Brushes: A Handbook for Artists and Artisans*, Design Books, New York, 1992.

43 B. A. Jubran, S. M. Habali, M. A. S. Hamdan and A. I. O. Zaid, *Mater. Struct.*, 1988, **21**, 364–369.

44 R. R. Pillai and A. Ramanathan, in *Third International Conference on Construction In Developing Countries (ICCIDC–III) "Advancing Civil, Architectural and Construction Engineering & Management"*, Bangkok, 2012.

45 EP Pat., 2035609A1, 2010.

46 Z. V. P. Murthy, G. Kaushik and R. Suratwala, *Indian J. Chem. Technol.*, 2004, **11**, 220–226.

47 R. D. Forrest, *J. R. Soc. Med.*, 1982, **75**, 198–205.

48 E. H. H. Windsor, *Pop. Mech. Mag. 1914*.

49 L. S. M. Curtin, in *Prophet of the Earth: Ethnobotany of the Pima*, ed. U. of A. Press, Tuscon, Ariz, USA, 1949.

50 V. D. Zheljazkov, *J. Environ. Qual.*, 2005, **34**, 2310–2317.

51 V. D. Zheljazkov, J. L. Silva and M. Patel, *Horttechnology*, 2008, **18**, 592–596.

52 K. R. Yadav, R. K. Sharma, M. P. Yadav and R. M. Kothari, *Fresenius Environ. Bull.*, 1995, **4**, 491–496.

53 D. Winterman, From food to fashion, the thriving market in human hair, http://news.bbc.co.uk/2/hi/uk_news/magazine/8753698.stm., (accessed 20 January 2005).

54 H. Lee, K. Noh, S. C. Lee, I. K. Kwon, D. W. Han, I. S. Lee and Y. S. Hwang, *Tissue Eng. Regen. Med.*, 2014, **11**, 255–265.

55 T. Fujii, D. Ogiwara and M. Arimoto, *Biol. Pharm. Bull.*, 2004, **27**, 89–93.

56 R. C. de Guzman, J. M. Saul, M. D. Ellenburg, M. R. Merrill, H. B. Coan, T. L. Smith and M. E. Van Dyke, *Biomaterials*, 2013, **34**, 1644–1656.

57 T. Fujii and Y. Ide, *Biol. Pharm. Bull.*, 2004, **27**, 1433–1436.

58 V. Verma, P. Verma, P. Ray and A. R. Ray, *Biomed. Mater.*, 2008, **3**, 025007.

59 P. M. Steinert and M. I. Gullino, *Biochem. Biophys. Res. Commun.*, 1976, **70**, 221–227.

60 H. Thomas, A. Conrads, K.-H. Phan, M. van de Locht and H. Zahn, *Int. J. Biol. Macromol.*, 1986, **8**, 258–264.

61 M. van de Locht, *Melliand Textilberichte*, 1987, **10**, 780–786.

62 F. Ikkai and S. Naito, *Biomacromolecules*, 2002, **3**, 482–487.

63 A. Tachibana, Y. Furuta, H. Takeshima, T. Tanabe and K. Yamauchi, *J. Biotechnol.*, 2002, **93**, 165–170.

64 H. Ito, T. Miyamoto and H. Inagaki, *Kobunshi Ronbunshu*, 1982, **39**, 221–227.

65 *US Pat. 6274163*, 2001.

66 *US Pat. 6159496*, 2000.

67 *WO Pat. 00/76437 A1*, 2001.

68 *US Pat. 6270793*, 2001.

69 *EP Pat. 2146738 A2*, 2008.

70 A. Tachibana, S. Kaneko, T. Tanabe and K. Yamauchi, *Biomaterials*, 2005, **26**, 297–302.

71 T. Aboushwareb, D. Eberli, C. Ward, C. Broda, J. Holcomb, A. Atala and M. Van Dyke, *Jounal Biomed. Mater. Res. - Part B Appl. Biomater.*, 2009, **90**, 45–54.

72 P. J. Apel, J. P. Garrett, P. Sierpinski, J. Ma, A. Atala, T. L. Smith, L. A. Koman and M. E. Van Dyke, *J. Hand Surg. (Am. Vol.)*, 2008, **33**, 1541–1547.

73 P. Sierpinski, J. Garrett, J. Ma, P. Apel, D. Klorig, T. Smith, L. A. Koman, A. Atala and M. Van Dyke, *Biomaterials*, 2008, **29**, 118–128.

74 K. Yamauchi, A. Yamauchi, T. Kusunoki, A. Kohda and Y. Konishi, *J. Biomed. Mater. Res.*, 1996, **31**, 439–444.

75 T. Tanabe, N. Okitsu, A. Tachibana and K. Yamauchi, *Biomaterials*, 2002, **23**, 817–825.

76 K. Yamauchi, H. Hojo, Y. Yamamoto and T. Tanabe, *Mater. Sci. Eng. C*, 2003, **23**, 467–472.

77 K. Y. Lee and W. S. Ha, *Polymer*, 1999, **40**, 4131–4134.

78 K. Y. Lee, S. J. Kong, W. H. Park, S. Ha and I. C. Kwon, *J. Biomater. Sci. Polym. Ed.*, 1998, **9**, 905–914.

79 K. Y. Lee, *Fibers Polym.*, 2001, **2**, 71–74.

80 A. Vasconcelos, G. Freddi and A. Cavaco-Paulo, *Biomacromolecules*, 2008, **9**, 1299–1305.

81 C. Tonin, A. Aluigi, C. Vineis, A. Varesano, A. Montarsolo and F. Ferrero, *J. Therm. Anal. Calorim.*, 2007, **89**, 601–608.

82 M. Zoccola, A. Montarsolo, A. Aluigi, A. Varesano, C. Vineis and C. Tonin, *e-Polymers*, 2007, **105**, 1–19.

83 K. Katoh, M. Shibayama, T. Tanabe and K. Yamauchi, *Biomaterials*, 2004, **25**, 2265–2272.

84 J. G. Rouse and M. E. Van Dyke, *Materials*, 2010, **3**, 999–1014.

85 C. S. Ki, E. H. Gang, I. C. Um and Y. H. Park, *J. Memb. Sci.*, 2007, **302**, 20–26.

86 J. Li, Y. Li, L. Li, A. F. T. Mak, F. Ko and L. Qin, *Polym. Degrad. Stab.*, 2009, **94**, 1800–1807.

87 H. L. Zhang, J. Wang, N. Yu and J. S. Liu, *J. Polym. Res.*, 2014, **21**, 329–337.

88 M. Boakye, N. Rijal, U. Adhikari and N. Bhattarai, *Materials*, 2015, **8**, 4080–4095.

89 D.-G. Yu, G. R. Williams, X. Wang, X.-K. Liu, H.-L. Li and S. A. Bligh, *RSC Adv.*, 2013, **3**, 4652–4658.

90 S. Sharma and A. Gupta, *Brazilian Arch. Biol. Technol.*, 2016, **59**, 1–14.

91 A. L. V. Villa, M. R. S. Aragão, E. P. D. Santos, A. M. Mazotto, R. B. Zingalli, E. P. de Souza and A. B. Vermelho, *BMC Biotechnol.*, 2013, **13**, 13–15.

92 Y. Shimomura and M. Ito, *J. Investig. Dermatology Symp. Proc.*, 2005, **10**, 230–233.

93 A. W. Lipkowski, B. Gajkowska, A. Grabowska and K. Kurzepa, *Polimery*, 2009, **54**, 386–388.

94 H. Xie, S. Li and S. Zhang, *Green Chem.*, 2005, **7**, 606–608.

95 S. Huda and Y. Yang, *J. Polym. Environ.*, 2009, **17**, 131–142.

96 R. J. Block, *Ann. N. Y. Acad. Sci.*, 1951, **53**, 608–612.

97 P. M. M. Schrooyen, P. J. Dijkstra, R. G. Oberthü, A. Bantjes and J. Feijen, *J. Agric. Food Chem.*, 2000, **48**, 4326–4334.

98 D. R. Goddard and L. Michaelis, *J. Biol. Chem.*, 1934, **106**, 605–614.

99 C. Jones and D. Mecham, *Arch. Biochem*, 1943, **3**, 193–202.

100 J. Maclaren, *Aust. J. Chem.*, 1962, **15**, 824–831.

101 A. J. Poole, J. S. Church and M. G. Huson, *Biomacromolecules*, 2009, **10**, 1–8.

102 R. Cecil and J. R. R. Mcphee, *Adv. Protein Chem.*, 1959, **14**, 255–389.

103 R. S. Asquith and N. H. Leon, in *Chemistry of Natural Protein Fibers*, ed. R. S. Asquith, Springer, Boston, 1977, pp. 193–265.

104 A. Mohd Idris, PhD Thesis, Monash University, 2014.

105 S. Pandey, *Anal. Chim. Acta*, 2006, **556**, 38–45.

106 A. Pinkert, K. N. Marsh, S. Pang and M. P. Staiger, *Chem. Rev.*, 2009, **109**, 6712–6728.

107 P. Wasserscheid and T. (Thomas) Welton, *Ionic Liquids in Synthesis.*, Wiley, Weinheim, 2008.

108 R. P. Swatloski, S. K. Spear, J. D. Holbrey and R. D. Rogers, *J. Am. Chem. Soc.*, 2002, **124**, 4974–4975.

109 M. Y. Lui, L. Crowhurst, J. P. Hallett, P. A. Hunt, H. Niedermeyer and T. Welton, *Chem. Sci.*, 2011, **2**, 1491–1496.

110 A. Idris, R. Vijayaraghavan, A. F. Patti and D. R. Macfarlane, *ACS Sustain. Chem. Eng.*, 2014, **2**, 1888–1894.

111 J. E. Plowman, S. Clerens, E. Lee, D. P. Harland, J. M. Dyer and S. Deb-Choudhury, *Anal. Methods*, 2014, **6**, 7305–7311.

112 Y. Kohno, S. Saita, K. Murata, N. Nakamura and H. Ohno, *Polym. Chem.*, 2011, **2**, 862–867.

113 K. Fujita, D. R. MacFarlane and M. Forsyth, *Chem. Commun.*, 2005, **38**, 4804–4806.

114 J. Zhang, J. Wu, J. Yu, X. Zhang, J. He and J. Zhang, *Mater. Chem. Front.*, 2017, **1**,

1273–1290.

115 A. Brandt, M. J. Ray, T. Q. To, D. J. Leak, R. J. Murphy and T. Welton, *Green Chem.*, 2011, **13**, 2489–2499.

116 H. Liu, K. L. Sale, B. M. Holmes, B. A. Simmons and S. Singh, *J. Phys. Chem. B*, 2010, **114**, 4293–4301.

117 H. Liu, G. Cheng, M. Kent, V. Stavila, B. A. Simmons, K. L. Sale and S. Singh, *J. Phys. Chem. B*, 2012, **116**, 8131–8138.

118 A. Pinkert, *J. Chem. Eng. Data*, 2012, **57**, 1338–1340.

119 F. Huo, Z. Liu and W. Wang, *J. Phys. Chem. B*, 2013, **117**, 11780–11792.

120 R. S. Payal and S. Balasubramanian, *Phys. Chem. Chem. Phys.*, 2014, **16**, 17458–17465.

121 B. D. Rabideau, A. Agarwal and A. E. Ismail, *J. Phys. Chem. B*, 2014, **118**, 1621–1629.

122 E. S. R. E. Hassan, F. Mutelet and M. Bouroukba, *Carbohydr. Polym.*, 2015, **127**, 316–324.

123 A. Benedetto and P. Ballone, *ACS Sustain. Chem. Eng.*, 2016, **4**, 392–412.

124 J. Xi, W. Du and L. Zhong, in *Cellulose: Medical, Pharmaceutical and Electronic Applications*, eds. T. van de Ven and L. Godbout, InTech, Croatia, 2013.

125 S. Zheng, Y. Nie, S. Zhang, X. Zhang and L. Wang, *ACS Sustain. Chem. Eng.*, 2015, **3**, 2925–2932.

126 A. Idris, R. Vijayaraghavan, U. A. Rana, A. F. Patti and D. R. MacFarlane, *Green Chem.*, 2014, **16**, 2857–2864.

127 Z. Zhang, Y. Nie, Q. Zhang, X. Liu, W. Tu, X. Zhang and S. Zhang, *ACS Sustain. Chem. Eng.*, 2017, **5**, 2614–2622.

128 J. Chen, K. Vongsanga, X. Wang and N. Byrne, *Materials*, 2014, **7**, 6158–6168.

129 S. Reichl, *Biomaterials*, 2009, **30**, 6854–6866.

130 A. L. Horvath, *Sci. World J.*, 2009, **9**, 255–271.

131 N. Singh and K. Prasad, *Green Chem.*, 2019, **21**, 3328–3333.

132 M. Wang, T. Zhao, G. Wang and J. Zhou, *Text. Res. J.*, 2014, **84**, 1315–1324.

133 A. Idris, R. Vijayaraghavan, U. A. Rana, D. Fredericks, A. F. Patti and D. R. MacFarlane, *Green Chem.*, 2013, **15**, 525–534.

134 A. Kelch, S. Wessel, T. Will, U. Hintze, R. Wepf and R. Wiesendanger, *J. Microsc.*,

2000, **200**, 179–186.

135 S. Spange, D. Keutel and F. Simon, *J. Chim. Phys.*, 1992, **89**, 1615–1622.

136 M. A. Ab Rani, A. Brant, L. Crowhurst, A. Dolan, M. Lui, N. H. Hassan, J. P. Hallett, P. A. Hunt, H. Niedermeyer, J. M. Perez-Arlandis, M. Schrems, T. Welton and R. Wilding, *Phys. Chem. Chem. Phys.*, 2011, **13**, 16831–16840.

137 L. Kyllönen, A. Parviainen, S. Deb, M. Lawoko, M. Gorlov, I. Kilpeläinen and A. W. T. King, *Green Chem.*, 2013, **15**, 2374–2378.

138 P. Bonhôte, A.-P. Dias, N. Papageorgiou, K. Kalyanasundaram and M. Grätzel, *Inorg. Chem.*, 1996, **35**, 1168–1178.

139 S. Zhang, X. Qi, X. Ma, L. Lu, Q. Zhang and Y. Deng, *J. Phys. Org. Chem.*, 2012, **25**, 248–257.

140 Y. Fukaya, K. Hayashi, M. Wada and H. Ohno, *Green Chem.*, 2008, **10**, 44–46.

141 H. Ohno and Y. Fukaya, *Chem. Lett.*, 2009, **38**, 2–7.

142 L. Crowhurst, R. Falcone, N. L. Lancaster, V. Llopis-Mestre and T. Welton, *J. Org. Chem.*, 2006, **71**, 8847–8853.

143 Z. S. Othman, N. H. Hassan and S. I. Zubairi, in *Progress and Developments in Ionic Liquids*, ed. S. Handy, InTech, Croatia, 2017, pp. 495–515.

144 S. Spange, R. Lungwitz and A. Schade, *J. Mol. Liq.*, 2014, **192**, 137–143.

145 L. Crowhurst, N. L. Lancaster, J. M. P. Arlandis and T. Welton, *J. Am. Chem. Soc.*, 2004, **126**, 11549–11555.

146 A. Xu, J. Wang and H. Wang, *Green Chem.*, 2010, **12**, 268–275.

147 L. K. J. Hauru, M. Hummel, A. W. T. King, I. Kilpeläinen and H. Sixta, *Biomacromolecules*, 2012, **13**, 2896–2905.

148 R. Sheldon, *Chem. Commun.*, 2001, **1**, 2399–2407.

149 W. Zheng, W. Xie, W. Sun and L. Zhao, *Chem. Eng. Sci.*, 2017, **166**, 42–52.

150 A. Castro Grijalba, E. F. Fiorentini and R. G. Wuilloud, *J. Chromatogr. A*, 2017, **1491**, 117–125.

151 S. Riaño and K. Binnemans, *Green Chem.*, 2015, **17**, 2931–2942.

152 J. Eßer, P. Wasserscheid and A. Jess, *Green Chem.*, 2004, **6**, 316–322.

153 M. H. Ibrahim, M. Hayyan, M. A. Hashim and A. Hayyan, *Renew. Sustain. Energy Rev.*, 2017, **76**, 1534–1549.

154 P. A. Z. Suarez, J. E. L. Dullius, S. Einloft, R. F. De Souza and J. Dupont, *Polyhedron*,

1996, **15**, 1217–1219.

155 L. Chen, C. Fink, Z. Fei, P. J. Dyson and G. Laurenczy, *Green Chem.*, 2017, **19**, 5435–5441.

156 J. Fuller, R. T. Carlin and R. A. Osteryoung, *J. Electrochem. Soc.*, 1997, **144**, 3881–3886.

157 A. Basile, A. I. Bhatt and A. P. O'Mullane, *Nat. Commun.*, 2016, **7**, ncomms11794.

158 J. L. Anthony, E. J. Maginn and J. F. Brennecke, *J. Phys. Chem. B*, 2001, **105**, 10942–10949.

159 J. McFarlane, W. B. Ridenour, H. Luo, R. D. Hunt, D. W. DePaoli and R. X. Ren, *Sep. Sci. Technol.*, 2005, **40**, 1245–1265.

160 P. M. Dean, J. Turanjanin, M. Yoshizawa-Fujita, J. L. Scott and D. R. MacFarlane, *Cryst. Growth Des.*, 2009, **9**, 1137–1145.

161 J. L. Shamshina, P. S. Barber and R. D. Rogers, *Expert Opin. Drug Deliv.*, 2013, **10**, 1367–1381.

162 S. P. F. Costa, A. M. O. Azevedo, D. P. C. A. G. Pinto, D. M. Lúcia and M. F. S. Saraiva, *ChemSusChem*, 2017, **10**, 2321–2347.

163 M. Wagner and C. Hilgers, *Ionic Liquids in Synthesis*, Wiley, Weinheim, 2008.

164 P. Weerachanchai and J. M. Lee, *Bioresour. Technol.*, 2014, **169**, 336–343.

165 L. A. Blanchard, D. Hancu, ric J. Beckman and J. F. Brennecke, *Nature*, 1999, **399**, 28–29.

166 L. Zhang, W. Cao, P. J. J. Alvarez, X. Qu, H. Fu, S. Zheng, Z. Xu and D. Zhu, *Appl. Surf. Sci.*, 2018, **440**, 821–829.

167 J. Kröckel and U. Kragl, *Chem. Eng. Technol.*, 2003, **26**, 1166–1168.

168 K. E. Gutowski, G. A. Broker, H. D. Willauer, J. G. Huddleston, R. P. Swatloski, J. D. Holbrey and R. D. Rogers, *J. Am. Chem. Soc.*, 2003, **125**, 6632–6633.

169 A. König, M. Stepanski, A. Kuszlik, P. Keil and C. Weller, *Chem. Eng. Res. Des.*, 2008, **86**, 775–780.

170 S. Hayashi and H. O. Hamaguchi, *Chem. Lett.*, 2004, **33**, 1590–1591.

171 N. V. Plechkova and K. R. Seddon, *Chem. Soc. Rev.*, 2008, **37**, 123–150.

172 N. Sun, M. Rahman, Y. Qin, M. L. Maxim, H. Rodrıguez and R. D. Rogers, *Green Chem.*, 2009, **11**, 646–655.

173 B. Kosan, C. Michels and F. Meister, *Cellulose*, 2008, **15**, 59–66.

174 J. B. Binder, M. J. Gray, J. F. White, C. Z. Zhang and J. E. Holladay, *Biomass Bioenergy*, 2009, **33**, 1122–1130.

175 W. Li, N. Sun, B. Stoner, X. Jiang, X. Lu and R. D. Rogers, *Green Chem.*, 2011, **13**, 2038–2047.

176 H. Wang, G. Gurau and R. D. Rogers, *Struct. Bond.*, 2013, **151**, 79–105.

177 D. M. Phillips, L. F. Drummy, D. G. Conrady, D. M. Fox, R. R. Naik, M. O. Stone, P. C. Trulove, H. C. De Long and R. A. Mantz, *J. Am. Chem. Soc.*, 2004, **126**, 14350–14351.

178 D. A. Fort, R. C. Remsing, R. P. Swatloski, P. Moyna, G. Moyna and R. D. Rogers, *Green Chem.*, 2007, **9**, 63–69.

179 A. George, K. Tran, T. J. Morgan, P. I. Benke, C. Berrueco, E. Lorente, B. C. Wu, J. D. Keasling, B. A. Simmons and B. M. Holmes, *Green Chem.*, 2011, **13**, 3375–3385.

180 I. Kilpeläinen, H. Xie, A. King, M. Granstrom, S. Heikkinen and D. S. Argyropoulos, *J. Agric. Food Chem.*, 2007, **55**, 9142–9148.

181 C. Li, B. Knierim, C. Manisseri, R. Arora, H. V. Scheller, M. Auer, K. P. Vogel, B. A. Simmons and S. Singh, *Bioresour. Technol.*, 2010, **101**, 4900–4906.

182 M. Zavrel, D. Bross, M. Funke, J. Buchs and A. C. Spiess, *Bioresour. Technol.*, 2009, **100**, 2580–2587.

183 M. Frederix, F. Mingardon, M. Hu, N. Sun, T. Pray, S. Singh, B. A. Simmons, J. D. Keasling and A. Mukhopadhyay, *Green Chem.*, 2016, **18**, 4189–4197.

184 B. Li, J. Asikkala, I. Filpponen and D. S. Argyropoulos, *Ind. Eng. Chem. Res.*, 2010, **49**, 2477–2484.

185 S. Singh, B. A. Simmons and K. P. Vogel, *Biotechnol. Bioeng.*, 2009, **104**, 68–75.

186 A. M. da Costa Lopes, K. G. Joao, D. F. Rubik, E. Bogel-Łukasik, L. C. Duarte, J. Andreaus and R. Bogel-Łukasik, *Bioresour. Technol.*, 2013, **142**, 198–208.

187 Q. Li, Y.-C. He, M. Xian, G. Jun, X. Xu, J.-M. Yang and L.-Z. Li, *Bioresour. Technol.*, 2009, **100**, 3570–3575.

188 Y. Qin, X. Lu, N. Sun and R. D. Rogers, *Green Chem.*, 2010, **12**, 968–971.

189 Y. Wu, I. Sasaki, T., S. Rie and K. Sakurai, *Polymer*, 2008, **49**, 2321–2327.

190 R. P. Swatloski, J. D. Holbrey and R. D. Rogers, *Green Chem.*, 2003, **5**, 361–363.

191 S. Ostadjoo, P. Berton, J. L. Shamshina and R. D. Rogers, *Toxicol. Sci.*, 2018, **161**, 249–265.

192 D. R. M. Passino and S. B. Smith, *Environ. Toxicol. Chem.*, 1987, **6**, 901–907.

193 J. Flieger and M. Flieger, *Int. J. Mol. Sci.*, 2020, **21**, 1–41.

194 S. K. Ruokonen, C. Sanwald, M. Sundvik, S. Polnick, K. Vyavaharkar, F. Duša, A. J. Holding, A. W. T. King, I. Kilpeläinen, M. Lämmerhofer, P. Panula and S. K. Wiedmer, *Environ. Sci. Technol.*, 2016, **50**, 7116–7125.

195 X.-Y. Li, X.-Q. Miao, L.-F. Zhang and J.-J. Wang, *Ecotoxicol. Environ. Saf.*, 2012, **75**, 180–186.

196 A. Ghosh, S. Clerens, S. Deb-Choudhury and J. M. Dyer, *Polym. Degrad. Stab.*, 2014, **108**, 108–115.

197 C. Tonin, M. Zoccola, A. Aluigi, A. Varesano, A. Montarsolo, C. Vineis and F. Zimbardi, *Biomacromolecules*, 2006, **7**, 3499–3504.

198 W. Zhao, R. Yang, Y. Zhang and L. Wu, *Green Chem.*, 2012, **14**, 3352–3360.

199 C. Bolduc and J. Shapiro, *Clin. Dermatol.*, 2001, **19**, 431–436.

200 C. R. Quinn, T. M. Quinn and A. P. Kelly, *Cutis*, 2003, **72**, 280–289.

201 T. C. de Sá Dias, A. R. Baby, T. M. Kaneko and M. V. Robles Velasco, *J. Cosmet. Dermatol.*, 2007, **6**, 2–5.

202 R. Schueller and P. Romanowski, *Cosmet. Toilet.*, 1998, **113**, 39–44.

203 M. F. R. G. Dias, *Int. J. Trichology*, 2015, 7, 2–15.

204 J. S. Church, G. L. Corino and A. L. Woodhead, *Biopolymers*, 1997, **42**, 7–17.

205 P. M. J. Barton, PhD Thesis, Queensland University of Technology, 2011.

206 R. Ogle and M. Fox, in *Atlas of Human Hair*, CRC Press, Bosa Roca, 1998, pp. 11–28.

207 C. B. Baddiel, *J. Mol. Biol.*, 1968, **38**, 181–199.

208 J. A. Swift, *Fundamentals of human hair science*, Micelle Press, 1997.

209 A. Barth and C. Zscherp, *Q. Rev. Biophys.*, 2002, **35**, 369–430.

210 A. C. Williams, H. G. M. Edwards and B. W. Barry, *J. Raman Spectrosc.*, 1994, **25**, 95–98.

211 A. Kuzuhara, N. Fujiwara and T. Hori, *Biopolymers*, 2007, **87**, 134–140.

212 A. Kuzuhara, *Biopolymers*, 2005, **79**, 173–184.

213 K. L. A. Chan, S. G. Kazarian, A. Mavraki and D. R. Williams, *Appl. Spectrosc.*, 2005, **59**, 149–155.

214 K. L. A. Chan, F. H. Tay, C. Taylor and S. G. Kazarian, *Appl. Spectrosc.*, 2008, **62**,

1041–1044.

215 K. R. Ackermann, J. Koster and S. Schlücker, *J. Biophotonics*, 2008, **1**, 419–424.

216 F. I. Bell, R. Skinner, I. M. Tucker, Y. Leray, T. E. Lyons, K. Devine, P. Pudney and T. Oikawa, *J. Cosmet. Sci.*, 2004, **55**, 19–24.

217 A. Kuzuhara, *J. Appl. Polym. Sci.*, 2011, **122**, 2680–2689.

218 C. Robbins, *Text. Res. J.*, 1967, **37**, 811–813.

219 R. C. Shah and R. S. Gandhi, *Text. Res. J.*, 1968, **38**, 874–875.

220 H. Alter and M. Bit-Alkhas, *Text. Res. J.*, 1969, **39**, 479–481.

221 H. H. Stein and J. Guarnaccio, *Text. Res. J.*, 1959, **29**, 492–496.

222 M. Joy and D. M. Lewis, *Int. J. Cosmet. Sci.*, 1991, **13**, 249–261.

223 V. Signori and D. M. Lewis, *Int. J. Cosmet. Sci.*, 1997, **19**, 1–13.

224 L. Rintoul, H. Panayiotou, S. Kokot, G. George, G. Cash, R. Frost, T. Bui and P. Fredericks, in *Analyst*, The Royal Society of Chemistry, 1998, vol. 123, pp. 571–577.

225 J. Jachowicz, *J. Soc. Cosmet. Chem*, 1987, **38**, 263–286.

226 A. Kuzuhara, *Biopolymers*, 2007, **85**, 274–283.

227 A. Kuzuhara, *Biopolymers*, 2006, **81**, 506–514.

228 D. J. Lyman, J. Murray-Wijelath and M. Feughelman, *Appl. Spectrosc.*, 2001, **55**, 552–554.

229 M. Gniadecka, O. F. Nielsen, D. H. Christensen and H. C. Wulf, *J. Invest. Dermatol.*, 1998, **110**, 393–398.

230 H. Panayiotou and S. Kokot, *Anal. Chim. Acta*, 1999, **392**, 223–235.

231 J. L. Bantignies, G. L. Carr, D. Lutz, S. Marull, G. P. Williams and G. Fuchs, *J. Cosmet. Sci.*, 2000, **51**, 73–90.

232 Y.-J. Chen, Y.-D. Cheng, H.-Y. Liu, P.-Y. Lin and C.-S. Wang, *Chang Gung Med. J.*, **29**, 518–527.

233 X. Wang, Z. Qi, X. Liu, S. Wang, C. Li, G. Liu, Y. Xiong, T. Li, J. Tao and Y. Tian, *Cancer Epidemiol.*, 2010, **34**, 453–456.

234 E. A. Carter, PhD Thesis, Queensland University of Technology, 1997.

235 L. Wang, Y. Nie, X. Zhang, S. Zeng, S. Zhang and S. Zheng, *Chem. Eng. Technol.*, 2016, **39**, 979–986.

236 C. Marcott, M. Lo, K. Kjoller, F. Fiat, N. Baghdadli, G. Balooch and G. S. Luengo,

Appl. Spectrosc., 2014, **68**, 564–569.

237 T. Lasisi, S. Ito, K. Wakamatsu and C. N. Shaw, *Am. J. Phys. Anthropol.*, 2016, **160**, 341–352.

238 G. Wei, B. Bhushan and P. M. Torgerson, *Ultramicroscopy*, 2005, **105**, 248–266.

239 F. Kaliyadan, B. B. Gosai, W. N. Al Melhim, K. Feroze, H. A. Qureshi, S. Ibrahim and J. Kuruvilla, *Int. J. Trichology*, 2016, **8**, 94–98.

240 T. Terlier, J. Lee and Y. Lee, *J. Vac. Sci. Technol. B, Nanotechnol. Microelectron. Mater. Process. Meas. Phenom.*, 2018, **36**, 03F131.

241 J. Dombovári, J. S. Becker and H.-J. Dietze, *Fresenius. J. Anal. Chem.*, 2000, **367**, 407–413.

242 I. Rodushkin and M. D. Axelsson, *Sci. Total Environ.*, 2003, **305**, 23–39.

243 A. D. Levin, V. A. Pribytkov, E. M. Rukin and I. F. Seregina, *Meas. Tech.*, 2001, **44**, 660–662.

244 S. Seidel, R. Kreutzer, D. Smith, S. McNeel and D. Gilliss, *J. Am. Med. Assoc.*, 2001, **285**, 67–72.

245 M. G. Birgani, R. Reiazi, M. A. Ardekani, H. Ghaffari, A. Shakeri-Zadeh and B. Mofid, *Med. J. Islam. Repub. Iran*, 2020, **34**, 1–6.

246 A. Du, N. Mangelson, L. Rees and R. Matheny, *Nucl. Instruments Methods Phys. Res. Sect. B Beam Interact. with Mater. Atoms*, 1996, **109–110**, 673–676.

247 A. A. Hosseini, A. Amirabadi, H. Afarideh, S. M. Hadji-Saeid and A. H. Behrozi, *Nucl Instrum Methods Phys Res B NUCL INSTRUM METH B*, 1996, **109–110**, 239–242.

248 I. M. Kempson, W. M. Skinner and P. K. Kirkbride, *Biochim. Biophys. Acta - Gen. Subj.*, 2003, **1624**, 1–5.

249 B. Flinders, E. Beasley, R. M. Verlaan, E. Cuypers, S. Francese, T. Bassindale, M. R. Clench and R. M. A. Heeren, *J. Am. Soc. Mass Spectrom.*, 2017, **28**, 2462–2468.

250 T. Kojima, H. Kitano, M. Niwa, K. Saito, Y. Matsushita and K. Fukushima, *Surf. Interface Anal.*, 2011, **43**, 562–565.

251 K. lshikawa, M. Okamoto and S. Aoyagi, *Biointerphases*, 2016, **11**, 02A315.

252 M. Okamoto, K. Ishikawa, N. Tanji and S. Aoyagi, *Surf. Interface Anal.*, 2012, **44**, 736–739.

253 A. Harvey, C. M. Carr and A. Pereira, *J. Cosmet. Sci.*, 2004, **55**, 265–279.

254 I. M. Kempson and W. M. Skinner, *Sci. Total Environ.*, 2005, **338**, 213–227.

255 J. M. Cardamone, *J. Mol. Struct.*, 2010, **969**, 97.

256 S. Kumar, J. K. Bhattacharyya, A. N. Vaidya, T. Chakrabarti, S. Devotta and A. B. Akolkar, *Waste Manag.*, 2009, **29**, 883–895.

257 M. Ferenetz, H. Myllymäki, K. Grahn, A. Sipilä and A. Harlin, *Autex Res. J.*, 2004, **4**, 164–174.

258 H. F. D. Almeida, J. N. C. Lopes, L. P. N. Rebelo, J. A. P. Coutinho, M. G. Freire and I. M. Marrucho, *J. Chem. Eng. Data*, 2016, **61**, 2828–2843.

259 S. A. Dharaskar, M. N. Varma, D. Z. Shende, C. K. Yoo and K. L. Wasewar, *Sci. World J.*, 2013, **9**, 578–587.

260 A. B. Pereiro, P. Verdía, E. Tojo and A. Rodríguez, *J. Chem. Eng. Data*, 2007, **52**, 377–380.

261 X. Liu, Y. Nie, Y. Liu, S. Zhang and A. L. Skov, *ACS Sustain. Chem. Eng.*, 2018, **6**, 17314–17322.

262 M. G. Freire, A. R. R. Teles, M. A. A. Rocha, B. Schröder, C. M. S. S. Neves, P. J. Carvalho, D. V. Evtuguin, L. M. N. B. F. Santos and J. A. P. Coutinho, *J. Chem. Eng. Data*, 2011, **56**, 4813–4822.

263 Y. Hiraga, A. Kato, Y. Sato and R. L. Smith, *J. Chem. Eng. Data*, 2015, **60**, 876–885.

264 M. Zoccola, A. Aluigi, A. Patrucco, C. Vineis, F. Forlini, P. Locatelli, M. C. Sacchi and C. Tonin, *Text. Res. J.*, 2012, **82**, 2006–2018.

265 J. Yin, S. Rastogi, A. E. Terry and C. Popescu, *Biomacromolecules*, 2007, **8**, 800–806.

266 G. S. J. Sturm, M. D. Verweij, A. I. Stankiewicz and G. D. Stefanidis, *Chem. Eng. J.*, 2014, **243**, 147–158.

267 A. Shavandi, T. H. Silva, A. A. Bekhit and A. E. D. A. Bekhit, *Biomater. Sci.*, 2017, **5**, 1699–1735.

268 U. Blume-Peytavi, A. Tosti, D. A. Whiting and R. M. Trüeb, *Hair growth and disorders*, Springer, Berlin, 2008.

269 W. Akhtar, H. G. M. Edwards, D. W. Farwell and M. Nutbrown, *Spectrochim. Acta - Part A Mol. Biomol. Spectrosc.*, 1997, **53**, 1021–1031.

270 V. F. Monteiro, A. P. Maciel and E. Longo, *J. Therm. Anal. Calorim.*, 2005, **79**, 289–293.

271 R. L. Weber, Y. Ye, S. M. Banik, Y. A. Elabd, M. A. Hickner and M. K. Mahanthappa,

J. Polym. Sci. Part B Polym. Phys., 2011, **49**, 1287–1296.

272 R. E. Daso, L. J. Osborn, M. F. Thomas and I. A. Banerjee, *ACS Omega*, 2020, **5**, 14543–14554.

273 O. Maroñas, J. Söchtig, Y. Ruiz, C. Phillips, Carracedo and M. V. Lareu, *Forensic Sci. Rev.*, 2015, **27**, 13–40.

274 The Human Protein Atlas, https://www.proteinatlas.org/, (accessed 29 September 2019).

275 L. Langbein, M. A. Rogers, S. Praetzel-Wunder, D. Böckler, P. Schirmacher and J. Schweizer, *J. Invest. Dermatol.*, 2007, **127**, 1532–1535.

276 R. Sinclair, M. J. Flagler, L. Jones, N. Rufaut and M. G. Davis, *Br. J. Dermatol.*, 2012, **166**, 27–32.

277 A. Basit, F. Asghar, S. Sadaf and M. W. Akhtar, *Biotechnol. Reports*, 2018, **20**, 1–6.

278 R. D. Rogers and K. R. Seddon, *Science*, 2003, **302**, 792–793.

279 C. K. Z. Andrade and L. M. Alves, *Cuurent Org. Chem.*, 2005, **9**, 195–218.

280 T. Y. Wu, S. G. Su, S. T. Gung, M. W. Lin, Y. C. Lin, C. A. Lai and I. W. Sun, *Electrochim. Acta*, 2010, **55**, 4475–4482.

281 J. S. Wilkes, *J. Mol. Catal. A Chem.*, 2004, **214**, 11–17.

282 C. E. Song, *Chem. Commun.*, 2004, **9**, 1033–1043.

283 M. Armand, F. Endres, D. R. MacFarlane, H. Ohno and B. Scrosati, *Nat. Mater.*, 2009, **8**, 621–629.

284 *U.S. Pat. 2927129A*, 1958.

285 *U.S. Pat. 2594044*, 1952.

286 *U.S. Pat. 2915569 A*, 1959.

287 S. A. Chowdhruy, R. Vijayaraghavan and D. R. MacFarlane, *Green Chem.*, 2010, **12**, 1023–1028.

288 W. Schroth, H. D. Schandler and J. Andersch, *ChemInform*, 1989, **29**, 129–135.

289 U. Hess, S. Dunkel and B. Muller, *Pharmazie*, 1993, **48**, 591–597.

290 A. E. Rosamilia, C. R. Strauss and J. L. Scott, *Pure Appl. Chem.*, 2007, **79**, 1869–1877.

291 S. A. Chowdhruy, P. Dean, R. Vijayaraghavan and D. R. MacFarlane, *Aust. J. Chem.*, 2011, **64**, 1624–1627.

292 A. I. Bhatt, A. M. Bond, D. R. MacFarlane, J. Zhang, J. L. Scott, C. R. Strauss, P. I.

Iotov and S. V. Kalcheva, *Green Chem.*, 2006, **8**, 161–171.

293 R. Vijayaraghavan and D. R. MacFarlane, *ACS Sustain. Chem. Eng.*, 2014, **2**, 1724–1728.

294 A. W. T. King, J. Asikkala, I. Mutikainen, P. Järvi and I. Kilpeläinen, *Angew. Chemie - Int. Ed.*, 2011, **50**, 6301–6305.

295 A. P. Bertolino and W. M. O'Guin, in *Disorders of hair growth: diagnosis and treatment*, ed. E. A. Olsen, McGraw-Hill, Medical Pub. Division, Durham, 1994, pp. 21–37.

296 V. D. Hodoroaba, S. Rades and W. E. S. Unger, *Surf. Interface Anal.*, 2014, **46**, 945–948.

297 B. Flinders, E. Cuypers, H. Zeijlemaker, J. Tytgat and R. M. A. Heeren, *Drug Test. Anal.*, 2015, **7**, 859–865.

298 I. and S. A. C. (ISAC), Time-of-Flight secondary ion mass spectrometry (ToF-SIMS), https://www.nottingham.ac.uk/isac/facilities/tof-sims/tof-sims.aspx, (accessed 1 February 2020).

299 R. Araújo, M. Fernandes, A. Cavaco-Paulo and A. Gomes, in *Biofunctionalization of Polymers and their Applications. Advances in Biochemical Engineering / Biotechnology*, Springer, Berlin, 2010, pp. 121–143.

300 M. Valéria, R. Velasco, T. Cristina, S. Dias, A. Zanardi De Freitas, N. Dias, V. Júnior, C. A. Sales De Oliveira Pinto, T. M. Kaneko and A. Rolim Baby, *Brazilian J. Pharm. Sci.*, 2009, **45**, 153–162.

301 J. E. Lai-Cheong and J. A. McGrath, *Medicine (Baltimore).*, 2009, **37**, 223–226.

302 B. Bhushan and N. Chen, *Ultramicroscopy*, 2006, **106**, 755–764.

303 B. A. Thomas Rutherford and P. B. Hawk, *J. Biol. Chem.*, 1907, **3**, 459–489.

304 W. Xu, L. Wang, J. Huang, G. Ren, D. Xu and H. Tong, *Aust. J. Chem.*, 2015, **68**, 825–829.

305 S. Chakraborty, T. J. Wadas, H. Hester, C. Flaschenreim, R. Schmehl and R. Eisenberg, *Inorg. Chem.*, 2005, **44**, 6284–6293.

306 S. Men and J. Jiang, *Russ. J. Phys. Chem. A*, 2018, **92**, 1627–1630.

307 S. T. Lin, M. F. Ding, C. W. Chang and S. S. Lue, *Tetrahedron*, 2004, **60**, 9441–9446.

308 R. Leones, F. Sentanin, S. C. Nunes, J. M. S. S. Esperança, M. C. Gonçalves, A. Pawlicka, V. D. Z. Bermudez and M. M. Silva, *Electrochim. Acta*, 2015, **184**, 171–

178.

309 K. Nakabayashi, Y. Sato, Y. Isawa, C. T. Lo and H. Mori, *Polymers*, 2017, **9**, 616–632.

310 H. Tokuda, S. Tsuzuki, M. A. B. H. Susan, K. Hayamizu and M. Watanabe, *J. Phys. Chem. B*, 2006, **110**, 19593–19600.

311 S. Holopainen, M. Nousiainen, J. Puton, M. Sillanpää, U. Bardi and A. Tolstogouzov, *Talanta*, 2011, **83**, 907–915.

312 C. Chiappe, P. Margari, A. Mezzetta, C. S. Pomelli, S. Koutsoumpos, M. Papamichael, P. Giannios and K. Moutzouris, *Phys. Chem. Chem. Phys.*, 2017, **19**, 8201–8209.

313 A. Brandt, J. P. Hallett, D. J. Leak, R. J. Murphy and T. Welton, *Green Chem.*, 2010, **12**, 672–679.

314 T. Erdmenger, J. Vitz, F. Wiesbrock and U. S. Schubert, *J. Mater. Chem.*, 2008, **18**, 5267–5273.

315 I. J. Villar-Garcia, S. Fearn, G. F. De Gregorio, N. L. Ismail, F. J. V Gschwend, A. J. S. Mcintosh and K. R. J. Lovelock, *Chem. Sci.*, 2014, **5**, 4404–4418.

316 U. Domańska, A. Pobudkowska and F. Eckert, *Green Chem.*, 2006, **8**, 268–276.

317 H. Lu, W. Chen and T. P. Russell, *Macromolecules*, 2009, **42**, 9111–9117.

318 M. T. Clough, C. R. Crick, J. Gräsvik, P. A. Hunt, H. Niedermeyer, T. Welton and O. P. Whitaker, *Chem. Sci.*, 2015, **6**, 1101–1114.

319 G. Qu, W. He, Y. Cai, X. Huang and P. Ning, *Carbohydr. Polym.*, 2016, **148**, 390–396.

320 S. Brica, L. Freimane, L. Kulikovska and A. Zicmanis, *Chem. Sci. Int. J.*, 2017, **19**, 1–9.

321 M. Biso, M. Mastragostino, M. Montanino, S. Passerini and F. Soavi, *Electrochim. Acta*, 2008, **53**, 7967–7971.

322 L. Magna, J. Bildé, H. Olivier-Bourbigou, T. Robert and B. Gilbert, *Oil Gas Sci. Technol. - Rev. lIFP*, 2009, **64**, 669–679.

323 W. Schroth, H.-D. Schädler and J. Andersch, *Z. Chem.*, 1989, **29**, 129–135.

324 Y. J. Lee, M. K. Kwon, S. J. Lee, S. W. Jeong, H.-C. Kim, T. H. Oh and S. G. Lee, *J. Appl. Polym. Sci.*, 2017, **134**, 44658.

325 Z.-D. Ding, Z. Chi, W.-X. Gu, S.-M. Gu, J.-H. Liu and H.-J. Wang, *Carbohydr. Polym.*, 2012, **89**, 7–16.

326 C. Marks, A. Mitsos and J. Viell, *J. Solution Chem.*, 2019, **48**, 1188–1205.

327 G. Bousrez, O. Renier, S. P. Kelley, B. Adranno, E. Tahavori, H. M. Titi, V. Smetana, S.-F. Tang, A.-V. Mudring and R. D. Rogers, *Eur. J. Chem.*, 2021, **27**, 13181.

328 A. M. J. McCarthy, Honours Thesis, Queensland University of Technology, 2006.

329 B. H. Stuart and D. J. Ando, *Biological applications of infrared spectroscopy*, John Wiley & Sons, Ltd, West Sussex, 1997.

Appendix:

TGA for Chapter 3

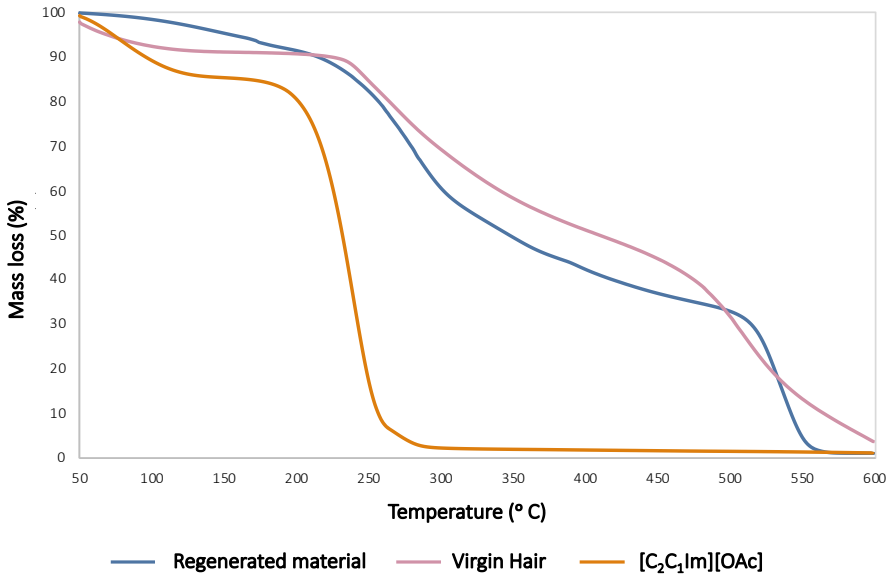


Figure 45. Thermogravimetric curves of European straight hair recovered hair material from $[C_2C_1Im][OAc]$ dissolution, chemically untreated European straight hair, precipitate from the water-soluble fraction and $[C_2C_1Im][OAc]$.

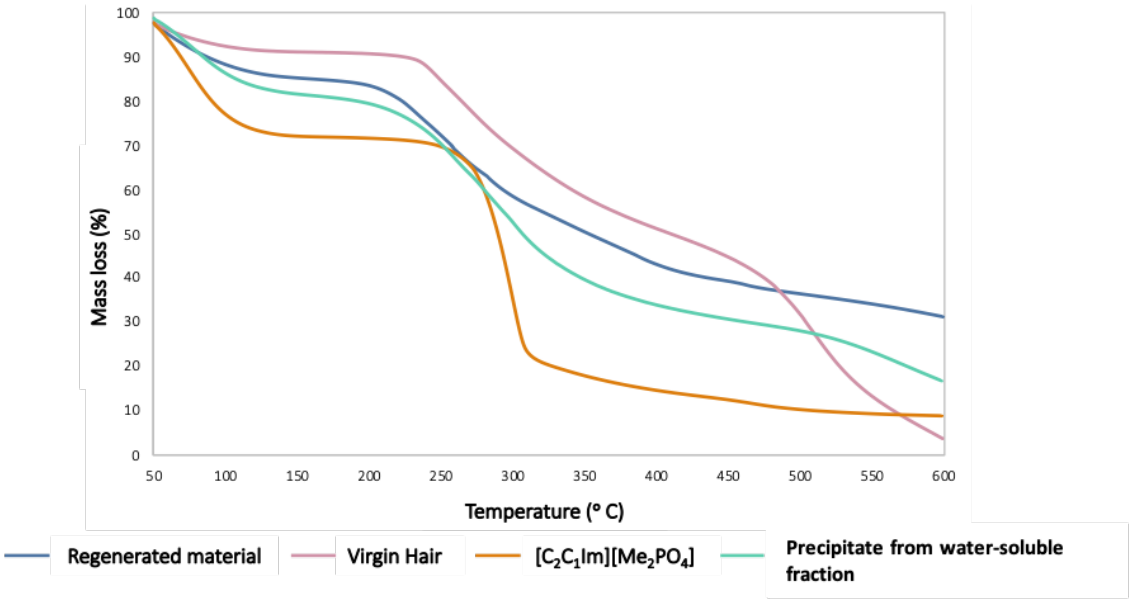


Figure 46. Thermogravimetric curves of European straight hair recovered hair material from $[C_2C_1Im][Me_2PO_4]$ dissolution, chemically untreated European straight hair, precipitate from the water-soluble fraction and $[C_2C_1Im][Me_2PO_4]$.

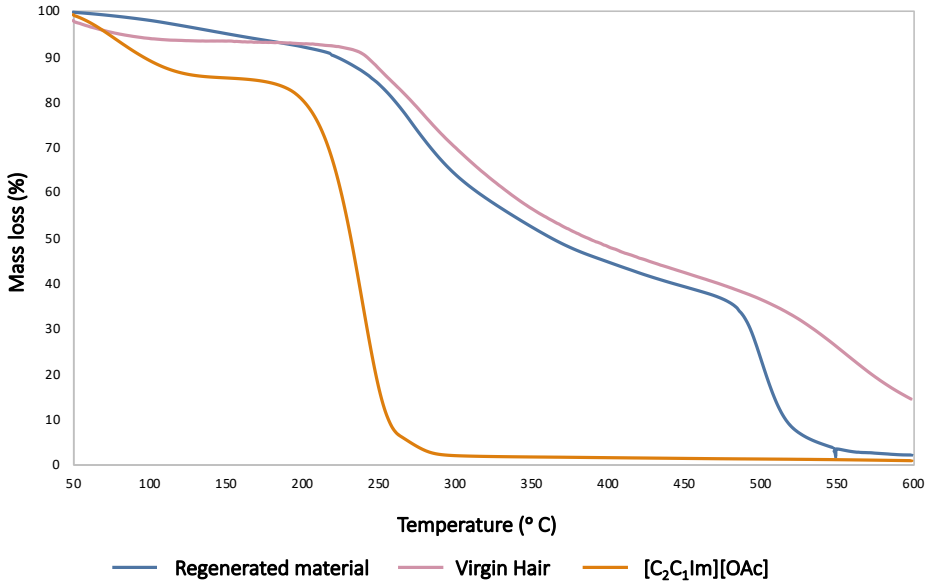


Figure 47. Thermogravimetric curves of European blonde hair recovered hair material from $[C_2C_1Im][OAc]$ dissolution, chemically untreated European blonde hair, precipitate from the water-soluble fraction and $[C_2C_1Im][OAc]$.

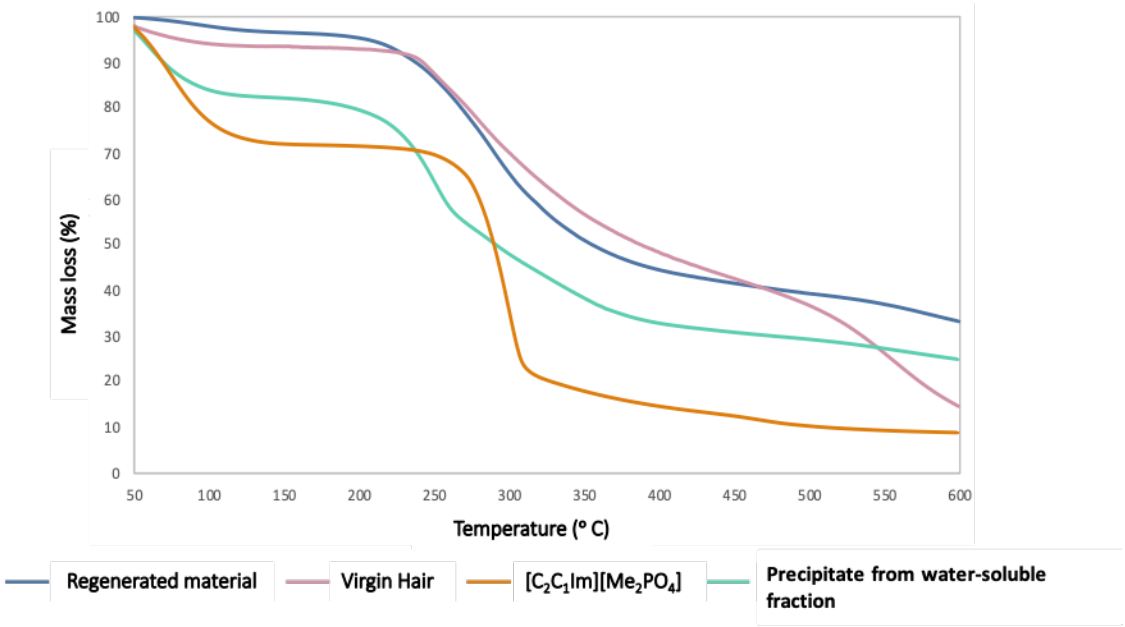


Figure 48. Thermogravimetric curves of European blonde hair recovered hair material from $[C_2C_1Im][Me_2PO_4]$ dissolution, European blonde hair, precipitate from the water-soluble fraction and $[C_2C_1Im][Me_2PO_4]$.

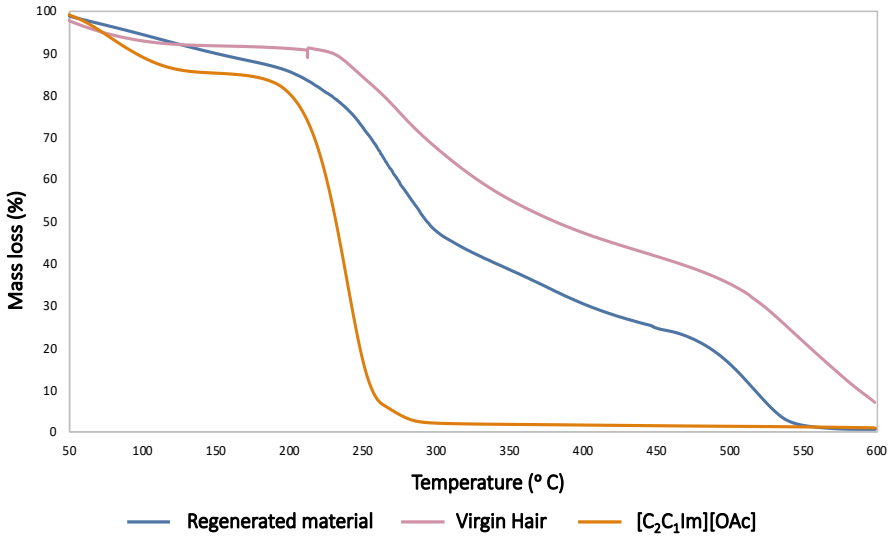


Figure 49. Thermogravimetric curves of Asian hair recovered hair material from $[C_2C_1Im][OAc]$ dissolution, chemically untreated Asian hair, precipitate from the water-soluble fraction and $[C_2C_1Im][OAc]$.

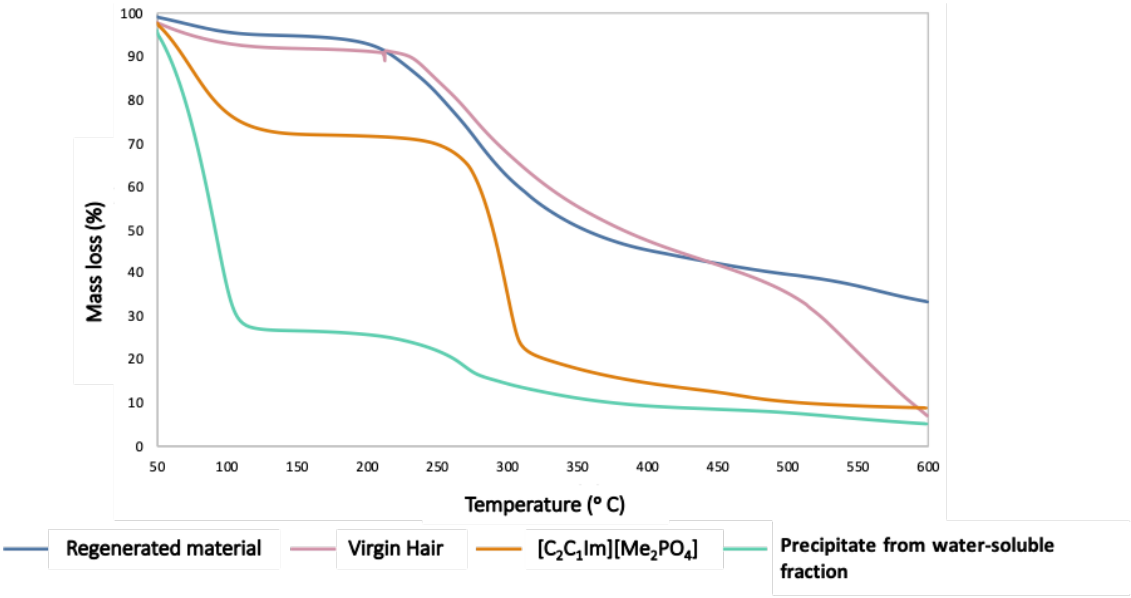


Figure 50. Thermogravimetric curves of Asian hair recovered hair material from $[C_2C_1Im][Me_2PO_4]$ dissolution, chemically untreated Asian hair, precipitate from the water-soluble fraction and $[C_2C_1Im][Me_2PO_4]$.

Distortion of hair fibres during ATR sampling for Chapter 4

At the beginning of this study it was originally presumed that the hair fibre morphology would not change throughout this investigation. The ATR-FTIR instruments is provided with an ATR-FTIR armature in order to increase the contact between solid samples and the ATR crystal. That means a force is imposed on the sample by the ATR-FTIR armature. Compressing of the fibre during ATR-FTIR analysis is expected. Previous studies in literature, suggests the ATR-FTIR armature compresses the fibre, which increases the width of the fibre letting the IR radiation to penetrate deeper into the fibre.[328]

To further investigate the impact of the ATR-FTIR armature on hair fibre, the analysed spot was observed by microscopy. Figure 51 shows the spot analysed after the ATR-FTIR analysis, as we can see the morphology of the chemically untreated fibre has changed. It is possible to compare the fibre before and after the analysis, which shows the change on the morphology of the fibre. This investigation was performed with a chemically untreated fibre, unless mentioned otherwise.

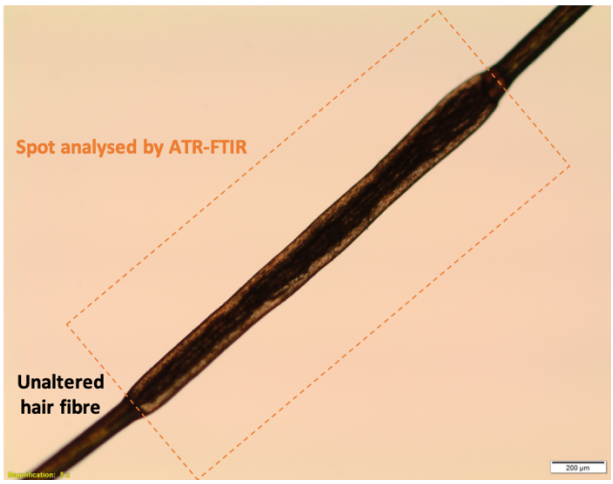


Figure 51. Hair fibre observed by Microscopy after ATR-FTIR analysis.

The morphology of the fibre changed, but it is not possible to conclude on the damaged on the surface of the fibre. This technique is not conclusive, therefore is not possible to determine why hair spectrum has changed during ATR-FTIR analysis.

To improve the examination of the fibre, another technique with better resolution and higher magnification was needed. For that reason, the scanning electron microscopy

(SEM) was the technique selected. Figure 52 shows two different fibres, these hair fibres present different thickness. The first top three images, designated as a) b) and c), show a top view of a thicker fibre after ATR-FTIR analysis. The compressing effect is visible, although on picture b) there are a few fractures that may suggest that the fibre has been fractured during analysis. The bottom three pictures represent a thinner hair fibre after ATR-FTIR analysis, however contrariwise to the other set of pictures, these ones show the side view. The thickness before and after the ATR-FTIR analysis were measured and it was possible to conclude the hair fibre decreases 34% of its initial width after this analysis.

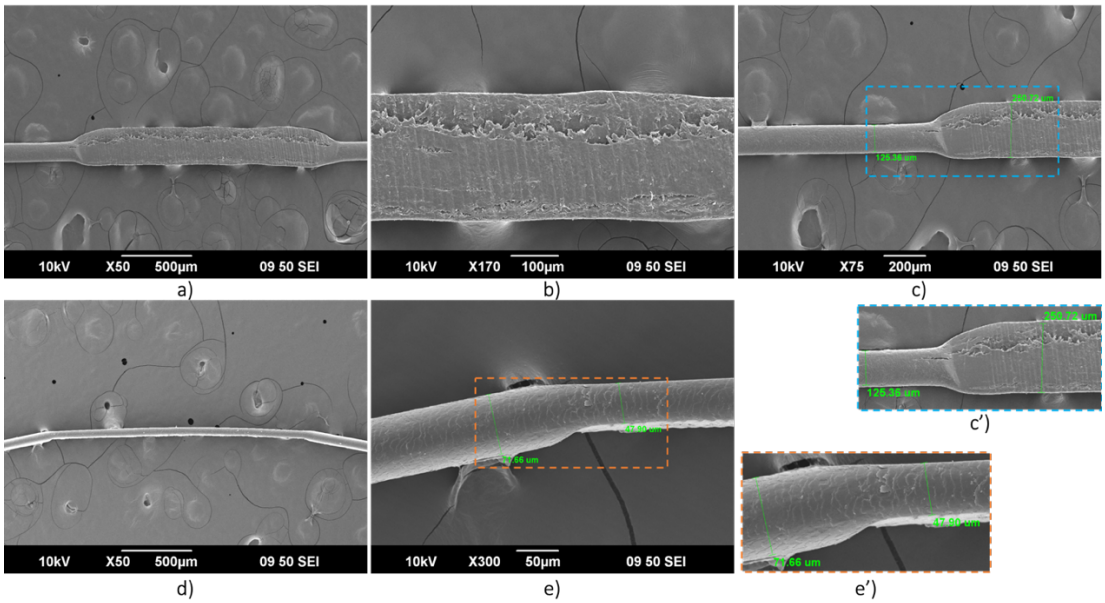


Figure 52. SEM analysis on hair fibres with different thicknesses. a), b) and c) top view of the thicker hair fibre on the spot analysed by ATR-FTIR analysis, different magnifications (X50, X170 and X75, respectively); d), e) and f) side view of a thinner hair fibre, different magnifications (X50 and X300, respectively). c') and e') highlight the measurements of the fibre thicknesses.

Also, the bottom part of picture e) fibre is uneven suggesting again the fibre has fractured.

The fractures of the fibre may affect the ATR-FTIR results since the cortex can be exposed.

To assess the impact of the fractured fibres on the ATR-FTIR analysis a fibre was analysed over an extended period of time.

The test was performed by analysing a single hair fibre for 100 minutes, in order to understand how the hair spectrum changes over this period of time. Or how long it takes to observe an intensification of the cortex in the ATR-FTIR spectrum. Our previous studies showed that the largest variation in the spectrum of hair occurs in the first 100 minutes. For this reason, the test was performed for 100 minutes to check the variation on the hair spectrum. The result of that test is represented in Figure 53, where is possible to detect several spectra on top of each other. That may suggest that the spectrum of a single hair fibre changes with time. Once again, Figure 53 is very similar to Figure 37, which shows the complexity of this technique in the analysis of hair.

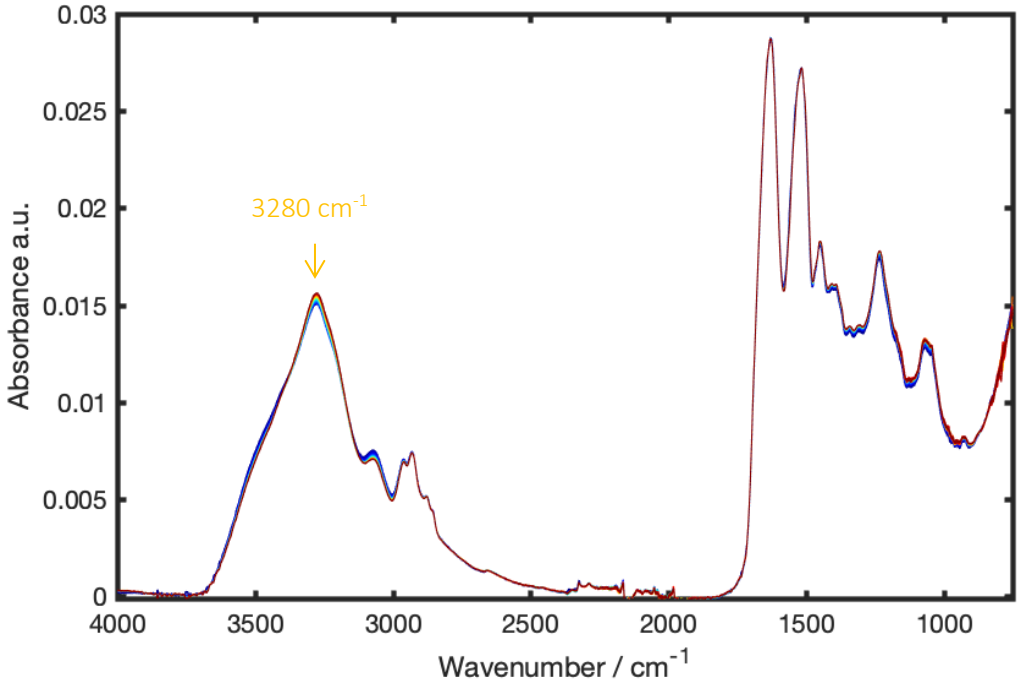


Figure 53. Spectra of chemically untreated European curly hair during 100 scans on same spot.

In order to verify if the variation is linear for this specific period of time, or if in some way the variation will reach a maximum, the absorbance at 3280 cm^{-1} was verified. To avoid the complexity of the fingerprint region, a band at higher wavenumbers were selected. The result of that test is presented in Figure 54, where after 100 minutes the variation on the spectrum after this period is nearly stable.

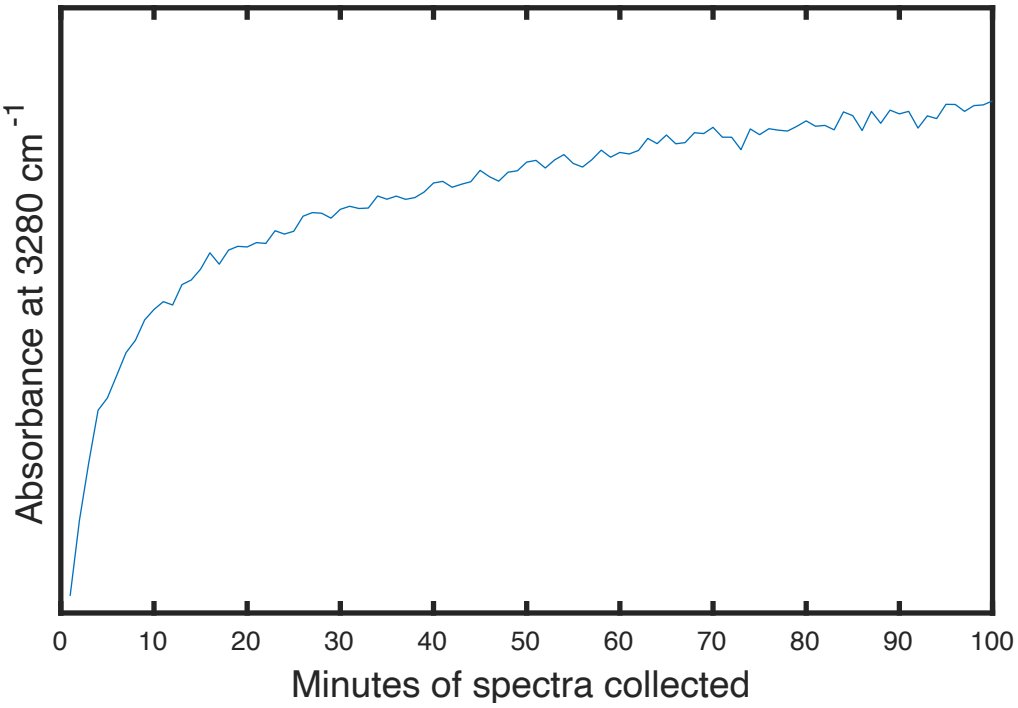


Figure 54. Variation of hair fibre spectrum during 100 minutes on a specific spot on the fibre.

Figure 54 shows that at the beginning of the test the variation is very accentuated, but after 20 minutes the data starts to reach a stable plateau. That means that something is changing within the fibre. That could be due to the rupturing of the fibre and the exposure of the cortex, where the contact of the fibre with the ATR crystal increases. All these reasons need to be considered during the analysis of the spectrum of the fibre.

At this point, we know the impact of the ATR-FTIR armature on the fibre morphology. So, now the natural variation of the fibre can be investigated.

In the next study, to guarantee the pressure and the way the fibre is compressed by the ATR armature is similar, 16 spots along the fibre were analysed. Each spectrum for each spot was subtracted from the first spectrum, this way it's possible to highlight the changes throughout time during pressure.

The next Figure 55 presents the comparison between a hair fibre and the variation during the ATR-FTIR analysis of a spot of chemically untreated hair fibre. The profile of the spectra regarding the variation on the hair fibre throughout time, and beside some variations discussed below, shows a profile that is recognised as biological material.

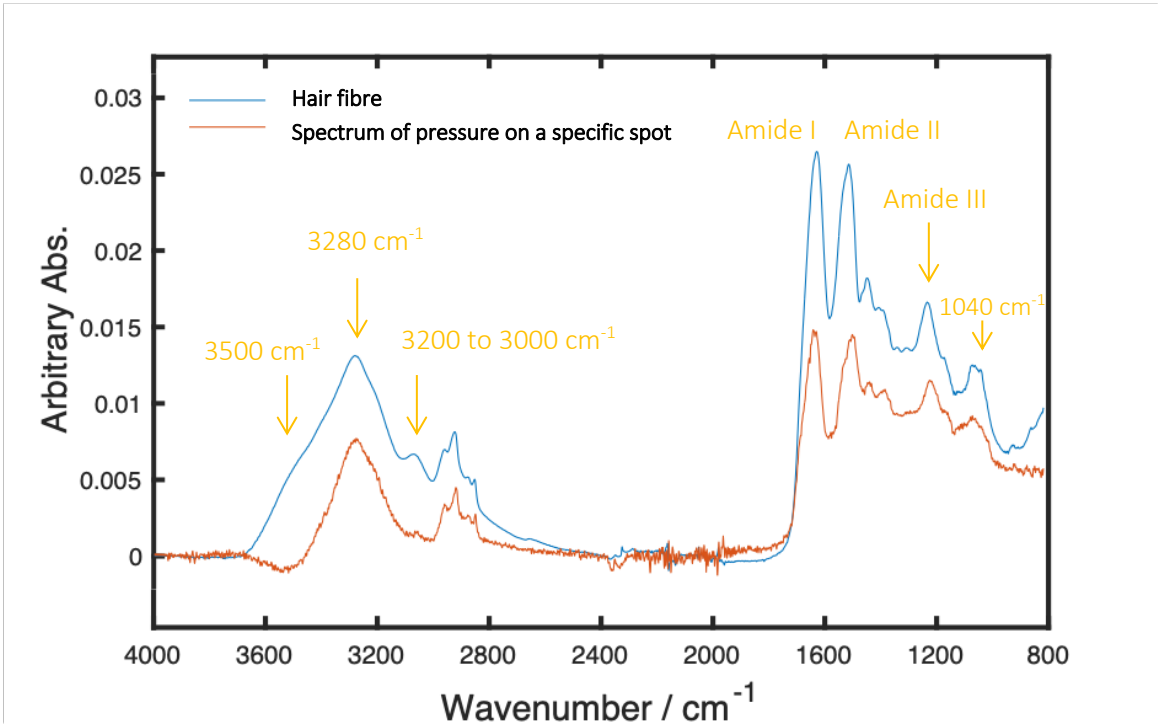


Figure 55. Comparison between hair fibre and variation on spectra of untreated hair fibre during ATR-FTIR armature pressure. Orange spectrum was subtracted from the first spectrum. For comparison purposes, chemically untreated hair spectrum is presented to better understand the bands affected by pressure.

The band at 3500 cm^{-1}, OH water network, showed a decrease on its intensity, which may suggest the fibre is dehydrating throughout the test due to pressure. Consequently, the dehydration of the fibre could be related to the realising of some lipids/oils from inside the fibre when pressure is applied, as previously discussed in subchapter 1.2.1. Also, band 1040 cm^{-1} presented a variation on its intensity and shape, this could be easily mistaken by chemical modifications if this study had not been done. The knowledge of the impact of the ATR armature pression on the hair structure is very important. Once this impact has been identified, the chemical modifications on the hair structure can be easily identified on the hair spectrum.

The following band, 3200 to 3000 cm^{-1}, reported as aromatic C-H stretching bands from Tyr, Phe and Trp groups, showed an increase of the intensity but it seems the proportion among the peaks looked unaffected.[236]

After the compressing effect, the fibre changed its conformation. According to the measurements performed during SEM analysis, the fibre reduced about 34% of its width.

The initial cuticle thickness of chemically untreated hair fibre was reported to be in the range 2.5-5μm[208], therefore according to the information available a rough calculation of the new cuticle size could be made. Assuming the 34% reduction of the hair fibre the cuticle after the compressing effect would have a size around 1.5-3μm. But it is important to remember that this is only a speculation, and the real dimension would be only determined after the cross section of the spot analysed. Nonetheless, that would not be an easy task.

Now that we have an idea of the size of the cuticle after ATR-FTIR armature pressure and the depth profile was calculated, between 0.92 and 6.91μm, it's easier to identify the hair components that are being analysed. The depth profile is the value how deep the evanescent wave goes through the sample, however the evanescent wave represents an exponential decay, so the higher region of the depth profile (cortex region) will not be sampled as the lower ones (cuticle region). The depth profile on this study was calculated to be around 0.92 and 6.91μm, according to these values only a small amount of the cortex may be sampled during the analysis.

The fingerprint region, besides the complexity reported before, have small variations that can be identified. The initial proportion among Amide I, II and III is not preserved after the modification on the morphology of the hair fibre. Amide III presents a higher increase when compared to Amide I and II. This may suggest Amide III is not as affected to the compression of the fibre as Amide I and II. Furthermore stated in literature, the study of the modification of hard α-keratin fibres during stretch, revealed native keratin fibres present predominantly the α-helix conformation, 1657 cm^{-1}.[133,329] Although, when stretch was applied on the fibre that conformation changed followed by a second maximum at 1631 cm^{-1}, that major frequency is related to the β-sheet conformation.[329]

It is important to emphasize that cortex is mainly composed by α-helix, while the cuticle is predominantly β-structures, as mentioned before.[204] Both Amide I and Amide II showed a shift towards lower wavenumbers and an increase on the right side of the band, related to the β-structures. That phenomenon might confirm that the cuticle is being analysed, since β-structures is the dominant conformation. However, in the case of our study the fibre was not stretched but compressed, these two phenomena are very different so it's not possible to confirm that the same is happening in this case.

After a certain period of time under the pressure of the ATR-FTIR armature, those are the major modifications identified on the hair spectrum. This was the analysis at one spot, but more spots were analysed to assurance pressure acts similarly on the hair fibre. The Figure 56 presents the variation on spectra of hair fibre during ATR-FTIR armature pressure at different spots along the hair fibre. Once again, each spectrum was subtracted from the first one. Despite the spikes presented in the spectra, regarding water vapour during the analysis, all spots present the same behaviour in both higher and lower wavenumbers.

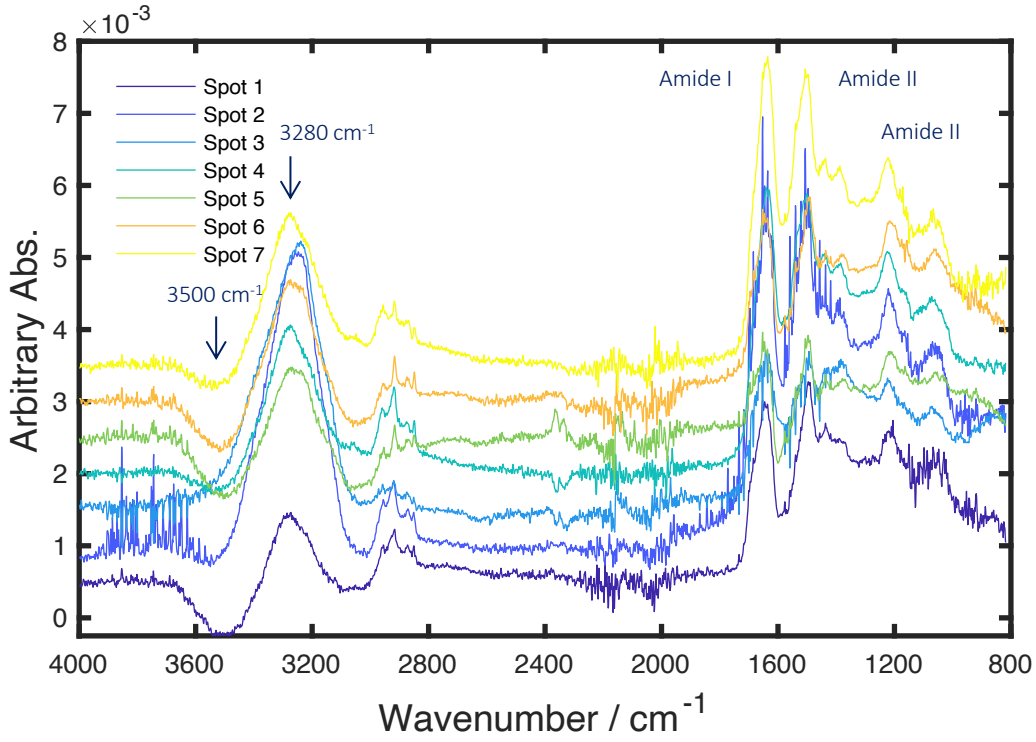


Figure 56. Variation on spectra of hair fibre during ATR-FTIR armature pressure at different spots along hair fibre. The spectra were collected from root (spot 1) to tip of hair (spot 7). The spectra should be read from spot 1, represented by deep blue colour, to spot 7 (yellow).

Small differences among spectra can be justified by the difference on the section being sampling. The thickness along the fibre may not be exactly the same along the fibre, as hair is a natural material. So, the area being sampled will be slightly different among spots.

The ATR-FTIR analysis is a non-invasive technique, nevertheless the natural morphology of the hair has been proven to change during this analysis. The identification on how

fibres are affected by pressure is very important, as chemical modifications on the fibre structure will not be confused by pressure alterations.

The major variations on the hair spectrum were regarding OH bands (3500 cm^{-1}), probably from the dehydration of the fibre and N-H stretching (3280 cm^{-1}) variations related to cuticle. At the fingerprint region, the main modifications are related to Amide I and II that showed to be shifted towards lower wavenumbers and a shoulder at β-conformations, suggesting the band has been affected by pressure. Also, the ratio between Amide I&II/Amide III changed drastically, suggesting Amide III may not be as affected by pressure as the other two Amide bands.

Pressure variation among different hair fibres

The variation along the fibre were also investigated for different hair types, European straight, European blonde, Asian and Indian hair. The fibres were investigated to confirm if the behaviour shown above was the same for all hair types. Each spectrum was subtracted from the first one for each spot, to highlight the changes throughout time during pressure, these variations are represented in Figure 57 for each hair type.

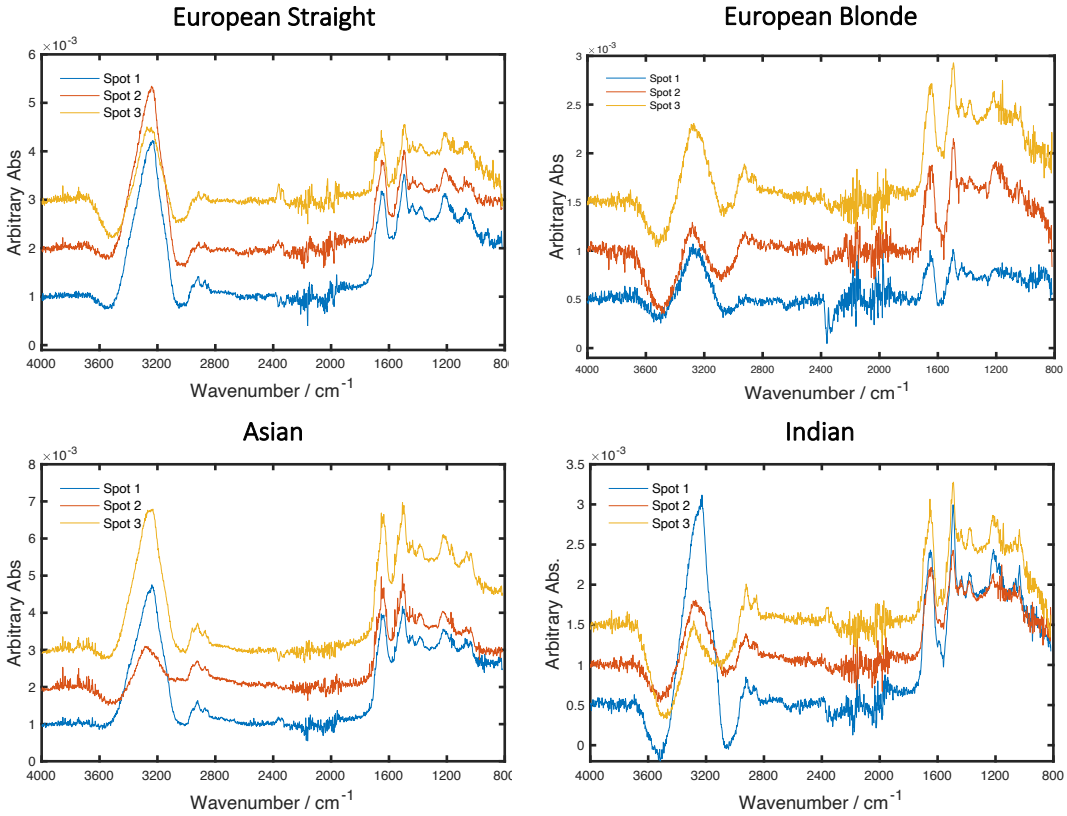


Figure 57. The study of the pressure effect during ATR-FTIR analysis on some spots along each fibre. Four hair types from different backgrounds were analysed, European straight, European blonde, Asian and Indian Hair.

All hair types seem to have a similar behaviour as European curly hair, shown in Figure 56. At higher wavenumber there is always one middle component (3280 cm^{-1} due to N-H stretching) that shows an increase on its intensity, while the outside components seem to decrease. But as not as intense as the middle one. Once again, is possible to detect that the proportion among Amide I & II/Amide III is not preserved throughout the ATR-FTIR analysis. However, the variation regarding the pressure throughout the analysis seems to be very consistent among hair types. Similarly, in the fingerprint region, despite its complexity, it is possible to observe the hair types follow the same pattern. So, even when analysing different hair fibres or different spots along the fibre the behaviour of hair with pressure seems to be similar for all hair types. Now, that the effect of the ATR armature pressure on different hair types is known, and how affected is the hair fibre during the ATR-FTIR analysis, it is possible to examine the natural variation along the hair fibres.

Differential Scanning Calorimetry (DSC)

Approximately 3 mg of the sample of interest was loaded into a T_{zero} (for solid samples) and hermetic (viscous liquid) DSC (TA-Q2000) pan and sealed.

Due to limitation of the machine, only ILs listed below were analysed.

The sample sequence was as follow:

1st Cycle

Ramp at 10° C/min from 25° C to -90° C

Isothermal for 5 min

Ramp at 10° C/min from -90° C to 500° C

Isothermal for 5 min

Ramp at 10° C/min from 500° C to -90° C

Isothermal for 5 min

2nd Cycle

Ramp at 10° C/min from -90° C to 500° C

Isothermal for 5 min

Ramp at 10° C/min from 500° C to -90° C

Ionic Liquid	DSC
1-ethyl-3-methylimidazolium bis(trifluoromethanesulfonyl)imide,$[C_2C_1Im][NTf_2]$	A glass transition was observed at -87° C and a melting transition was observed at > 280° C.
1-butyl-3-methylimidazolium chloride, $[C_4C_1Im]Cl$	A glass transition was observed at -41° C and a melting transition was observed at 73° C.
1-butyl-3-methylimidazolium methylsulphate, $[C_4C_1Im][CH_3O_4S]$	A glass transition was observed at -41.0° C and a melting transition at 72.8° C.
1-butyl-1-methylpyrrolidinium trifluoromethanesulfonate, $[C_4C_1Pyrr][CF_3SO_3]$	A melting transition was observed at 276.0° C.

1,1,3,3-tetramethylguanidinium acetate, [TMGH][OAc]	A melting transition was observed between 90-97° C.